

Retinal Neuronal Remodelling in a Model of Optic Atrophy

Peter Alexander Williams

A thesis submitted to Cardiff University in accordance with the requirements for the degree of
Doctor of Philosophy in the disciplines of Visual Neuroscience and Molecular Biology

School of Optometry and Vision Sciences
Cardiff University
December 2011

Declaration

Declaration

This work has not previously been accepted in substance for any degree and is not concurrently submitted in candidature for any degree.

Signed.....

Date.....

Statement 1

This thesis is being submitted in partial fulfilment of the requirements for the degree of PhD.

Signed.....

Date.....

Statement 2

This thesis is the result of my own independent work / investigation, except where otherwise stated. Other sources are acknowledged by explicit references.

Signed.....

Date.....

Statement 3

I hereby give consent for my thesis, if accepted, to be available for photocopying and for interlibrary loan, and for the title and the summary to be made available to outside organisations.

Signed.....

Date.....

Acknowledgments

I would like to gratefully acknowledge everyone who has helped me over the last 2 years including Drs Paulina Samsel and Lilian Kisiswa for their gene gun expertise, Ed Pritchard for teaching me retinal dissection techniques, Tim Gould and Stephen Cross for teaching me immunohistochemistry, Caroline Waters for her help with plasmid preps, Dr Jan Hobot and Chris Von Ruhland for their help with electron microscopy, Elaine Taylor for her support with mouse work and western blots, Dr Steven Hughes for the melanopsin staining technique, Dr Tatjana Jakobs for the gift of the PSD-95:GFP plasmid and all the supporting staff within the department who have helped me within this time.

I would also like to acknowledge Miss Rebecca Thirgood for the hippocampal sections and Central Bioscience Services, Cardiff University who performed the qPCR.

I would like to make an especial thank you to my parents for their ever-present support, all my grandparents for a continual supply of hot meals and Hattie Jackson for putting up with me while I undertook this PhD.

Many thanks of course go to my two supervisors; Professors James Morgan and Marcela Votruba for their continual support and guidance, without whom I would not have got this far.

Abstract

The heterozygous mutation, B6;C3-*Opa1*^{Q285STOP}, leads to a 50% reduction in Opa1 transcript and protein in the mouse retina and neural tissues and models autosomal dominant optic atrophy and presents with visual dysfunction and structural changes in the retina and optic nerve. This thesis explores the intimate relationship between retinal ganglion cell dendritic architecture, health and synaptic connectivity as influenced by the mitochondrial fusion protein Opa1.

Using a range experimental paradigms it is reported here retinal ganglion cell dendritic atrophy which is exacerbated with age and localised exclusively to sublamina b of the inner plexiform layer. There is a marked reduction in the number of glutamatergic synaptic sites and PSD95 levels on ON-centre retinal ganglion cells. In addition, there is a significant increase in synaptic vesicle number and density in both ON and OFF bipolar cells.

These processes cast light on the intimate relationship between normal mitochondrial fusion and fission balances, as influenced by the OPA1 protein, in neural cell connectivity in the mammalian retina and the changes shown here serve as an exciting biomarker for disease and rescue and recovery therapeutics.

Abbreviations

%Δ	Percentage Change
AF	AlexaFluor
ATP	Adenosine Triphosphate
BSA	Bovine Serum Albumin
CMT	Charcot-Marie-Tooth Disease
CNS	Central Nervous System
C _v	Coefficient of Variation
DNA	Deoxyribonucleic Acid
DOA	Dominant Optic Atrophy
Drp1	Dynamin Related Protein 1
ENU	<i>N</i> -ethyl- <i>N</i> -nitrosourea
ERG	Electroretinogram
Fis1	Mitochondrial Fission 1 Protein
GABA	γ-Aminobutyric Acid
GCL	Ganglion Cell Layer
GFP	Green Fluorescent Protein
GTPase	Guanosine Triphosphate
HBSS	Hank's Balanced Salt Solution
INL	Inner Nuclear Layer
IPL	Inner Plexiform Layer
ipRGC	Intrinsically Photosensitive Retinal Ganglion Cell
LGN	Lateral Geniculate Nucleus
Mfn1	Mitofusin 1
Mfn2	Mitofusin 2
mtDNA	Mitochondrial DNA
n	Number

NS	Non-Significant
OCT	Optimal Cutting Temperature
OKN	Optokinetic Drum
ONL	Outer Nuclear Layer
<i>OPA1</i>	Optic Atrophy 1 (gene)
Opa1	Optic Atrophy 1 (protein)
<i>Opa1+/-</i>	Heterozygous Opa1 Mutant Mouse
OPL	Outer Plexiform Layer
P	Post-Natal Day
PBS	Phosphate Buffered Saline
PBST	PBS with 0.1% Triton-X
PERG	Pattern Electroretinogram
PFA	Paraformaldehyde
PhNR	Photopic Negative Response
PKC- α	Protein Kinase C Alpha
PSD-95	Post-Synaptic Density 95
RGC	Retinal Ganglion Cell
ROS	Reactive Oxygen Species
RT	Room Temperature
S_{EM}	Standard Error of the Mean
Thy-1	Thymocyte Differentiation Antigen 1
VEP	Visual Evoked Potential
<i>wt</i>	Wild Type
XFP	X Fluorescent Protein
YFP	Yellow Fluorescent Protein
ΔE_{Cl}	Chloride Equilibrium Potential

Contents

Declaration.....	2
Acknowledgments.....	3
Abstract.....	4
Abbreviations.....	5
List of Figures	10
List of Tables	12
Chapter 1: Introduction	13
1.1: Mitochondria	13
1.2: Mitochondria: Fusion and Fission.....	17
1.2.1: Opa1.....	17
1.2.2: Mfn1.....	18
1.2.3: Mfn2.....	19
1.2.4: Drp1	20
1.2.5: Fis1	21
1.3: Mitochondria: Importance in Neuronal Health and Survival.....	23
1.4: The Retina	25
1.5: Retina Ganglion Cells: Morphology, Structure and Function	29
1.6: Dendrites: Structure, Function and Importance.....	33
1.7: The Inner Plexiform Layer: Neurotransmitters and Localisation.....	35
1.8: Synapses: Structure, Function and Importance.....	38
1.9: Dominant Optic Atrophy.....	40
1.10: Mouse Models of Dominant Optic Atrophy: A Comparison.....	43
1.10.1: Mouse Model of Dominant Optic Atrophy	43
1.10.2: Generation of the B6;C3-Opa1 ^{Q285STOP} and B6;C3-Opa1 ^{329-355del} Opa1 Mutant Mice	47
1.10.3: Visual, Neurological and Neuromuscular Abnormalities	48
1.10.4: Retinal Ganglion Cell Populations.....	50
1.10.5: Optic Nerve Pathology	52
1.10.6: Clinical Relevance of the B6;C3-Opa1 ^{Q285STOP} and B6;C3-Opa1 ^{329-355del} Mouse Models	53
1.11: Aims and Hypothesis.....	56
Chapter 2: Materials and Methods.....	58
2.1: <i>Opa1</i> ^{+/-} Mice	58
2.2: Retinal Dissections and Flat Mounts.....	60

2.3: Hippocampal Sections.....	62
2.4: Quantitative RT-PCR.....	62
2.5: Western Blots.....	63
2.6: Electron Microscopy	64
2.7: Immunohistochemistry.....	64
2.8: Custom Media.....	66
2.9: DiOlistic Labelling Using the Gene Gun.....	66
2.10: Bacterial Cell Cultures and Plasmid Preparation	67
2.11: Biolistic Transfection of Plasmid DNA.....	69
2.12: Analysis: Image and Statistical.....	70
Chapter 3: Aberrant Mitochondrial Morphology in <i>Opa1</i> ^{+/-} Dendrites	75
3.1: Introduction	75
3.2: Mitochondrial Morphology.....	75
3.3: Mitochondrial Location and Distribution.....	76
3.4: Summary	76
Chapter 4: Retinal Ganglion Cell Dendropathy in <i>Opa1</i> ^{+/-} Mice Occurs Without Cell Loss, Is Exacerbated With Age and Localised Exclusively to Sublamina b of the Inner Plexiform Layer	79
4.1: Introduction	79
4.2: Retinal Cell Populations	80
4.2.1: Retinal Ganglion Cells	80
4.2.2: Bipolar Cells.....	81
4.2.3: Photoreceptors	81
4.3: Retinal Ganglion Cell Dendropathy.....	84
4.3.1: Dendropathy with Age	84
4.3.2: Localisation	86
4.4: Summary	86
Chapter 5: <i>Opa1</i> ^{+/-} Deficiency Leads to the Selective Loss of Glutamatergic Synapses on ON-Centre Retinal Ganglion Cells	95
5.1: Introduction	95
5.2: Neurotransmitters	95
5.3: Synapses.....	97
5.4: Synaptic Vesicles.....	101
5.5: Summary	101
Chapter 6: Dendritic Spine Atrophy in CA1 Region Pyramidal Neurones.....	106

6.1: Introduction	106
6.2: Changes in Dendritic Spine Density and Morphology	107
6.3: Quantification of Post-Synaptic Sites (PSD95) in Opa1+/- Mice.....	108
6.4: Western Blot and qPCR Analysis of Post-Synaptic Sites and Pre-Synaptic Vesicles	108
6.5: Summary	109
Chapter 7: Method Development of Magnetofections for Neuronal Cell Transfection.....	112
7.1: Introduction	112
7.2: Method Development.....	115
7.2.1: <i>In vitro</i> retinal labelling using lipophilic dye coated magnetic nanoparticles.....	115
7.2.2: <i>In vivo</i> retinal labelling using lipophilic dye coated magnetic nanoparticles.....	116
7.2.3: <i>In vitro</i> retinal and neuronal labelling using plasmid coated magnetic nanoparticles	116
7.2.4: <i>In vivo</i> retinal labelling using plasmid coated magnetic nanoparticles	117
7.2.5: Plasmid validation	117
7.3: Results.....	118
7.3.1: <i>In vitro</i> labelling of retinal ganglion cells using lipophilic dyes.....	118
7.3.2: <i>In vivo</i> labelling of retinal ganglion cells using lipophilic dyes.....	120
7.3.3: <i>In vitro</i> labelling of cell cultures using plasmid DNA.....	122
7.3.4: <i>In vivo</i> labelling of retinal cells using plasmid DNA.....	124
7.3.5: Plasmid validation	126
7.5: Magnetofections Discussion	128
Chapter 8: Discussion.....	130
8.1: Retinal Ganglion Cell Dendropathy in a Mouse Model of Dominant Optic Atrophy.....	130
8.2: Mechanism of Disease	134
8.3: The Pharmacological Properties of Retina Ganglion Cells Determines Their Fate	138
8.4: The Importance of Mitochondria in Neuronal Health, Survival and Plasticity	142
8.5: Implications for Therapeutics Interventions.....	144
References	146
Appendix: DiOlistic Method Development	161
Papers Arising From This Thesis.....	163

List of Figures

Figure I: Mitochondrial structure	15
Figure II: Mitochondrial fusion and fission I	16
Figure III: Mitochondrial fusion and fission II	22
Figure IV: Mammalian retina and visual system	28
Figure V: Melanopsin in the visual system	31
Figure VI: Neurotransmitters in the retina	37
Figure VII: Opa1 mutations	42
Figure VIII: DOA disease progression timeline	44
Figure IX: Retinal dissections	61
Figure X: Sholl analysis	73
Figure XI: Retinal ganglion cell count locations	74
Figure XII: Mitochondria morphometrics	74
Figure XIII: Aberrant mitochondrial morphology in <i>Opa1</i> ^{+/-} mice	77
Figure XIV: Retinal cell populations are preserved in <i>Opa1</i> ^{+/-} mice	82
Figure XV: DiOlistically labelled ON-centre retinal ganglion cells	87
Figure XVI: Dendritic pruning in ON-centre retinal ganglion cells	88
Figure XVII: Sholl analysis of ON-centre retinal ganglion cells	89
Figure XVII: Reduction in ON-centre secondary and tertiary dendrites	91
Figure XIX: OFF-centre retinal ganglion cells are unaffected by Opa1 deficiency	92
Figure XX: Selective pruning of ON-centre retinal ganglion cells	94
Figure XXI: Glutamatergic synapses are specifically eliminated in <i>Opa1</i> ^{+/-} mice	96
Figure XXII: Reduced retinal connectivity in <i>Opa1</i> ^{+/-} mice	98
Figure XXIII: Mitochondrial and synapses ON-centre retinal ganglion cells	100
Figure XXIV: Increased synaptic vesicle density in <i>Opa1</i> ^{+/-} mice	103

Figure XXV: Western blot densitometry of <i>wt</i> and <i>Opa1</i> ^{+/-} retinas	104
Figure XXVI: qPCR analysis of <i>wt</i> and <i>Opa1</i> ^{+/-} retinas	105
Figure XXVII: Dendritic spine and synapse loss in <i>Opa1</i> ^{+/-} mice	110
Figure XXVIII: Opa1, PSD95 and synaptophysin protein and transcript levels	111
Figure XIX: Magnetolistically labelled retinal ganglion cells	119
Figure XXX: Magnetolistically labelled retinal ganglion cell axons <i>in vivo</i>	121
Figure XXXI: Magnetofections: RGC-5 cultures	123
Figure XXXII: Magnetofections: Intraocular injections	125
Figure XXXIII: DiOlistic method development	162

List of Tables

Table I: Comparative retinal ganglion cell classes across species	32
Table II: Comparison of Opa1 mouse models	46
Table III: Mouse ages	59
Table IV: Individual nuclear layer thicknesses in <i>wt</i> and <i>Opa1</i> ^{+/-} retina sections	83
Table V: Magnetofection trials	127

There are no small problems. Problems that appear small are large problems that are not understood.

Ramón y Cajal

from Advice for a Young Investigator (1897)

Chapter 1: Introduction

1.1: Mitochondria

Mitochondria are essential organelles in almost all eukaryotic cells and serve a bioenergetic function. They provide this role through a series of well-defined biochemical reactions that lead to the generation of ATP through oxidative phosphorylation (Lawrence, 2005; Chan, 2006a; Chen and Chan, 2006). Mitochondria also have a role in cell signalling (calcium signalling), apoptosis (Delivani and Martin, 2006) and steroidogenesis (Poderoso et al., 2008) and, further to this, provide structure and organisation to the synaptic bouton (Chan, 2006a) (*Figure 1*).

Within eukaryotic cells there is a substantial ionic gradient between the cytosolic concentration of Ca^{2+} ions ($\sim 100\text{nM}$) and the extracellular concentration of Ca^{2+} ions ($\sim 1\text{mM}$) which is kept in balance, in part, by ions pumps, Ca^{2+} exchangers ($\text{Na}^+/\text{Ca}^{2+}$ exchanger found in plasma membranes, ER and mitochondria), Ca^{2+} binding proteins (*e.g.* calmodulin) and the mitochondria (Rizzuto et al., 2009). Here the mitochondria can have a role buffering changes in intracellular Ca^{2+} and sequestering Ca^{2+} as they readily take up Ca^{2+}

when the concentration in the cytosol is high. This allows Ca^{2+} to rapidly accumulate within the mitochondria lowering the cytosolic Ca^{2+} concentration (Rossier, 2006).

Mitochondria display considerable morphological diversity in terms of their number and distribution as well as their inner membrane structure which is mostly in part due to their dynamic behaviour driven by the balance of mitochondrial fusion and fission (Cervený et al., 2007). When this balance shifts towards fusion the mitochondria become long and interconnected and when this balance shifts towards fission the mitochondria become fragmented (Zhang and Chan, 2007) (*Figure II*). Ultimately mitochondrial fusion and fission play a key role in cell physiology and homeostasis (Liesa, Palacin and Zorzano, 2009) and an improper balance in this can lead to mitochondrial dysfunction leading on to neurodegenerative diseases including, but not limited to Parkinson's disease (Abou-Sleiman, Muqit and Wood, 2006), Alzheimer's disease (Knott and Bossy-Wetzell, 2008; Wang et al., 2008), Huntington's disease (Kieper et al., 2010), Charcot-Marie-Tooth disease (Cervený et al., 2007), Leber's hereditary optic neuropathy (Carelli et al., 2009) and dominant optic atrophy (Olichon et al., 2006).

There are several proteins that have a role in mitochondrial dynamics (fusion and fission) and these shall be discussed.

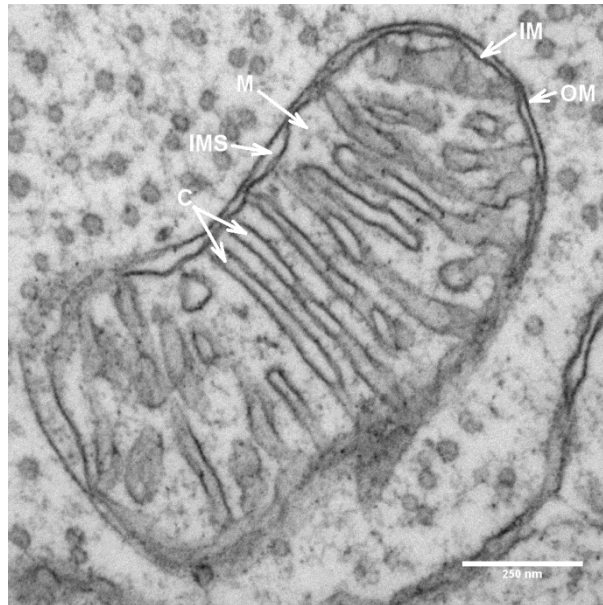


Figure 1: Mitochondrial structure

An electron micrograph showing the internal organisation of a mitochondrion within a retinal ganglion cell dendrite. Mitochondria are found at a high density within the retinal ganglion cell especially within the axon where they are required for efficient saltatory conduction of action potentials and within the dendrite for synaptic transfer.

Key: C = cristae, IM = inner membrane, IMS = intermembrane space, M = matrix, OM = outer membrane

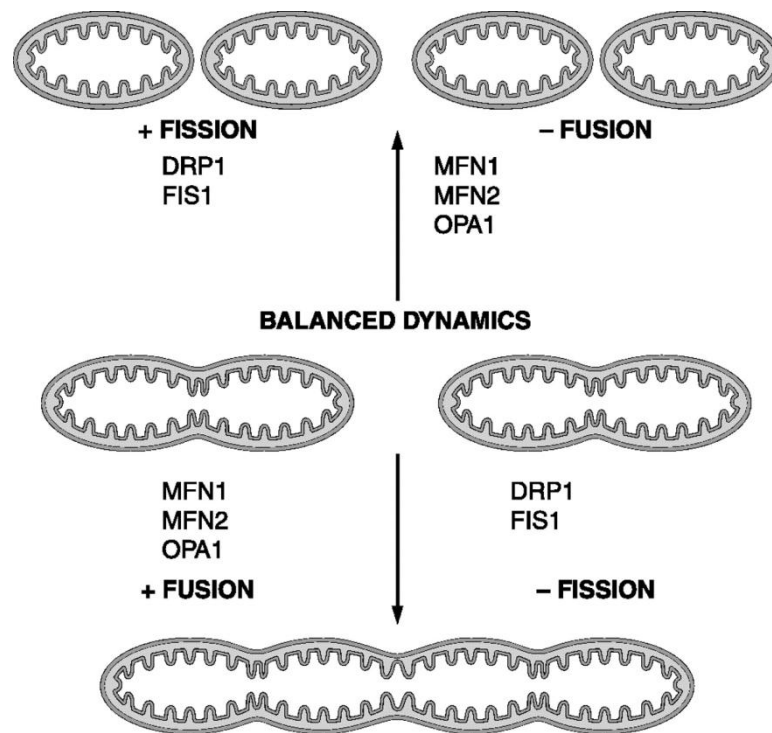


Figure II: Mitochondrial fusion and fission I

Schematic showing the balance of mitochondrial fusion and fission as regulated by the proteins Drp1, Fis1, Mfn1, Mfn2 and Opa1. Increased fusion leads to elongated mitochondria, whereas increased fission leads to small, fragmented mitochondria. Adapted from Liesa et al., 2009.

1.2: Mitochondria: Fusion and Fission

1.2.1: Opa1

The *OPA1* gene codes for the protein Opa1 a dynamin-like mitochondrial related guanosine triphosphatase (GTPase) and a 100K member of the GTPase superfamily (Hinshaw and Schmid, 1995; Votruba, Thiselton and Bhattacharya, 2003; Ju et al., 2005) located primarily in the mitochondrial inner membrane, the mitochondrial outer membrane, the cristae and the inner membrane space (Ju et al., 2005) and is homologous with the yeast (*S. cerevisiae*) gene Mgm1 (Olichon et al., 2002). Mgm1 has roles in the maintenance of mitochondrial morphology (which is important for mitochondrial stability due to its role in the mitochondrial inner membrane structure and integrity), endocytosis, vesicular traffic and coated vesicle formation (Hinshaw and Schmid, 1995), the structure and maintenance of mitochondrial networks, mitochondrial motility and dynamics (including mitochondrial fission and fusion) (*Figure III*) as well as ensuring an appropriate distribution of mitochondria and ensuring a good ATP supply to cytoplasmic regions. OPA1 can act as an anti-apoptotic GTPase protecting the cells from the “detrimental consequences of apoptotic stimuli” (Davies et al., 2007) by modifying the mitochondrial cristae (for which the inner membrane rhomboid protease, PARL, is required) which regulates cytochrome c release (Frezza et al., 2006; Tang et al., 2009). In addition, Opa1 has roles in oxidative phosphorylation and, in ADOA, the activity of OXPHOS complexes II and III is significantly increased (Van Bergen et al., 2011).

The *OPA1* gene comprises 90kb of genomic DNA coded for by 31 exons (of which the last one is non-coding) and there are eight splice variants. The peptide comprises 960 amino acids. The mature protein is 90/80kDa (depending on the isoform) (Davies et al., 2007). The

gene is located on chromosome 3q28 (Votruba, Moore and Bhattacharya, 1997; Alexander et al., 2000; Delettre et al., 2002) and mutations occur throughout the gene (Votruba, 2004).

Opa1 protein is expressed ubiquitously throughout the body with high levels in the retina, brain (Misaka, Miyashita and Kubo, 2002), liver and heart. Within the retina it is predominantly found in the ganglion cell layer of the retina with lower levels of expression in the IPL, OPL and INL (Aijaz et al., 2004).

The exact mechanism of how Opa1 mediates mitochondrial fusion is yet to be fully elucidated although it is known that Opa1 is essential for mitochondrial fusion. Mitochondrial fusion, as influenced by Opa1, is essential for the redistribution of mtDNA that, over time, may become damaged (Chan, 2006b). Opa1 exists primarily in the inner mitochondrial membrane and is not exposed to the cytosol yet yeast deficient in Mgm1 show no evidence of outer membrane fusion. It is unclear whether this is a direct effect or as a consequence from aberrant inner membrane fusion events. Members of the GTPase superfamily are involved in the curvature and moulding of the inner mitochondrial membrane and as Opa1 shows a high homology to members of this family it is likely that Opa1 also has a role.

1.2.2: Mfn1

Mfn1 is the human homologue of the *Drosophila* GTPase Fzo and is an outer mitochondrial membrane protein helps regulates mitochondrial morphogenesis through mitochondrial fusion by mitochondrial tethering and the merging of lipid bilayers (Santel et al., 2003; Cervený et al., 2007). The gene, MFN1, is located on chromosome 3 at 3q27.1 and, in humans, shows a 63% sequence identity with another mitochondrial fusion protein; Mfn2.

MFN1 and MFN2 are widely expressed throughout the body with high levels in the heart, liver and pancreas although there are higher levels of Mfn1 over Mfn2. Both Mfn1 and Mfn2 have a role in tethering of mitochondria (Mfn1 being required on both mitochondria) and this again is shown to be at a higher level in Mfn1 (Chen et al., 2003; Zhang and Chan, 2007; Liesa et al., 2009).

Mfn1 is seen to be essential to the mammalian system and embryonic development as deficient mice show severely fragmented mitochondria which lead to embryonic lethality (Chen et al., 2003; Zhang and Chan, 2007). Over expression of MFN1 leads to an increase in the number of Mfn1 protein which, in turn, leads to the formation of perinuclear clusters of mitochondria (Santel et al., 2003).

1.2.3: Mfn2

Mfn2 is located in the outer mitochondrial membrane (Liesa et al., 2009) and has a secondary role in mitochondrial fusion working in concert with Opa1 and Mfn1 (Merkwirth and Langer, 2008; de Brito and Scorrano, 2009). Mfn2 was first identified by homology with the *Drosophila* protein Fzo where disruption of Fzo prevents mitochondrial fusion. Recent studies (Chen et al., 2003; Chen and Chan, 2006) have shown Mfn2 to be essential for embryonic development in mice where Mfn2 knockout mice show reduced mitochondrial fusion and motility due to fragmented mitochondria. This leads to a disruption in placental development and ultimately Mfn2 knock-out mice die mid-gestation. It has been shown that cells with high metabolic demands are more susceptible to Mfn2 disruptions. More recent work (de Brito and Scorrano, 2009) shows that Mfn2 has a role in tethering mitochondria

and ER by forming interorganellar bridges which are essential for the funnelling of Ca^{2+} (Rizzuto et al., 1998). *Mfn2*^{-/-} cells are shown to have much smaller mitochondria and have an alteration in their ER morphology.

In human mutations in *Mfn2* can lead to Charcot-Marie-Tooth neuropathy type 2A (CMT2A); a primary neuropathy that affects both the sensory (including optic atrophy) and muscle systems leading to muscle atrophy over time. CMT2A disease is one of the most common hereditary diseases affecting 1 in 2500 with a loss of deep tendon reflexes and feet deformities among its symptoms (Chen and Chan, 2006; Liesa et al., 2009).

1.2.4: Drp1

The GTPase Drp1 has been shown to have a role in several intracellular functions including, but not limited to, controlling ER morphology, as a driver for mitochondrial fission as well as a role in mitochondria-dependent apoptosis (Frank et al., 2001; Lackner and Nunnari, 2009). Identified by its yeast homologue, Dnm1, it has been shown that Drp1 has a role in the scission of the mitochondrial membrane. Drp1 itself possesses a highly conserved GTPase domain and is found in all tissues tested with the highest levels found in the brain, heart and skeletal muscle (Liesa et al., 2009). Although Drp1 has a role in mitochondrial fission only a fraction of the protein actually exists in the mitochondria, the rest being dispersed throughout the cytosol. Drp1 can regulate mitochondria morphology without actually affecting endocytic pathways or triggering apoptosis.

During mitochondrial fission Drp1 acts by assembling into oligomeric complexes that then form rings or spirals around the mitochondrial outer membrane, compressing it and

effectively causing mitochondrial fission. An absence of Drp1 (homozygous negative) in *C. elegans* shows no membrane scission (Frank et al., 2001; Knott and Bossy-Wetzel, 2008).

A recent clinical case showed that, in one patient, a deficiency in the Drp1 gene lead to defective mitochondrial fission causing tubular, elongated and interconnected mitochondria which lead to severe, lethal brain abnormalities (microcephaly as well as optic atrophy) with the subject dying after 37 days (Waterham et al., 2007).

1.2.5: Fis1

Fis1, the mammalian homologue of the yeast protein Fis1p (and human homologue hFis1), is a small 17kDa protein comprising of 152 amino acids found on the mitochondrial outer membrane and is ubiquitous across tissues (Liesa et al., 2009). Recent work has found that Fis1 has a role in mitochondrial fission (Mozdy, McCaffery and Shaw, 2000; Knott and Bossy-Wetzel, 2008) by recruiting Drp1 to the mitochondrion (Stojanovski et al., 2004). Fis1 is coupled to the mitochondrion at its C-terminus leaving the majority of its structure in the cytosol (Yu et al., 2005). The cytosolic N-terminus forms six α (α 1-6) helices which mediate protein-protein interactions with Drp1 which leads to mitochondrial fission in a multistep pathway (Mozdy et al., 2000; Yoon et al., 2003; Dohm et al., 2004). *In vitro* Fis1 overexpression has been shown to cause mitochondrial fragmentation mediated by Drp1 (Yu et al., 2005) and to cause cytochrome c release (Liesa et al., 2009). Cells lacking Fis1 have been shown to have flat, elongated mitochondria and deletions in hFis1 and *OPA1* leads to mitochondrial fragmentation (Lee et al., 2007).

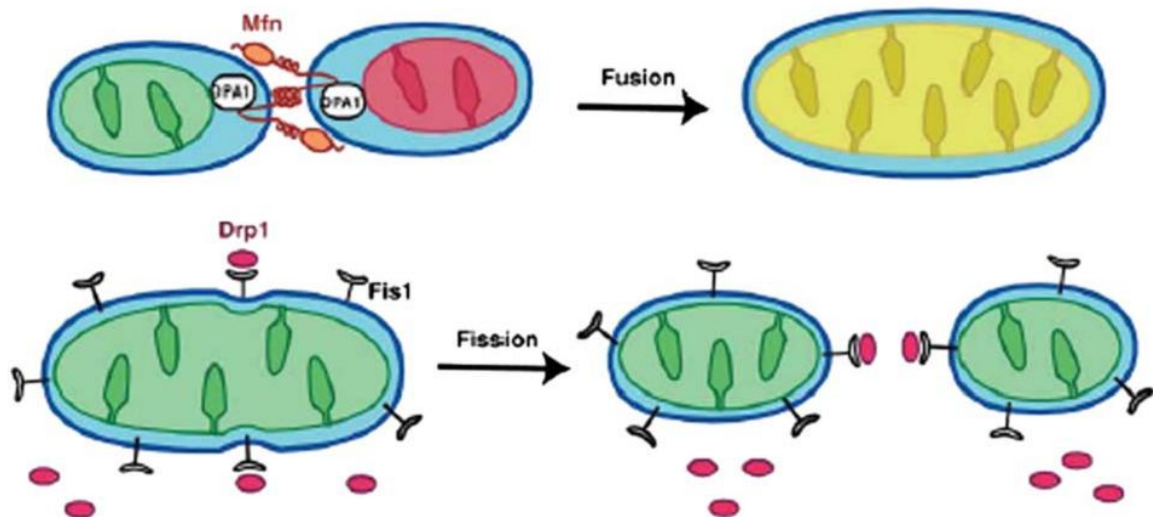


Figure III: Mitochondrial fusion and fission II

Mitochondrial fusion is mediated by Mfn, a mitochondrial outer membrane protein (orange molecule) with the coiled C-terminus mediates oligomerization between Mfn molecules on adjacent mitochondria, and Opa1 situated in the intermembrane space (*top*).

Mitochondrial fission is mediated by Drp1 within the cytosol, and Fis1 located on the mitochondrial outer membrane (*bottom*). Adapted from (Chen and Chan, 2005).

1.3: Mitochondria: Importance in Neuronal Health and Survival

The appropriate intracellular distribution and morphology of mitochondria is crucial in most eukaryotic cells and this is even more so in neural tissue where neurons exist on a 'metabolic knife-edge' which relates to the level of energy dependence over the level of energy produced. If the bioavailability of ATP is too low neurons will not function properly, cell atrophy and dendropathy (dendritic atrophy) will ensue resulting in cell death. High metabolic rates and associated lipid peroxidation can increase mitochondrial ROS release, resulting in ATPase and glucose transport dysfunction. This in turn can lead to excitotoxicity and cell death (Li et al., 2004; Chen and Chan, 2006; Mattson and Magnus, 2006).

The intracellular distribution of the mitochondria plays a role in neuron health since neurons have high energy demands. In the healthy neuron mitochondria are found in abundance throughout the cell especially near sites of concentrated bioenergetics, for example the dendrites and synapses where mitochondria are required to regulate ATP and buffer Ca^{2+} levels to maintain proper synaptic function (Chen and Chan, 2006; Knott and Bossy-Wetzel, 2008).

Mitochondria are highly dynamic organelles and mitochondrial dysfunction is increasingly recognised as a key contributor to neuronal dysfunction and loss in classic neurodegenerative diseases such as Alzheimer's (Wang et al., 2008), Huntington's (Kieper et al., 2010) and Parkinson's disease (Abou-Sleiman et al., 2006; Mattson, Gleichmann and Cheng, 2008) as well as dominant optic atrophy (driven by deficits in Opa1) and CMT disease (deficits in Mfn2). In these disease states, the rate of neuronal loss is slow and accompanied by prolonged periods of neural dysfunction in the absence of demonstrable neuronal loss and atrophy. The high dependence of neurons on mitochondria leaves them highly

susceptible to any changes in energy stasis (Mattson and Magnus, 2006). Mitochondrial structure, number and their distribution within the axon, dendrite and synapse are thus integral to neuronal physiological function and health (Selkoe, 2002; Mattson et al., 2008; Cheng, Hou and Mattson, 2010; Cho, Nakamura and Lipton, 2010; Saxena and Caroni, 2011).

In dominant optic atrophy quite how a mitochondrial mutation manifests as a specific loss or degeneration of retinal ganglion cells is currently unknown, however, retinal ganglion cells face a unique challenge in the central nervous system. Retinal ganglion cells have, by far, the most extended processes in the retina, and the axons of these cells only myelinate in the retrolaminar part of the optic nerve head. These unmyelinated sections of axons can be as long as 1cm for retinal ganglion cells in the human peripheral retina and these axons have a huge metabolic demand that needs to be met by the mitochondria within the cell as, at this point in the axon, action potential transmission is non-saltatory.

1.4: The Retina

The neuronal structure of the retina has been studied intensely for over a century. The visual cells, the photoreceptors (rods and cones), were once thought to make direct connections from the eye to the brain and thanks, in part, to Ramón y Cajal's work in the late 19th century we now know that this is not the case. Cajal improved on Golgi's silver nitrate staining of neurones (Ramon y Cajal, 1889ab) and thanks to his meticulous method he showed that retina is made up of many different layers of cells, each with distinct morphologies and functions and these groups of cells work as a unit with one another to form a very approachable part of the brain (Dowling and Werblin, 1969; Werblin and Dowling, 1969; Werblin, 1972; Dowling, 1987; Matthews, 2005).

The neural retina is designed to perform two major roles; to respond to photons in light at the level of the photoreceptive cells through the isomerisation of photopsins or rhodopsins and to convert these biochemical changes into a series of coordinated, filtered neural responses. The structural organisation of the mammalian retina is organised to perform this role with two synaptic layers (the inner and outer plexiform layers) and which are intercalated between three somal layers (the ganglion cell layer and the inner and outer nuclear layers).

The outer nuclear layer is the start of the phototransduction pathway. The outer nuclear layer contains the photoreceptors; rods, the most populous which are used for scopic vision; and cones, used for photopic vision. Photons in light are absorbed by the photoreceptive cells causing rhodopsin (in rods) or a photopsin (cones) to isomerise between their *cis* and *trans* isoforms. This instigates a series of biochemical reactions that leads to a change in the photoreceptor's membrane potential, closing the voltage-gated

calcium channels and causing a decrease in the intracellular calcium concentration. This lack of calcium leads to less glutamate being released onto the bipolar cell which can have an inhibitory or excitatory effect leading to depolarisation or hyperpolarisation. This takes place in the outer plexiform layer, the junction between the inner and outer nuclear layers which contains the processes and synapses of bipolar cells and horizontal cells and their connections to the photoreceptive cells.

The inner nuclear layer is home to the cell bodies of three classes of cells that connect between the photoreceptors (biochemical transduction of light) and the retinal ganglion cells (the neural conductors of filtered neuronal information to the visual regions of the brain). These cells are the amacrine cells, horizontal cells and two classes of bipolar cells; the rod bipolar cells and cone bipolar cells. Amacrine cells are the axonless interneurons of the retina functioning in feedback and feedforward loops with bipolar cells and retinal ganglion cells with dendrites that ramify in the inner plexiform layer. Horizontal cells integrate signals from the photoreceptive cells and their dendrites travel distally, ramifying in the outer plexiform layer, whereas their axons carry on horizontal to the cell body and ramify in the inner nuclear layer. Bipolar cells transmit signals between the photoreceptive cells and the retinal ganglion cells. Essentially; bipolar cells copy rod information and converge cone colour channels to produce the functional dichotomy of the mammalian retina; ON and OFF channels (Boycott, Dowling and Kolb, 1969; Nelson, Famiglietti and Kolb, 1978). ON bipolar cells have a depolarising response to light with processes that ramify distally to their soma in sublamina b of the inner plexiform layer close to the ganglion cell layer. OFF bipolar cells have a hyperpolarising response to light with processes that ramify proximal to their soma in sublamina a of the inner plexiform layer close to the inner nuclear layer.

The ganglion cell layer contains the cell bodies of the majority of retinal ganglion cells and of displaced amacrine cells. The unmyelinated axons of retinal ganglion cells trace towards the optic disc where they myelinate and form the optic nerve leading to the lateral geniculate nucleus and superior colliculus. The dendrites of retinal ganglion cells ramify within the inner plexiform layer where they form the first true neural synapses with amacrine cells and bipolar cells (Dacey and Petersen, 1992; Bodnarenko, Jeyarasasingam and Chalupa, 1995; Chalupa and Werner, 2004; Dong et al., 2004).

A detailed diagram and schematic of the mammalian neural retina can be seen in *Figure IV*.

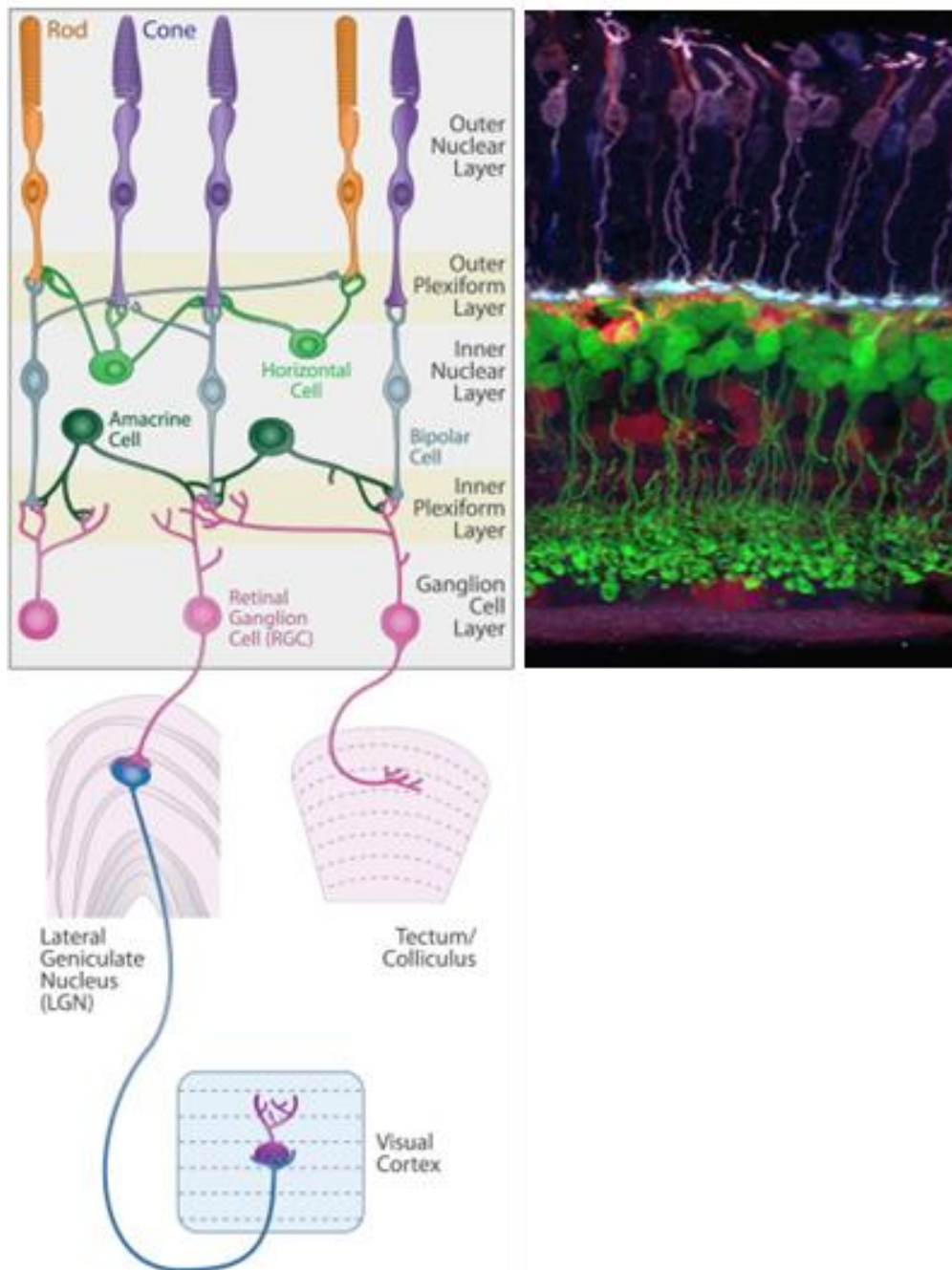


Figure IV: Mammalian retina and visual system

Mammalian visual system (*left*) showing cell somas, dendrites and axons of cells in the retina with the axons of retinal ganglion cells leading through to the LGN (and its projections to the primary visual cortex) and SC. Immunostained mature mouse retina (*right*) showing photoreceptors (*purple*), horizontal cells (*bright red*), bipolar cells (*green*) and amacrine cells (*crimson*). Adapted from (Morgan and Wong, 2007; Sanes and Zipursky, 2010).

1.5: Retina Ganglion Cells: Morphology, Structure and Function

In the early 19th century Treviranus made the first description of what would later be referred to as 'retinal ganglion cells', "papillae" on the vitreal/inner surface of the retina. Further work by the anatomists Müller and Kölliker lead to understanding that the major direction of retinal flow was from the photoreceptive cells to the ganglion cells and the optic nerve. Thanks to Ramón y Cajal's meticulous method later that century, using Golgi's silver nitrate staining, gave further qualitative information towards the understanding of the retina. Ramón y Cajal showed that the retina was more than just photoreceptive cells and their afferent fibres but that there were further subsets of cells, the retinal ganglion cells, with interconnecting bipolar cells in between them. He showed retinal ganglion cells to have multiple morphological subtypes based on their patterns of dendritic arborisation within the inner plexiform layer.

RGCs are the on-off visual information cells of the retina with the cell soma found in the ganglion cells layer (with an average density of 3300cells/mm² in the mouse (Jeon, Strettoi and Masland, 1998)) and their dendrites ramifying in the inner plexiform layer. It is here that the RGCs can be subcategorised as, although all retinal ganglion cell dendritic trees show laminar or multi-laminar radiation, they vary massively in terms of both structure and function (Dowling, 1987; Stuart, Spruston and Hausser, 1999; Coombs et al., 2006; Marc, 2008).

The morphology of RGC dendritic architecture can be used as a guide to retinal ganglion cell function, with retinal ganglion cells in mice subcategorised into as many as 14 different classes (Sun, Li and He, 2002b; Kong et al., 2005; Coombs et al., 2006). A comparison of retinal ganglion cells classes of different species can be seen in *Table 1*. Grossly, retinal

ganglion cells can be categorised into ON- and OFF- centre and ON-OFF (bistratified) where each have their own morphology. ON-centre retinal ganglion cells ramify in sublamina b of the IPL making, but not exclusive to, glutaminergic synapses with bipolar cells forming a light-sensitive pathway. OFF-centre retinal ganglion cells on the other hand ramify in sublamina a of the IPL making, as well as the glutaminergic synapses with bipolar cells, GABA-ergic synapses with amacrine cells forming a dark sensitive pathway (Nelson et al., 1978; Dowling, 1987). Bistratified cells ramify in a multi-lamina fashion in both sublaminae of the IPL and are involved with colour vision and may also be motion sensitive.

Some retinal ganglion cells are also receptive to light (intrinsically photosensitive retinal ganglion cells [ipRGCs]), make direct connections to the suprachiasmatic nucleus and have a role in pupil-light reflex and circadian rhythms (*Figure V*).

Figure V: Melanopsin in the visual system (overleaf)

(A) Schematic of the retina showing the conventional ON- and OFF-centre retinal ganglion cells (*black*) and the relationship between photoreceptors (*blue, green*) and intrinsically photoreceptive retinal ganglion cells (*red*). Traditionally, the light transduction pathway starts at the level of the photoreceptors which makes its way to the retinal ganglion cells and the brain. Here melanopsin containing ipRGCs receive light input and transfer this directly to the brain without intermediary retina cell types. (B) The principle targets for ipRGC axons (*blue*) are the suprachiasmatic nucleus (SCN) as well as the ventral lateral geniculate nucleus (LGNv), the intergeniculate leaflet (IGL) and the olivary pretectal nucleus (OPN) which is part of the pupil-light reflex (circuit in *cyan*). Primary synapses and targets of this pathway are the iris (I), the ciliary ganglion (CG) and the Edinger-Westphal nucleus (EW). The *orange* pathway shows a polysynaptic circuit that regulates melatonin release from the pineal gland (P) in a circuit that includes the paraventricular nucleus (PVN), the intermediolateral nucleus (IML) and the superior cervical ganglion (SCG). Adapted from (Berson, 2003).

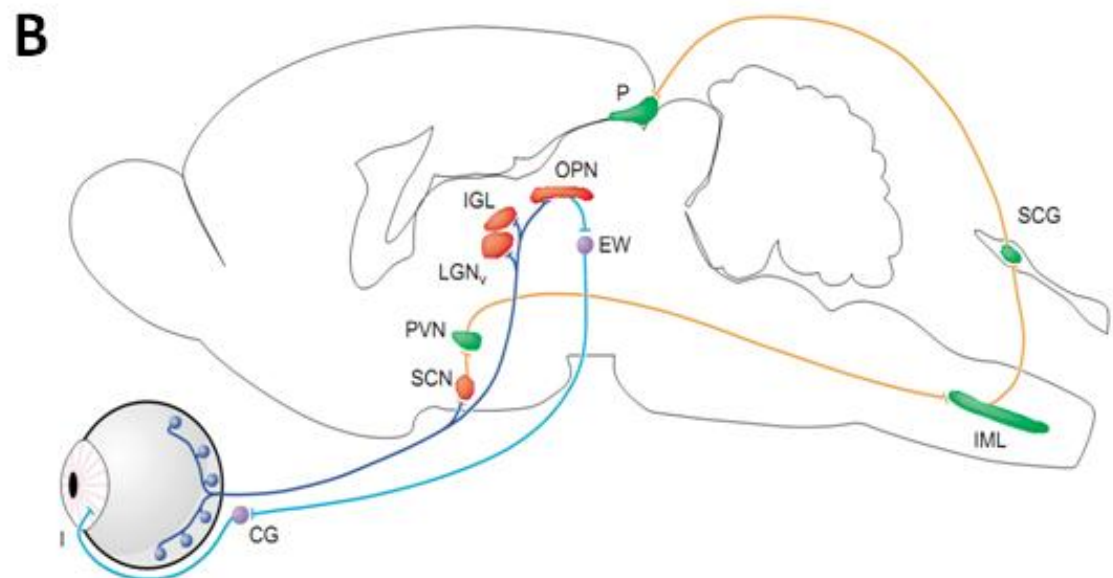
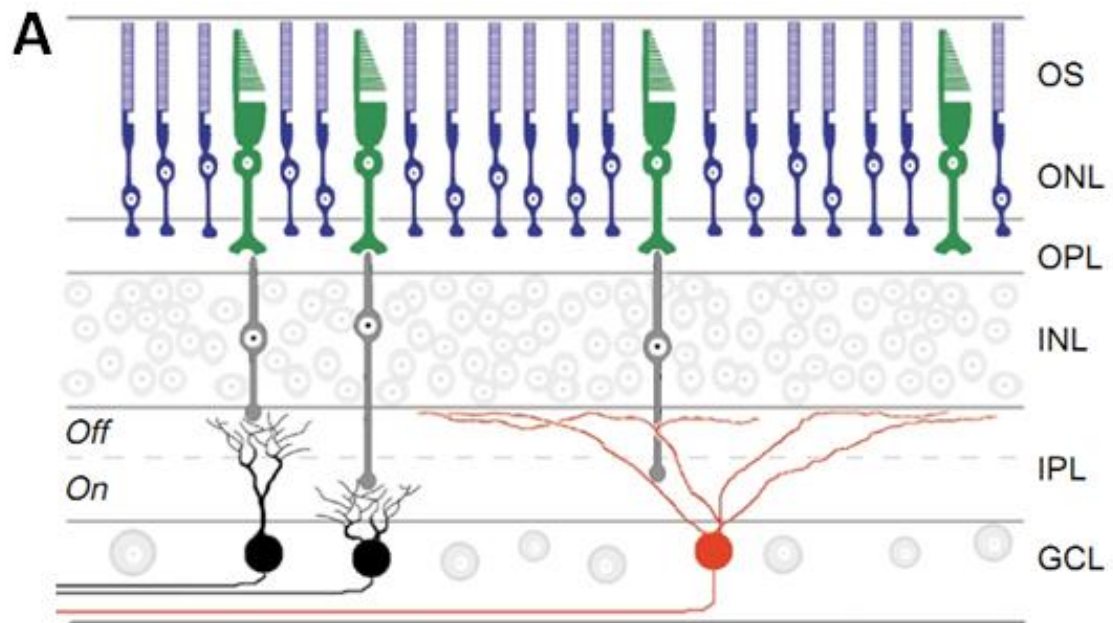


Table I: Comparative retinal ganglion cell classes across species

The retinal ganglion cell population is a morphologically diverse group and many variants in nomenclature exist between species. Table I compares the various retinal ganglion cell subcategories in animals from the order *Primate*, *Rodentia*, *Lagomorpha* and *Scandentia*. Names marked with ‘*’ indicate nomenclature individual to this researcher (Boycott et al., 1969; Watanabe and Rodieck, 1989; Dacey and Petersen, 1992; Akaishi et al., 1995; Doi, Uji and Yamamura, 1995; Ghosh et al., 1996; Jeon et al., 1998; Yamada et al., 2001; Sun et al., 2002b; Diller et al., 2004; Coombs et al., 2006; Ghosh et al., 2006; Laycock, Crewther and Crewther, 2007; Dhruv et al., 2009; Ruggiero et al., 2009).

	Midget (Parvocellular)	Parasol (Magnocellular)	BiStratified (Koniocellular)	Photosensitive (ipRGC)
Mouse (Sun*)	RG _B	RG _A	RG _D	
Alternate Mouse	Type III	Type II	M11, M12, M13, M14	Melanopsin-Expressing Cells
Rabbit	β	α		
Pika	Type I	Type III		
Tree Shrew	Group A	Group B		ipRGC
Owl Monkey	Midget	Parasol		
Capuchin	Midget	Parasol		
Rhesus Macaque	Midget	Parasol		
Baboon	Midget	Parasol		
Marmoset (Ghosh*)	Group B	Group A	Group C	
Alternate Primate	Pβ	Pα		
2nd Alternate Primate	A	B		
3rd Alternate Primate	P1/P2	M		

1.6: Dendrites: Structure, Function and Importance

Ramón y Cajal called neurons the “mysterious butterflies of the soul” and, although a rather beautiful analogy was made of the neuron, little was said about their processes and extensions; the dendrite. The reality is that dendrites are far much more than just passive neuronal extensions (Johnston and Narayanan, 2008). Dendrites are elaborate processes extending from the cell body of neurons. Here they receive almost all synaptic inputs to the cell. Synapse formation on the dendrite involves communication between both the pre- and post- synaptic cell although not all dendrites receive synaptic input (for example some sensory neurones) (Jan and Jan, 2001).

Dendrites act by increasing the total cell surface area and in some neural populations as much as 97% of the total surface area can be attributed to dendritic processes (Ulfhake and Kellerth, 1981). The dendritic architecture of neurones show considerable differences in organisation and morphology between different neuronal populations and within the groups themselves. Dendritic architecture and morphology therefore is often used to categorise the many types of neuronal cells (Akaishi et al., 1995; Stevens, 1998; Sun, Li and He, 2002a; Sun et al., 2002b).

Many dendrites are further specialised in that they have specialised extensions on themselves, dendritic spines. Increased activity at dendritic spines can increase their size and promote morphological changes (Stuart et al., 1999). However, dendritic spines are not present in all neuronal cell groups, for example RGCs, and instead, for RGCs at least, synaptic contact is conducted on the actual shaft of the dendrite. In RGCs dendrites act by increasing the total cell surface area by many times, ramifying in distinctly lamina fashion allowing differing stimuli to affect different cell populations with differing local

neurotransmitter demands (Stuart et al., 1999; Johnston and Narayanan, 2008; Shah, Hammond and Hoffman, 2010).

Neuronal processing also occurs within dendrites. In the axon and soma of a neurone, sodium and potassium channels are required to generate action potentials which is initiated by the initial depolarization of the soma by synaptic inputs in the dendrite (Chalupa and Werner, 2004; Silver, 2010). Action potentials generated in the soma can back propagate into the dendrite which informs synapses in the dendrite that neuronal output has occurred. Therefore, to allow the neuron to generate controlled action potentials, sodium and potassium channels on the dendrite are necessary (Hausser, Spruston and Stuart, 2000; Jan and Jan, 2001). Sodium channels are also present on direction-selective retinal ganglion cells. The direction-selective retinal ganglion cells fire action potentials in a specific direction which signals the direction of an image motion across their receptive field (Oesch, Euler and Taylor, 2005). When the image moves in the preferred direction across the dendritic field, the direction-selective cell exhibits a large excitatory post-synaptic potential and a large inhibitory post-synaptic potential in the opposite direction (Sun et al., 2006). In addition to sodium and potassium there is considerable calcium ion (Ca^{2+}) influx into the cytoplasm of dendrites which can arise from several sources including synaptically from glutamate receptors (both NMDA and AMPA type) and voltage sensitive calcium channels as well as from the mitochondria (and other internal stores such as the smooth endoplasmic reticulum). Ca^{2+} influx into dendrites and dendritic spines has been shown to regulate different forms of long- and short- term synaptic plasticity including long-term depression (LTD) and long-term potentiation (LTP) (Higley and Sabatini, 2008). This regulation of LTP and LTD is dependent on the frequency and the timing of Ca^{2+} influx (Bear, 1995).

1.7: The Inner Plexiform Layer: Neurotransmitters and Localisation

Synaptic transmission within the mammalian retina encodes pre-synaptic voltages and biochemical changes into a coordinated neurotransmitter release which is decoded post-synaptically into a filtered neuronal message. This role is fulfilled by several major retinal neurotransmitters acting on a sub-population of cell. These neurotransmitters are, most notably, glutamate, GABA (γ -aminobutyric acid), glycine, dopamine and acetylcholine.

At the level of the outer plexiform layer two major glutamatergic signalling pathways have been observed; metabotropic glutamatergic signalling between photoreceptors and ON bipolar cells and ionotropic glutamatergic signalling between photoreceptors and horizontal cell and OFF bipolar cells. Glutamatergic signalling in the outer plexiform layer occurs as photoreceptors hyperpolarise, decreasing the synaptic glutamate levels and depolarizing bipolar cells. Depolarised bipolar cells pass this neural message onto retinal ganglion cells through ionotropic glutamatergic signalling where the encoded neural message continues towards the brain's visual centres.

While this vertical channel of glutamatergic signalling is taking place amacrine cells act to oppose this neural firing through lateral, fast inhibition onto bipolar cells, retinal ganglion cells and other amacrine cells. Amacrine cells perform this function through ionotropic and metabotropic GABA and glycine release. In ionotropic inhibitory signalling GABA and / or glycine release from amacrine cells bind to ionotropic receptors opening Cl^- channels. This hyperpolarises the target cell and leads to inhibition. In metabotropic inhibitory signalling GABA release from amacrine cells bind to metabotropic GABA receptors decreasing the voltage sensitivity of Ca^{2+} channels which depresses glutamate release. Amacrine cells can also excite each other through acetylcholine signalling, dopamine is also expressed in

amacrine cells acting as a synaptic modulator (*Figure VI*) (Pourcho, 1982; Davanger, Ottersen and Stormmathisen, 1991; Crooks and Kolb, 1992; Pourcho, 1996; Marc, 2008).

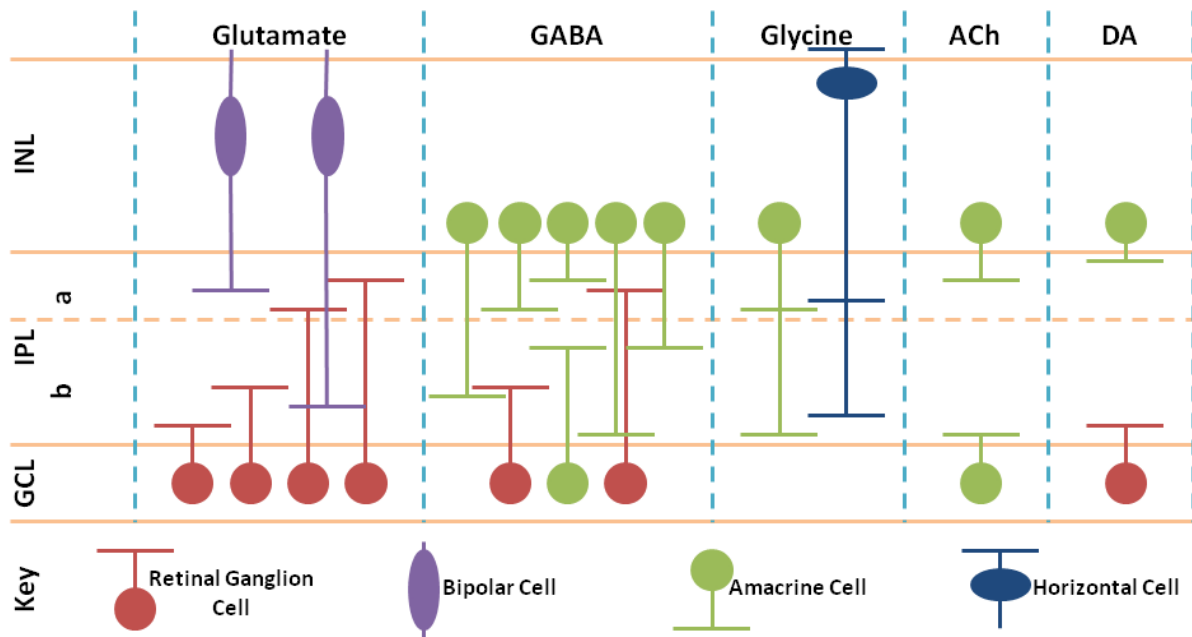


Figure VI: Neurotransmitters in the retina

Schematic showing the various neurotransmitters involved in synaptic transfer within the inner plexiform layer. The two most common neurotransmitters, glutamate and GABA, are present across the whole inner plexiform layer, less common neurotransmitters, glycine, acetylcholine and dopamine, are present only at synapses between specific cell classes.

1.8: Synapses: Structure, Function and Importance

Chemical synapses (from the Greek; *syn* – together, *haptein* – to clasp) are the functional connections between neurons be that axon – axon (axoaxonal), axon – dendrite (axodendritic) or dendrite – dendrite (dendrodendritic). Chemical synapses are the most common synapse in the mammalian nervous system and are asymmetrical in structure (*i.e.* they have a pre- and a post- synaptic site). Take, for example, a dendrodendritic synapse; at the presynaptic site, the presynaptic bouton, neurotransmitters are encased in synaptic vesicles (made from lipid bilayers) which dock at the active zone to form the readily releasable pool of synaptic vesicles. When the membrane potential is reduced by graded fluctuations from an action potential calcium channels open and Ca^{2+} diffuses into the dendrite. This triggers synaptic vesicle fusion to the plasma membrane at the pre-synaptic site releasing the stored neurotransmitter into the synaptic cleft (the area between the pre- and post- synaptic sites). On the opposite side of the cleft, on the postsynaptic membrane, are specialised neurotransmitter receptors. The released neurotransmitter binds to the complimentary receptor causing it to be activated allowing ions to enter or exit the neuron resulting in a change in voltage leading to either an excitatory or inhibitory response which subsequently becomes an EPSP (excitatory post-synaptic potential) or IPSP (inhibitory post-synaptic potential). At the post-synaptic site the bound neurotransmitter molecule must be removed in order for an EPSP or IPSP to occur either through reuptake from the pre-synaptic site for reuse (recycling) or metabolically broken down. Depending on the neurotransmitter synaptic transfer maybe rapid or protracted. Rapid synaptic transfer occurs when specific neurotransmitters (for example GABA) bind to ionotropic receptors forming active ion channels in the membrane. Slower synaptic transfer occurs in the case of

slowly acting neurotransmitters (for example glutamate) which bind to metabotropic receptors associated with G-proteins (G-protein coupled receptors). Metabotropic receptors are also involved with channel opening, but, unlike ionotropic receptors, do not form the ion pore themselves. Instead this involves a range of intracellular second messaging systems.

One important factor governing neuronal connectivity is the ability for synaptic transmission to be modulated (either depression or potentiation) by previous synaptic activity or through the number of receptors located on the synapse, *i.e.* synaptic plasticity. Synaptic plasticity can occur in the short-term or long-term. Short-term synaptic plasticity happens at the level of the microsecond to the second and exists to strengthen or weaken existing synaptic sites. Synaptic enhancement occurs after synaptically active periods resulting in an increased chance that the synapse will release neurotransmitters by increasing the vesicle pool or increasing the amount of neurotransmitter in the synaptic vesicles. Long-term synaptic plasticity (long-term potentiation; LTP) is an increase in synaptic response following a continued burst of electrical stimulus (a tetanus) and is important, among other reasons, for memory formation in the hippocampus (Malenka, 1995).

1.9: Dominant Optic Atrophy

Mutations in *OPA1* lead to dominant optic atrophy, (Alexander et al., 2000; Delettre et al., 2002) the most common optic neuropathy, with an estimated prevalence of 1:12,000 (Carelli, Ross-Cisneros and Sadun, 2002) rising to 1:10,000 in certain populations (Danish; (Kjer, Jensen and Klinken, 1983)) (Delettre et al., 2002). DOA typically presents in the first decade of life as bilateral visual loss with pallor of the optic disc, centrocaecal visual field scotoma and tritanopia (Votruba, Moore and Bhattacharya, 1998; Delettre et al., 2002). Visual loss may be slowly progressive. There is considerable intra- and inter-familial variability in severity of visual loss ranging from legally blind to asymptomatic carriers. Some pedigrees have associated clinical features such as ptosis, myopathy and progressive external ophthalmoplegia. Histological assessment from donor eyes shows thinning of the retinal ganglion cell layer suggesting degeneration of retinal ganglion cells. Demyelination has been observed in the optic nerve, chiasm and tract (Kjer et al., 1983; Milea et al., 2010). The shape of the optic nerve has been reported to be characteristic (Fournier et al., 2001; Votruba et al., 2003) and the size of the optic nerve head is reduced (Barboni et al., 2010).

Over 200 different *OPA1* mutations have been reported to date (Ferré et al., 2005; Olichon et al., 2006) (*Figure VII*). Isolated mutations in the *OPA1* gene have also been shown to cause a 'DOA plus syndrome', in which optic atrophy is accompanied by sensorineural deafness, ataxia, axonal sensory-motor polyneuropathy, chronic progressive external ophthalmoplegia and mitochondrial myopathy with cytochrome c oxidase negative and Ragged Red Fibres (Amati-Bonneau et al., 2009; Huang, Santarelli and Starr, 2009; Milone et al., 2009; Yu-Wai-Man et al., 2010). Remarkably, it has recently emerged that, in rare

cases, *OPA1* mutations can be associated with hearing loss, ptosis and oculomotor deficits in the absence of any detectable optic atrophy (Milone et al., 2009).

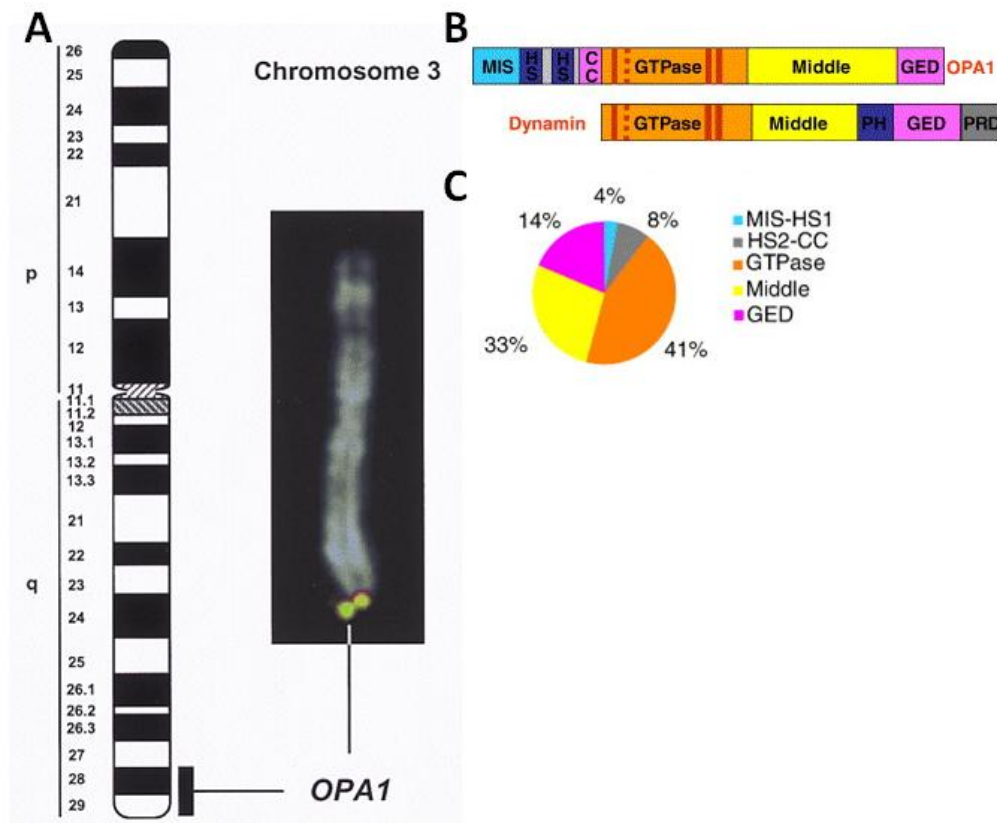


Figure VII: *Opa1* mutations

Diagrammatic and image of an unstained chromosome (A) shows the location of the *Opa1* gene, the structure of which is seen in B in comparison to dynamin. Note the similar features between *Opa1* and dynamin including an almost identical GTPase domain and GTPase effector domain (GED). *Opa1* contains an N-terminal coiled region (CC), two hydrophobic segments (HS) and a mitochondrial import sequence (MIS) whereas dynamin contains a pleckstrin homology domain for lipid binding and a C-terminal regulator proline rich domain (PRD). The majority of *Opa1* mutations occur within the GTPase domain or middle domain (C, mutations by domain). Adapted from (Delettre et al., 2000; Olichon et al., 2006).

1.10: Mouse Models of Dominant Optic Atrophy: A Comparison

1.10.1: Mouse Model of Dominant Optic Atrophy

Ocular and CNS tissue from patients with DOA is scarce and the published histology of DOA has come from a very small number of elderly patients with severe disease (Johnston et al., 1979; Kjer et al., 1983). This limitation has created a pressing need for an animal model of DOA. Such a model must combine the genetic and clinical characteristics of DOA in animals that are suitable for genetic analysis. Mice are widely used as genetic disease models due to the relative ease of genetic manipulation and high homology to the human genome. The murine retina shows relatively good homology to the human retina rendering the mouse suitable for modelling a wide range of human visual diseases with a genetic basis (Smith et al., 2002). However, there is a range of anatomical limitations, and it should be recognised that although the murine eye is a good model for human eye disease it is by no means perfect. Despite this, much has been learnt from mouse models of human genetic eye disease. In the last five years two mouse models of Opa1 DOA (based on OPA1 haploinsufficiency) have been published: the B6;C3-*Opa1*^{Q285STOP} Opa1 mutant mouse (Davies et al., 2007) and the B6;C3-*Opa1*^{329-355del} Opa1 mutant mouse (Alavi et al., 2007). Both display a broad correlation with the human DOA phenotype. (The two models are compared and contrasted in *Table II* and a timeline of disease progression for the B6;C3-*Opa1*^{Q285STOP} mutant mouse is seen in *Figure VIII*).

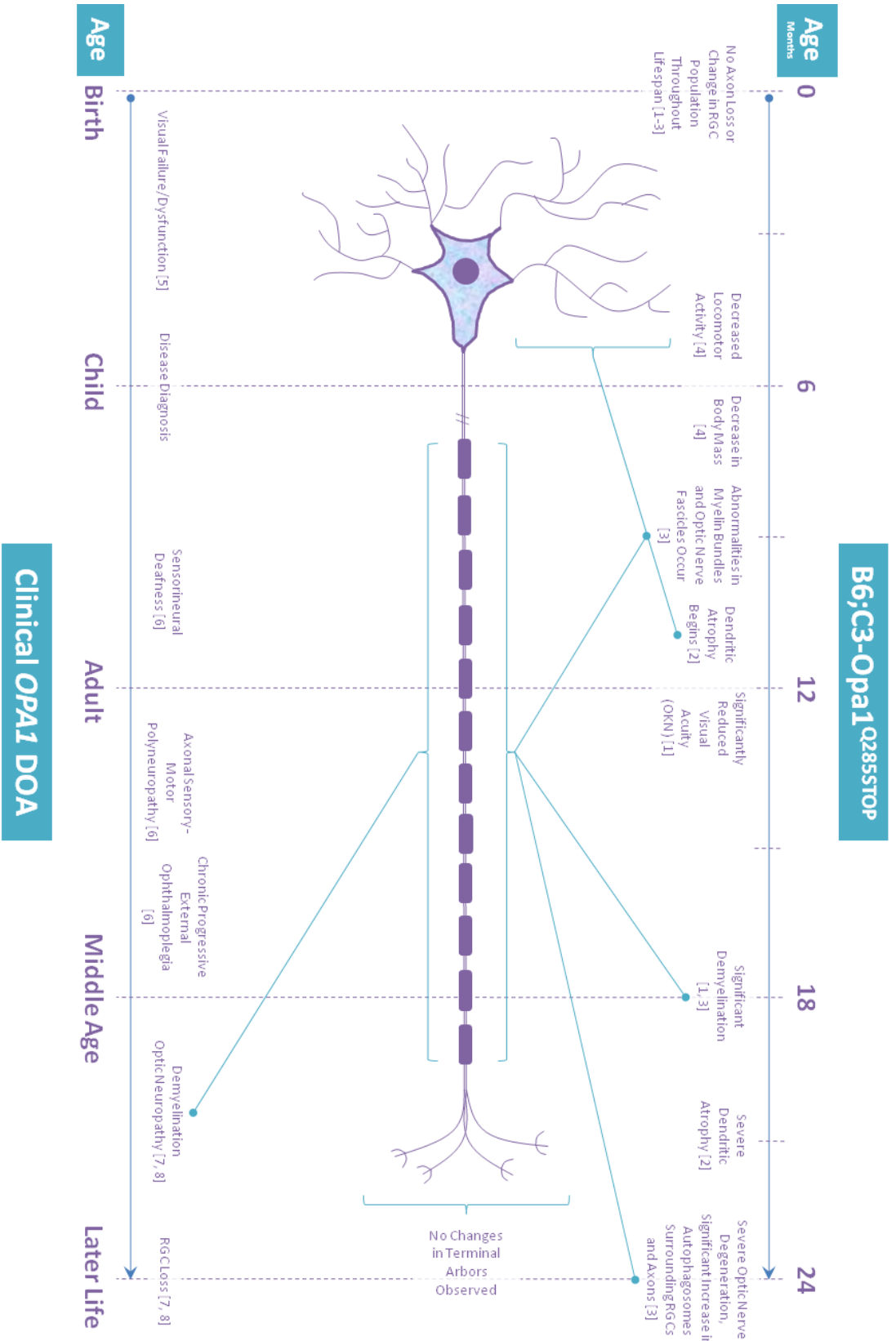


Figure VIII: DOA disease progression timeline (previous page)

Timeline showing the disease progression of DOA in patients (*lower*) and the B6;C3-Opa1^{Q285STOP} mouse model (*upper*). References: [1] (Davies et al., 2007), [2] (Williams, Morgan and Votruba, 2010), [3] (White et al., 2009), [4] (Taylor et al., 2010), [5] (Votruba et al., 1998), [6] (Yu-Wai-Man et al., 2010), [7] (Kjer et al., 1983), [8] (Johnston et al., 1979).

Table II: Comparison of Opa1 mouse models (overleaf)

A comparison of the B6;C3-Opa1^{Q285STOP} and B6;C3-Opa1^{329-355del} Opa1 mouse models. References: (Barnard et al.; Johnston et al., 1979; Kjer et al., 1983; Kjer et al., 1996; Holder et al., 1998; Votruba et al., 1998; Carelli et al., 2002; Ferré et al., 2005; Alavi et al., 2007; Davies et al., 2007; Alavi et al., 2009; Amati-Bonneau et al., 2009; Lenaers et al., 2009; White et al., 2009; Yu-Wai-Man et al., 2009; Heiduschka et al., 2010).

	Clinical Phenotype <i>Opa1</i> DOA	B6;C3-<i>Opa1</i>^{Q285STOP}	B6;C3<i>Opa1</i>^{329-355del}
Mutation	All exons except exon 4, 4b and 5 Substitutions, deletions and insertions Evidence for haploinsufficiency	Exon 8 Nonsense mutation At DNA level: c.1051 C>T At protein level: p.Q285X 50% reduction in protein levels	Intron 10. Splice site mutation At DNA Level: c.1065+5G>A At Protein Level: p.329-355del 50% reduction in protein levels
Mitochondria	Loss of mtDNA in 'plus' mutations Morphology: fragmentation in patient fibroblasts	mtDNA copy number: no significant difference compared to <i>wt</i> counterparts Morphology: powdered appearance Increased mitophagy	mtDNA copy number: no significant difference compared to <i>wt</i> counterparts. Morphology: disorganised cristae
Mouse	N/A	Strain: C ₃ H:C57Bl/6J. Generation: >G4	Strain: C ₃ H:C57Bl/6 Generation: Inter-crosses of F1
Homozygous Mutant	Presumed embryonic lethal	Embryonic lethality <E13.5	Embryonic lethality ca. E8.5
Phenotype			
Age Observed (Months, * = Most Significant)			
Visual Function and Electrophysiology	Acuity range from 6/6 to registered blind Optic atrophy with disc pallor VEP decreased amplitude, +/- increased latency, PERG P50:N95 ratio decreased	Decreased visual function assessed by OKN (6, 12*) Reduction in PhNR (light adapted ERG)(11-13*) Reduction in P2 (Light adapted Flash-VEP)(11-13*)	Decrease in VEP amplitude (20-24*) No significant change in ERG even in aged mice (2, 9, 24)
'Plus' Phenotype	Sensorineural deafness, ataxia, axonal sensory-motor polyneuropathy, chronic progressive external ophthalmoplegia and mitochondrial myopathy with cytochrome c oxidase negative and Ragged Red Fibres	Increased transfer arousal Longer freezing periods Decreased locomotor activity No COX-SDH ragged red fibres (6* for all)	Abnormal clutching reflex. Tremor (22*) Decreased locomotor activity (22*) Lighter than <i>wt</i> counterparts (22*) Less body fat than <i>wt</i> counterparts (21*) No COX-SDH ragged red fibres (21*)
RGC Population and Morphology	RGC loss	No significant difference in population Dendritic atrophy with age limited to sublamina b (10-15, >20*)	Reduction with age starting in peripheral retina confirmed by retrograde labelling (13, 17, 20*)
Optic Nerve	Demyelination Ascending optic neuropathy	Demyelination (24*) Myelin clumping (18, 24*) Watery degeneration (9, 24*) Dark degeneration (9, 24*) No axon loss (6, 9, 24)	Demyelination Disorganisation Swollen and distorted axons Complete loss of large axons Significant loss of small axons (8* for all)

1.10.2: Generation of the B6;C3-*Opa1*^{Q285STOP} and B6;C3-*Opa1*^{329-355del} *Opa1* Mutant Mice

Both the B6;C3-*Opa1*^{Q285STOP} mutant mouse (Davies et al., 2007) and the B6;C3-*Opa1*^{329-355del} mutant mouse (Alavi et al., 2007) were generated after screening an ENU-mutagenized DNA library of mouse DNA (Ingenium, Martinsried, Germany) for mutants with sequence changes in *Opa1*.

The B6;C3-*Opa1*^{Q285STOP} *Opa1* mutant mouse was generated by screening an ENU-mutagenized DNA archive from C3HeB/FeJ males for point mutations in *Opa1* exons 1, 8, 9, 10, 12 and 28, selecting a heterozygous nonsense mutation in exon 8, which codes for a C-T transition at 1051 bp (Q285STOP). This mutation causes protein truncation at the beginning of the dynamin GTPase, close to the location of a number of human disease mutations (c.868C>T (R290W) and c.869G>T (R290Q) (Ferré et al., 2005)). The *Opa1* mutant mouse line (B6;C3-*Opa1*^{Q285STOP}) was produced through *in vitro* fertilization with mutant sperm and C57Bl/6J females to produce a heterozygous, *Opa1*^{+/-}, mouse. The founder (F1) generation was then systematically outcrossed to C57Bl/6J up to at least G4. The *pdeβ* (RD1 mutation), carried by the C3H line, was excluded by systematic genotyping and breeding. Heterozygous *Opa1*^{+/-} mice were intercrossed to generate generation cohorts.

The B6;C3-*Opa1*^{329-355del} *Opa1* mutant mouse was also generated by screening an ENU-mutagenized DNA library of mouse DNA and this time identifying a splice site mutation in murine *Opa1* intron 10: c.1065 + 5G → A. Using a purebred C3HeB/FeJ outcross on C57Bl/6 a mouse model for DOA carrying this splice site mutation in the *Opa1* gene was created. The mutation is close to three reported human mutations (c.1065 +2T > C, c.1065 + 2T > G and c.1065 + 3A > C (Ferré et al., 2005)) and results in skipping of exon 10 in the OPA1 gene causing an in-frame deletion of 27 amino acid residues in the dynamin GTPase domain.

Both models show ~50% reduction in *Opa1* transcript in retinal tissue and a ~50% reduction in *Opa1* protein across a range of tissues, suggesting that haploinsufficiency underlies the pathophysiological mechanism. Both the B6;C3-*Opa1*^{Q285STOP} and B6;C3-*Opa1*^{329-355del} mutant mouse are embryonic lethal when homozygous; at <E13.5 in the B6;C3-*Opa1*^{Q285STOP} mutant mouse (Davies et al., 2007) and ca. E8.5 (between E3.5 and E12) in the B6;C3-*Opa1*^{329-355del} mutant mouse (Alavi et al., 2007).

1.10.3: Visual, Neurological and Neuromuscular Abnormalities

Visual function in the B6;C3-*Opa1*^{Q285STOP} mutant mouse has been assessed with a rotating optokinetic drum (OKN) using high (2°, corresponding to 0.25 cycles/degree) to low (4° and 8°, 0.125 and 0.0625 cycles/degree) resolution gratings. Two studies (Davies et al., 2007; Yu-Wai-Man et al., 2009) have looked at visual function at 6, 12, 13 and 18 month old mice. Significantly decreased mean tracking frequencies from 12 months in *Opa1*^{+/−} mice were detected at high and low spatial frequencies. Furthermore, reduced detection of the low resolution gratings was documented from 18 months onwards in *Opa1*^{+/−} mice. Visual electrophysiological testing (ERG and Flash-VEP) has recently been performed on 11-13 month B6;C3-*Opa1*^{Q285STOP} mice. There were no detectable differences in a- or b-wave in dark and light adapted ERG; however there was a significant reduction in the PhNR in the light adapted ERG. There was also a decrease in the P2 deflection in the dark adapted Flash-VEP (Barnard et al., 2011). The results of the visual electrophysiological testing are consistent with retinal ganglion cell dysfunction.

Given the ubiquitous expression of *Opa1* (Alexander et al., 2000) an *Opa1* deficiency may be expected to adversely affect other organ systems, especially those with high levels of

mitochondria and high metabolic demands. Detailed (non ocular) phenotyping of the B6;C3-*Opa1*^{Q285STOP} mouse model by SHIRPA neurological testing has revealed subtle systemic neurological and neuromuscular abnormalities (Davies et al., 2007), such as decreased locomotor activity.

There are several reported neurological and metabolic abnormalities in the B6;C3-*Opa1*^{329-355del} mutant mouse phenotype (Alavi et al., 2009). SHIRPA testing showed that over a half of the *Opa1* mutant mice had an abnormal clutching reflex with a third (11 males and 2 females) suffering a tremor by 22 months of age. *Opa1* mutant mice also performed significantly worse than controls on the Rotarod; a rotating rod used to test the physical performance of rodents. Although *Opa1* mutant mice maintained a normal food intake they were significantly lighter than controls regardless of sex. Post-mortem examination revealed significantly less body fat than controls though the muscle fibre morphology was unaffected. The extra-ocular phenotype reported in the B6;C3-*Opa1*^{329-355del} mutant mouse has recently been supported by findings on Rotarod in the B6;C3-*Opa1*^{Q285STOP}. This also applies to the tendency for B6;C3-*Opa1*^{Q285STOP} mutants to have lower body weight (Taylor et al., 2010). Of significance is the fact that neither model displayed hearing loss.

Both models have been aged up to 24+ months but no robust quantitative data on life expectancy has been published.

1.10.4: Retinal Ganglion Cell Populations

Both models show normal clinical fundal appearances on dilated ophthalmoscopy. Pattern electroretinogram (PERG) data from patients with DOA show a consistent reduction in the retinal ganglion cell specific P50: N95 ratio (Holder et al., 1998; Holder, 2004). Visually evoked potential (VEP) data in DOA patients show variable reduction in amplitude with occasional delay documented in some patients, consistent with axon dysfunction/damage. Further electrophysiological testing (ERG) (Miyata et al., 2007) shows a reduction in oscillatory potential and PhNR suggestive of retinal ganglion cell loss / dysfunction.

Electroretinography (ERG) in the B6;C3-*Opa1*^{329-355del} mutant mouse at 2 and 9 months was normal (Alavi et al., 2007). Reductions in the ERG could not be detected at 24 months of age when the disease might be regarded as 'end-stage' (Heiduschka et al., 2010). (Reductions were seen in the scotopic a-wave (photoreceptors) and b-wave (rod bipolar cells (Pinto et al., 2007)) and photopic b-wave amplitudes in the *Opa1* mice). However, assessment of the visual pathway by visual evoked potential (VEP) (Heiduschka et al., 2010) showed a significant reduction in the amplitude of scotopic VEPs in *Opa1* mice and a reduction in the amplitude of photopic VEPs, but in neither case was the VEP delayed. This was interpreted as a loss of RGCs, which could be confirmed by retrograde labelling.

Retrograde labelling from both superior colliculi using hydroxystilbamidine and by Haematoxylin and Eosin staining was undertaken to quantify any changes in RGC populations (Alavi et al., 2007). RGC counts were unchanged in 2 and 4 month old *Opa1* mutant mice but showed a slight reduction by 13 months. These changes were first seen at 9 months, appearing first in the peripheral and mid peripheral retina. By 23 months *Opa1* mutant mice showed a marked reduction in RGC layer counts which was confirmed by

retrograde RGC labelling. RGCs were reported to be phagocytosed by retinal microglia (Heiduschka et al., 2010). Histology of the retina confirms that there is no abnormality in the photoreceptor or other retinal layers.

Conversely, histological examination of B6;C3-*Opa1*^{Q285STOP} mutant mouse retinas by Haematoxylin and Eosin, Hoechst 33258 staining and TUNEL staining reveals no significant cell loss in the retinal ganglion cell layer or death across all age groups, even at 24 months of age (Davies et al., 2007). Retinal architecture and morphology is normal on histology with no defect in photoreceptors, however, there was a significant increase in the number of autophagosomes in the RGCs in the retina and surrounding the axons in the 24 month old *Opa1*^{+/−} mice (White et al., 2009) compared to age matched wild type littermate controls. Since *Opa1* is downregulated by ca. 50%, it is hypothesised that there is a reduction in mitochondrial membrane potential forming dysfunctional depolarized mitochondria, which must be eliminated by autophagosomes, or recovered by mitochondria fusion. Since mitochondrial fusion is impaired in this mouse model of DOA, autophagy of mitochondria (mitophagy) is a likely outcome. These data suggest that RGC dysfunction rather than significant RGC loss underlies visual dysfunction in this mouse model.

1.10.5: Optic Nerve Pathology

Although optic nerve pallor is a cardinal feature of human DOA, clinical optic atrophy is hard to categorise in the mouse eye and it has not been a robust phenotypic marker in either model. In the B6;C3-*Opa1*^{Q285STOP} mouse model transmission electron microscopic analyses have indicated little change relative to controls in the optic nerves of 6 month old *Opa1*^{+/-} mice. However, from 9 months to 18 months there were significant abnormalities in the optic nerve fascicles and myelin bundles, which appeared as large abnormal whirls of myelin as well as the appearance of noticeable demyelination (Davies et al., 2007) associated with significant intra-axonal changes (White et al., 2009). From 9 months of age these were evident as early signs of watery and dark axonal degeneration in the *Opa1*^{+/-} mice, and reached statistical significance by 24 months, by which time axons counts were significantly reduced. Since axon loss was evident in both the 24 month *Opa1*^{+/-} mice and age matched wild-type controls, it is likely that the changes reflected age related axon loss and not just the effects of *Opa1* deficiency.

Similar electron microscopic analysis on the B6;C3-*Opa1*^{329-355del} mutant mouse (Alavi et al., 2007) has shown a more severe phenotype to that of the B6;C3-*Opa1*^{Q285STOP} mutant mouse showing a complete loss of large axons and a significant loss of small axons by 8 months of age indicative of RGC degeneration. Optic nerve axons were swollen and distorted with associated demyelination and the presence of membranous whorls. The neurofibrillary and collagen contents were both reduced in the optic nerve.

1.10.6: Clinical Relevance of the B6;C3-*Opa1*^{Q285STOP} and B6;C3-*Opa1*^{329-355del} Mouse Models

The B6;C3-*Opa1*^{Q285STOP} mouse model is a useful resource for the study of DOA disease mechanisms since it shows late onset and subtle changes in RGCs and optic nerve which are associated with slow progression of the disease. The precise mechanisms linking defects in mitochondrial fusion to visual dysfunction remain unknown. The B6;C3-*Opa1*^{Q285STOP} model shows evidence of mitochondrial dysfunction with *Opa1*^{+/-} mouse muscle fibroblast culture displaying punctuated and dispersed mitochondria, giving an abnormal ‘powdered’ appearance (Davies et al., 2007). Apoptosis of RGCs has been proposed as a pathophysiological mechanism in DOA, but cell counts and TUNEL labelling in this mouse model show that visual dysfunction must exist prior to widespread RGC loss. Thus, this model supports dysfunction of RGCs as an early stage in DOA pathophysiology. From the data presented it appears that dendritic pruning of RGCs precedes visual deficit as well as changes in RGC axons and the optic nerve giving a potential timescale for the progression of the disease. The B6;C3-*Opa1*^{Q285STOP} mutant mouse harbours no mtDNA deletions associated with the DOA ‘plus’ phenotype in patients yet there are subtle extra-ocular neurological abnormalities present suggesting that even those OPA1 mutations not associated with mtDNA loss in patients can be associated with neuromuscular defects. This highlights the importance of conducting full neurological assessments in all DOA patients (Aijaz et al., 2004; Amati-Bonneau et al., 2009; Yu-Wai-Man et al., 2009).

The B6;C3-*Opa1*^{329-355del} mutant mouse provides a good model of DOA since it retains the key clinical features documented in patients with similar mutation in OPA1 close to intron 10 c.1065 (c.1065 +2T > C, c.1065 + 2T > G and c.1065 + 3A > C (Pesch et al., 2001; Ferré et al., 2005; Puomila et al., 2005)). The B6;C3-*Opa1*^{329-355del} mouse model of DOA displays no

mtDNA deletions (Alavi et al., 2009). Changes in the optic nerve, RGC populations and abnormal mitochondria (Alavi et al., 2007) are all present and these follow clinical observations in patients with DOA. The Opa1 mutant mouse also has reduced VEP amplitude strongly suggesting RGC loss, a finding supported by retrograde labelling of RGCs.

The evidence for retinal ganglion cell loss as the only mechanism of disease in clinical DOA is partly based on histological data conducted over 30 years ago on a small cohort of two very elderly patients with severe visual loss/‘end stage’ disease (Johnston et al., 1979; Kjer et al., 1983). This histology shows retinal thinning and widespread retinal ganglion cell loss. Recent OCT data (Milea et al., 2010) confirm the retinal nerve fibre layer thinning. Based on this data widespread retinal ganglion cell loss in DOA must be a relevant mechanism, but it may not be the earliest change and not necessarily even the only one (*Table II*).

VEP data from patients, with reduced amplitude, supports retinal ganglion cell loss; however, some patients’ VEP readings show an increased VEP latency (Holder et al., 1998) indicative of retinal ganglion cell dysfunction, in association with cell loss. With over 200 mutations recorded (Ferré et al., 2005) and electrophysiology available for only a proportion of these, it may be possible that retinal ganglion cell dysfunction precedes loss as the driver for visual dysfunction, and this effect may be mutation specific. Unfortunately, due to the constraints of human retinal phenotyping in patients with early disease it may prove difficult to explore this hypothesis fully.

Drawing from murine models of other neurodegenerative diseases, such as Alzheimer’s and Parkinson’s disease, there is evidence of both dendritic atrophy (Grutzendler et al., 2007) and widespread neural cell loss (Beal, 2001) as drivers for the disease and as the major mouse phenotype. Mitochondrial fusion and fission are essential for proper dendritic

morphology and we see rapid dendritic remodelling in terms of dendritic spine morphology when the fusion/fission balance is disturbed (Li et al., 2004). Retinal ganglion cells do not possess dendritic spines but there is evidence for dendritic remodelling over a longer time frame (Marc et al., 2003). It is feasible that this process is happening in a subset of DOA patients as an early disease marker (as in the B6;C3-*Opa1*^{Q285STOP} mouse) and that widespread retinal ganglion cell loss (as in the B6;C3-*Opa1*^{329-355del} mouse) occurs prior to gross visual dysfunction in that same way that there is a 70% neural loss in the substantia nigra in Parkinson's disease patients before the disease is clinically apparent.

1.11: Aims and Hypothesis

As outlined here, Opa1 is shown to be essential for embryonic growth in mice, dendritic architecture in neuronal cell culture and retinal ganglion cell integrity (as shown by its role in dominant optic atrophy both clinically and in animal models) through its roles in, but not exclusive to, mitochondrial fusion, oxidative phosphorylation, apoptosis and mtDNA content control.

Using a range of experimental paradigms this thesis aims to uncover the mechanism that underpins visual deficit in the B6; C3-Opa1^{Q285STOP} mouse model of dominant optic atrophy which occurs without retinal ganglion cell loss, a hallmark feature of the clinic phenotype.

In the absence of observable retinal ganglion cell loss this thesis first aims to establish the morphology and distribution of mitochondria within the retinal ganglion cells themselves using electron microscopy for mitochondrial ultrastructure and biolistic transfection for mitochondrial distribution within the retinal ganglion cells as previous reports have primarily focused on mitochondrial morphology in muscle biopsies and mouse embryonic fibroblasts. This thesis hypothesises abnormal mitochondrial morphology similar to that seen in previous ultrastructure analysis (abnormal cristae structure) that may drive retinal ganglion cell dysfunction.

Previous retinal ganglion cell counts in patient histology come from two elderly patients with end stage disease and cell counts in animal models come from either generic nuclear cell labelling (unspecific for retinal ganglion cells; B6; C3-Opa1^{Q285STOP} model) or retrograde labelling (which may not give a true count of retinal ganglion cells if the optic nerve is damaged; B6; C3-Opa1^{329-355del} model). Using specific cell labels (through

immunohistochemistry) this thesis next aims to establish a full count of retinal ganglion cells populations and their input cells, the bipolar cells. This thesis hypothesises that previous reports in this model are correct and that there is indeed no cell loss across the retina.

In the absence of cell loss in retina this thesis next aims to seek for an anatomical basis for the retinal ganglion dysfunction and the changes seen in the optic nerve by analysing the connections between the retinal ganglion cells and the bipolar cells using DiOlistics to label the soma and dendritic tree of the retinal ganglion cells, biolistics to image synapse distribution along the dendrite, immunohistochemistry, western blotting and qPCR to analyse specific synapse and synaptic receptor distribution and number in the inner plexiform layer as well as electron microscopy to analyse the number and distribution of bipolar cell to retinal ganglion cell synapses. This thesis hypothesises a decrease in retinal ganglion cell dendritic architecture coupled with the associated degeneration or loss of synaptic sites.

The methods used throughout this thesis will now be discussed.

Chapter 2: Materials and Methods

2.1: *Opa1*^{+/-} Mice

Mice were kept in a 12 hour light (10 lux) / 12 hour dark cycle with food and water available *ad libitum*. Breeding and all experimental procedures were undertaken in accordance with the ARVO Statement for the Use of Animals in Ophthalmic and Vision Research and approved by ethical and legal authorities (Home Office). The mutant strain has been described in detail elsewhere (B6; C3-*Opa1*^{Q285STOP}) (Davies et al., 2007). All animals were out-crossed to a C57Bl6/J background (F1) and the experiments were performed on mice bred to generations F4 to F5. Animals were genotyped by *Opa1* allele-specific PCR (Davies et al., 2007). A table detailing exact mouse numbers and ages is seen in *Table III*.

Table III: Numbers and ages of mice used per experiment

Table detailing the exact age and genotype of each mouse used throughout this series of experiments. Upper table, *wt*; lower table, *Opa1+/-*.

<i>wt</i>		
Experiment	Total Number Used	Ages (n x Month)
DiOlistics	22	2 x 4, 2 x 7, 4 x 10, 6 x 15, 1 x 20, 1 x 23, 5 x 24
Biolistics	3	3 x 12
Immunohistochemistry	12	4 x 12, 4 x 14, 4 x 15
γ-Synuclein Labelling	2	2 x 24
Melanopsin Labelling	2	1 x 23, 1 x 4
Western Blots	6	2 x 12, 2 x 14, 2 x 15
Electron Microscopy	6	2 x 12, 2 x 14, 2 x 15
Total	53	

<i>Opa1+/-</i>		
Experiment	Total Number Used	Ages (n x Month)
DiOlistics	28	2 x 4, 2 x 7, 4 x 10, 7 x 15, 2 x 20, 2 x 21, 4 x 23, 5 x 24
Biolistics	3	3 x 12
Immunohistochemistry	12	4 x 12, 4 x 14, 4 x 15
γ-Synuclein Labelling	2	2 x 24
Melanopsin Labelling	4	2 x 23, 2 x 4
Western Blots	6	2 x 12, 2 x 14, 2 x 15
Electron Microscopy	6	2 x 12, 2 x 14, 2 x 15
Total	61	

2.2: Retinal Dissections and Flat Mounts

For dendritic morphology of retinal ganglion cells using DiOlistic labelling adult *Opa1+/-* experimental mice (*Opa1+/-*) and their age and sex matched littermate controls (*wt*) were analysed as 3 age groups; less than 10 months old (<10 month), between 10 and 15 months old (10-15 month) and older than 20 months (>20 month). For synaptic and mitochondrial number and morphology using Biolistics adult *Opa1+/-* and their age and sex match *wt* controls were analysed at 12 months.

Mice were killed by cervical dislocation and the eyes immediately enucleated and placed in chilled (4°C) HBSS (Invitrogen, UK) in 7ml bijoux. The eye was punctured at the limbus and a slit cut in sclera to remove the cornea and sclera anterior to the ora serrata, lens and vitreous. Three cuts were made in the retina using micro-ophthalmic scissors before being flat-mounted ganglion cell layer up on a cell culture insert (Millipore, Billerica, MA) and submerged in custom media containing Neurobasal media, 1% N-2 supplement and 0.5mM glutamine (Invitrogen, UK) (*Figure IX*). Retinas were incubated at 37°C and 4% CO₂ ready for DiOlistic labelling using a gene gun or labelling with Hoechst 33258 stain. The total time between death and labelling was less than 10 minutes.

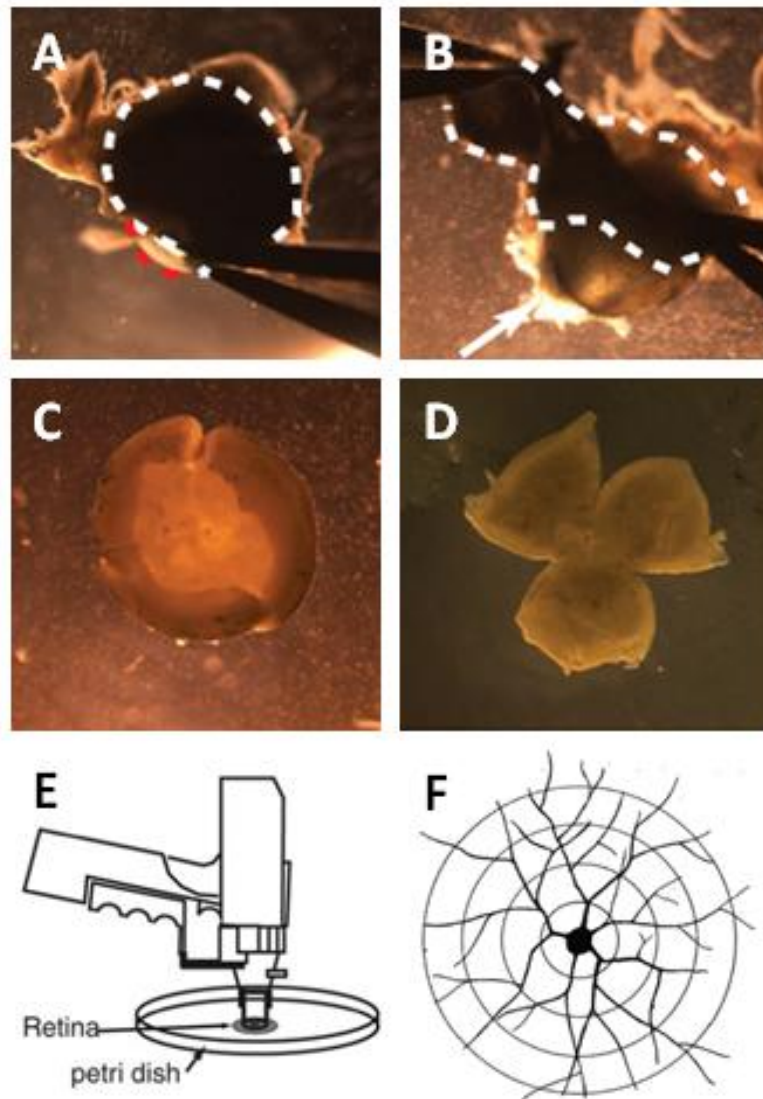


Figure IX: Retinal dissections

In order to perform DiOlistic and Biolistic labelling of retinal ganglion cells, mouse retinas were first dissected and maintained in culture. Once the eye is enucleated a hole is made (A) at the site of the limbus between the cornea (*red line*) and the sclera (*white line*) allowing the cornea to be fully removed (B) by cutting around the limbus. Several slits are then made in the retina (C) in order to flat mount the retina (D) ganglion cell layer up on a cell culture membrane in custom media. Following this, the retina can be DiOlistically or Biolistically labelled (E), imaged and analysed (F). Adapted from (Sholl, 1953; Sawamiphak, Ritter and Acker-Palmer, 2010)

2.3: Hippocampal Sections

The animals were killed by cervical dislocation and brain sectioned sagittally at 250 μ m in ice cold PBS using a Leica VT1000S vibratome (Leica Microsystems, UK). Hippocampal sections were immediately placed into 6 well plates containing HBSS (Invitrogen, UK). The HBSS was then removed in preparation for DiOlistic labelling. Sections were then immersed in Neurobasal media (Invitrogen) and incubated at 37°C and 4% CO₂ for 30 minutes. Total time between death and DiOlistic labelling of brain slices was less than 25 minutes.

2.4: Quantitative RT-PCR

Retina and hippocampus tissue from 12 month *wt* and *Opa1*^{+/-} mice were harvested and placed in RNAlater (Ambion). Total RNA was isolated using Trizol-Reagent and purified using the RNeasy Clean Up kit (Qiagen). 1 μ g of total RNA from each sample was reverse-transcribed using the High Capacity cDNA reverse transcription kit (Applied Biosystems). Quantitative PCR reactions were prepared using TaqMan[®] Universal PCR Master Mix, No AmpErase[®] UNG (Applied Biosystems) and mixed with cDNA, Taqman primers and probe gene specific assay mix. TaqMan gene expression assays (Applied Biosystems) were used for *Mus musculus* *Opa1* (Assay ID: Mm00453879_m1), *Syp* (Mm00436850_m1) and *Psd95* (Mm00492193_m1). qPCR was performed using an ABI Prism 7900HT (Applied Biosystems). Assays were carried out in triplicate with the mean CT values used to calculate the relative gene expression levels after normalizing to 18S RNA levels (endogenous control: VIC/MGB Probe, Primer Limited). Analysis of relative gene expression data was performed using the 2- $\Delta\Delta$ C T method. Statistical analysis was carried out by Tukey Post Test and expressed as ANOVA p-values. This was performed at Central Biological Services, Cardiff University.

2.5: Western Blots

Retina and hippocampus protein samples from *Opa1^{+/-}* and *wt* mice aged 12, 14 and 15 months were boiled for 5min at 95°C in a sample loading buffer. 20µg of protein extracts were separated by 8% SDS-PAGE (sodium dodecyl sulphate-polyacrylamide gel electrophoresis) in Tris/Glycine/SDS running buffer (Bio-Rad, UK).

Precision Plus Protein Standard (Bio-Rad, UK) was loaded in a volume of 10µl/ lane to show the location of proteins at the distinct size in the gel. Electrophoresis was run for 1hr15min at 100V followed by transfer to 0.2µm nitrocellulose membrane (Bio-Rad, UK) for 75 mins at 250mA in a cold Tris/Glycine transfer buffer (Bio-Rad, UK) with 20% methanol (v/v). After the transfer, membranes were blocked with 5% BSA (Bovine Serum Albumin (Sigma)) in PBST for 1hr at room temperature.

The membranes were incubated with either rabbit anti-PSD95 as a marker of NMDA and AMPA receptors (monoclonal; 1:500), rabbit anti-synapsophysin as a marker of synaptic vesicles (polyclonal; 1:500), rabbit anti-GABA A R α S1; the most populous receptor on OFF-centre retinal ganglion cells (polyclonal; 1:500) or rabbit anti-mGluR2&3; the most populous receptors on ON-centre retinal ganglion cells (polyclonal; 1:500) (Abcam, UK) in 1% BSA in PBST; β -actin (monoclonal; 1:400) was used a loading control. The membranes were washed three times in PBST and incubated for another hour with a secondary goat anti-rabbit antibody (1:10000) or goat anti-mouse (1:10000) in 1% BSA in PBST. After three washing in PBST blots were subjected to chemiluminescent detection with Pierce ECL Western Blotting Substrate (Thermo-Fisher Scientific, Rockford, IL) for 5mins and exposed to blue sensitive radiographic film (Kodak, UK).

2.6: Electron Microscopy

Electron microscopy was done in collaboration with Medical Microscopy Sciences, Cardiff University School of Medicine. *wt* and *Opa1^{+/-}* mice were killed by cervical dislocation and their whole retinas fixed in 1% glutaraldehyde in Sorensen's PB. Retinas were post fixed in 1% osmium tetroxide for 2hrs, thoroughly washed, dehydrated through graded ethanol (50, 70, 90 and 100% for 15 minutes each) followed by 3 exchanges of propylene oxide for 10 minutes each. Retinas were then infiltrated for 45 minutes in 50% TAAB embedding resin (TER) (TAAB Laboratories Equipment Ltd. UK) in propylene oxide, followed by 3 x 1 hour in 100% TER before being embedded in 100% TER at 60°C for 48 hours. 80nm thick sections were collected onto 300 mesh copper grids and stained for 30 minutes in saturated uranyl acetate, washed, and stained again using Reynolds lead citrate (Reynolds, 1963) for 15 minutes before being air dried. Samples were examined in a Philips CM12 TEM (FEI U. K. Ltd. UK) at 80kV. Images captured with a Megaview III camera and AnalySIS software (Soft Imaging System GmbH, Munster, Germany).

2.7: Immunohistochemistry

Mice were killed by cervical dislocation and the eyes quickly enucleated, punctured at the limbus and then submerged in 4% PFA at 4°C for 1 hour. Eyes were washed (1% PBS) and placed in a 25% sucrose solution in PBS at 4°C for 24 hours. Eye cups were then frozen in OCT compound (Sakura Finetek, UK) and cut at 20µm using a cryostat at (-23°C). For immunohistochemical (IHC) staining the techniques outlined in the literature (Chetkovich et al., 2002) were followed with a few alterations. Briefly, slide mounted sections were

warmed to room temperature (RT) for 30 minutes and then permeabilised with 0.2% Tween (PBST). Sections were blocked with 5% chick serum in PBS at RT for 1 hour and then incubated with rabbit anti-PSD95 as a marker of NMDA and AMPA receptors (monoclonal; 1:400), rabbit anti-PKC- α as a marker of rod bipolar cells (monoclonal; 1:200), rabbit anti-synaptophysin as a marker of synaptic vesicles (polyclonal; 1:250), rabbit anti-GABA A R α S1; the most populous receptor on OFF-centre retinal ganglion cells (polyclonal; 1:250), rabbit anti-mGluR2&3; the most populous receptors on ON-centre retinal ganglion cells (polyclonal; 1:250)(Abcam, UK) or rabbit anti- γ -synuclein as a specific marker of retinal ganglion cells (monoclonal; 1:200) in 5% chick serum in PBS at 4°C overnight. Sections were washed 3 times for 2 minutes in PBST and incubated with donkey anti-rabbit AF488-conjugated antibody (1:500) and To-Pro-3-Iodide (1:500) (Invitrogen, UK) at RT for 2 hours. They were washed again 3 times for 2 minutes in PBST, mounted in ProLong Gold AntiFade Reagent, coverslipped and sealed with nail polish. For ipRGC labelling, retinal flat-mounts were warmed to RT for 30 minutes and permeabilised with 0.2% Tween (PBST), blocked with 5% chick serum in PBS at RT for 1 hour and then incubated with rabbit anti-melanopsin (monoclonal; 1:2500) in 5% chick serum in PBS at 4°C for 72 h. Following this; sections were washed 3 times for 2 minutes in PBST and incubated with chick anti-rabbit AF488-conjugated antibody (1:500) and To-Pro-3-Iodide (1:500) at 4°C for 72 h. Retinas were washed again 3 times for 2 minutes in PBST, mounted in ProLong Gold AntiFade Reagent, coverslipped and sealed with nail polish.

2.8: Custom Media

Custom media for supporting retinal and hippocampus tissue for both short term (DiOlistics) and long term (Biolistics) are detailed below. Components were added in the order below to a sterile 25ml Falcon tube, warmed to 37°C and used immediately.

Culture media components:

- i. 10ml of neurobasal media
 - i. Used for the long-term maintenance of retina in culture.
- ii. 100µl of 1% N-2 supplement
 - i. Contains: Human transferrin, Insulin recombinant full chain, Progesterone, Putrescine and Selenite.
 - ii. Used for neuronal growth and survival
- iii. 100µl of 0.8mM penicillin/streptomycin complex
 - i. Used as an antibiotic/antimycotic to limit infection and contamination that may damage the culture.
- iv. 50µl of 0.5mM glutamine
 - i. Used to promote viability of retinal ganglion cells in culture. There is a lower recorded survival of retinal ganglion cells long term without the use of glutamine

2.9: DiOlistic Labelling Using the Gene Gun

The setting for the bead delivery and preparation was followed used published methods (Gan et al., 2000; Sun et al., 2002b; Pignatelli and Strettoi, 2004). For preparation of the DiOlistic bullets; 100mg of tungsten particles (1.7µm; Bio-Rad, Hercules, CA) was placed in a thin even layer on a clean, glass slide in a fume cupboard. Following this 80mg of 1,1'-dioleoyl-3,3',3'-tetramethylindocarbocyanine methanesulfonate (DiI; Invitrogen, UK) or 3,3'-dihexadecyloxycarbocyanine perchlorate (DiO; Invitrogen, UK) was suspended in 800µl

of methylene chloride, mixed, and applied over the tungsten particles. The methylene chloride evaporated quickly to leave DiI or DiO coated tungsten particles which were then scraped off using a surgical blade onto clean wax-paper. This powder was then funnelled into a length of tubing (Bio-Rad, Hercules, CA), gently inverted and vortexed before being allowed to settle resulting in a light application of the powder upon the inside of the tubing. Excess powder was funnelled off and the tubing was cut into 1.2cm lengths using a surgical blade for storage in the dark at room temperature ready for use.

Retinas were shot once at 100psi using a Helios gene gun (Bio-Rad, Hercules, CA) from 5cm with a 3.0 μ m pore size, high pore density, cell culture insert (Becton Dickinson, Franklin Lakes, NJ) to block clumps of tungsten particles that were not properly separated. Retinas were then incubated for 25 minutes to facilitate dye diffusion before being placed in 4% paraformaldehyde at room temperature for a further 35 minutes. Retinal preparations were then mounted on a slide with ProLong Gold AntiFade Reagent (Invitrogen, UK) and sealed with nail polish. Additional retinas were mounted with a 1 μ g/ml Hoechst 33258 stain for retinal ganglion cell counts. Retinas were imaged within 48 hours of being labelled.

2.10: Bacterial Cell Cultures and Plasmid Preparation

For Biolistic labelling the preparation of large numbers of plasmid DNA was required. DH5- α cells (*E.Coli*) were chosen as the competent cell line for the transformation reaction. For the transformation reaction 50 μ l of DH5- α competent cells and 1 μ l of stock plasmid DNA (either: PSD95:GFP [with ampicillin resistance], pDsRed2-Mito [with kanamycin resistance], pCMV-E2-Crimson [kanamycin] or pEGFP-N1 [kanamycin]) were thawed on ice for 20 minutes before being gently added together in an Eppendorf tube. This was left on ice for a

further 30 minutes, heat shocked at 42°C for 30 seconds and then returned to ice for a further 30 minutes. Following this the cell and plasmid solution was added to 80µl of S.O.C. medium (Invitrogen) (Super Optimal broth with Catabolite repression) and incubated at 37°C for 60 minutes in an orbital incubator. Fresh agar plates were prepared using agar powder (Invitrogen) and the relevant antibiotic (1:500) in a fume cupboard and the cell suspension was spread on dry agar plates using glass spreaders at a ratio of 60:40 or 80:20. Plates were inverted and incubated at 37°C overnight. After this period individual colonies were selected and isolated carefully using a 10µl pipette tip and placed into 10ml of LB (lysogeny broth; Invitrogen) containing the relevant antibiotic (1:500) before being incubated in an orbital incubator at 37°C overnight. 2ml of this culture was removed and used for miniprep kits.

For isolation of plasmids from the DH5- α *E.Coli* cells a PureLink Quick Plasmid Miniprep Kit was used (Invitrogen). 1ml of culture was centrifuged at 12000g to pellet cells and the supernatant removed before being resuspended in 250µl resuspension buffer, 250µl lysis buffer, inverted 5 times and incubated for 5 minutes. Following this 350µl of precipitation buffer was added, solution centrifuged at 12000g for 10 minutes and loaded into a spin column inside a wash tube. The spin column was centrifuged at 12000g for 1 minute and the flow-through discarded and 700µl of wash buffer with ethanol was added and centrifuged at 12000g for 1 minute. The flow-through was discarded and the process repeated once again before the DNA was eluted into 75µl of either TE buffer or MilliQ water. Plasmid DNA was aliquotted into small Eppendorf tubes and stored at -20°C for up to 1 month before use. Plasmid DNA concentrations were tested using a Picodrop Spectrophotometer.

2.11: Biolistic Transfection of Plasmid DNA

For biolistic transfection retinas from 12 month old mice were used. The preparation and delivery of plasmid DNA biolistically was followed using available published material (O'Brien and Lummis, 2006). For Biolistic bullet preparation 100 μ l of 0.05M Spermidine was added to 20 μ g of gold particles (1 μ g per bullet; 1 μ m in diameter; Bio-Rad, Hercules, CA) plus the addition of plasmid DNA material; either PSD-95:GFP and pCMV-E2-Crimson (Crimson) (Clontech, CA) for synaptic analysis or pDsRed2-Mito (MitoDsRed) (Clontech) and pEGFP-N1 (GFP) (Clontech) (1 μ g DNA per bullet). The mixture was vortexed and 100 μ l of 2M CaCl₂ was added drop-wise before being incubated at room temperature for 15 minutes. 1ml of ethanol was added before being vortexed and then centrifuged at 12,000rpm for 5 seconds. The supernatant was removed and an additional 300 μ l of fresh ethanol was added. A 20cm length of tubing was purged using N₂ and the solution funnelled in using a 50ml syringe. The N₂ flow was reduced and the tubing gently rotated allowing an even dispersion of the plasmid-coated gold particles. Once dry (approx. 20 minutes), N₂ flow was turned off, tubing removed and stored in a sealed, dark container at 4°C. 1.2cm bullets were cut when required and used within 2 weeks of preparation.

For Biolistic labelling flat-mounted retinas were shot at approx. 150 psi using the Helios Gene Gun (Bio-Rad). Transfected retinas were incubated on cell culture inserts in a custom media described above at 37°C / 4% CO₂ for 48 h before being fixed for 30 mins in 4% PFA, mounted on slides using ProLong Gold AntiFade Reagent, coverslipped and sealed using nail polish. Retinas were imaged within 24 hours of being mounted.

2.12: Analysis: Image and Statistical

For analysis of dendritic morphology of DiOlistically labelled retinal ganglion cells image stacks of retinal ganglion cells were collected using a Zeiss LSM 510 confocal microscope (Carl Zeiss Ltd, UK) captured at a 20x objective allowing the whole dendritic field to be shown. Cells were considered to be retinal ganglion cells if an axon running towards the optic disc was present. Cells were pseudo-coloured cyan using a custom LUT (look up table) for better contrast. Specific dendritic morphologies were analysed using ImageJ to measure dendritic field area (measured using the convex polygon tool to join the outer most points of the dendritic tree), an ImageJ plugin, NeuronJ to measure total dendritic length, and a custom Matlab macro to run a Sholl analysis which quantitatively analyses dendritic morphology and architecture (Sholl, 1953; Gutierrez and Davies, 2007) (*Figure X*). All retinal ganglion cells imaged were analysed.

For cell counts and populations retinas were stained with the nuclear Hoechst 33258 stain. Images were taken from the retinal ganglion cell layer at 3 locations of the retina 1mm from the optic disc (directly dorsal to the centre of the optic disc, at 120° to this; ventral-nasally, and at 120° to this again; ventral-temporally, *Figure XI*) using a Leica DM6000 B confocal microscope (Leica Microsystems, UK) with a 20x objective. Cells were manually counted in a 250µm² area using the ImageJ counter plugin. Data were expressed as a percentage change between *wt* and *Opa1*^{+/-}. For bipolar cell counts and retinal ganglion cell counts 20µm thick sections were labelled with either PCK-α (rod bipolar cells) or γ-synuclein (retinal ganglion cells). Z-stack images of were imaged using a Zeiss LSM510 confocal microscope using a 20x objective. Stacks were Z-projected and the total number of PKC-α or γ-synuclein positive cells were counted and expressed as a percentage change between *wt*.

For analysis of mitochondria and synapses using a Biolistic method retinas were mounted and image stacks of retinal ganglion cell dendrites were acquired using a Zeiss LSM510 confocal microscope at 40x. Dendrites and mitochondria were measured using ImageJ's freehand measure tool and 'cell counter' plugin, a modified Sholl analysis of synaptic and mitochondria numbers was performed using SynD and MATLAB (Schmitz et al., 2011).

For analysis of synaptic and neurotransmitter receptor density 20 μm sections were labelled with a variety of antibodies (see above), image stacks were created at 20x using a Zeiss LSM510 confocal microscope and the relative density of the secondary fluorophore was recorded using ImageJ and compared to a negative control (*i.e.* sections labelled as above but without a primary antibody of which the optic density was measured and then subtracted from the experimental data).

For mitochondrial analysis, synaptic counts and synaptic vesicle counts images of a high magnification were taken using electron microscopy. Average mitochondria length and total mitochondrial and cristae areas were measured using the freehand selection tool in ImageJ (*Figure XII*). Synapses were counted using ImageJ's Cell Counter Plugin with a region of interest with fixed area of 85 μm^2 selected from sublaminae a and b of the IPL. For vesicle densities, bipolar cell terminal areas were measured and all synaptic vesicles counted with and results expressed as a density (synaptic vesicles/ μm^2).

For Western blot protein analysis blots were scanned and the optical density was recorded using the cell lane and densitometry tools in ImageJ to form a graph of optical density. The area under the curve minus background was measured and was taken as the true optical density.

For dendritic spine analysis, high resolution, image stacks of hippocampal pyramidal dendrites were taken from the CA1 region of the hippocampus at x40 using a Zeiss LSM510 confocal microscope. Dendrites were subcategorised (apical proximal, apical distal, basal proximal and basal distal) with proximal dendrites considered to be no further than 120µm from the cell soma (Perez-Cruz et al., 2011). The length of the dendritic spines was measured and the number of dendritic spines counted to calculate a density. All image analysis was done using ImageJ.

Statistical analyses were performed using Minitab 14 and Microsoft Excel. Data sets were checked for normality using the Anderson-Darling test for normality (Minitab 14) with a 95% confidence level. If $P > 0.05$ the data was assumed to be normal, if $P \leq 0.05$ the data was assumed to not be normally distributed. Normally distributed data ($P > 0.05$) were analysed using Student's t-test (Excel) with a confidence level of 95%. Data that were not normally distributed ($P \leq 0.05$) were analysed using a non-parametric statistic test, Mann-Whitney-U (Minitab 14), with a confidence level of 95%. To test for variance between groups (*e.g.* the effect of genotype and age) an ANOVA was performed (Excel). If $F < F_{crit}$ and $P \geq 0.05$ the H_0 (null hypothesis) was accepted (*i.e.* no significant difference).

P values are displayed within the text and figure legends along with the name of the corresponding test. Unless stated otherwise, data were displayed as mean values \pm the standard error of the mean (SEM). All analyses of *wt* and *Opa1*^{+/-} data were performed in a masked fashion.

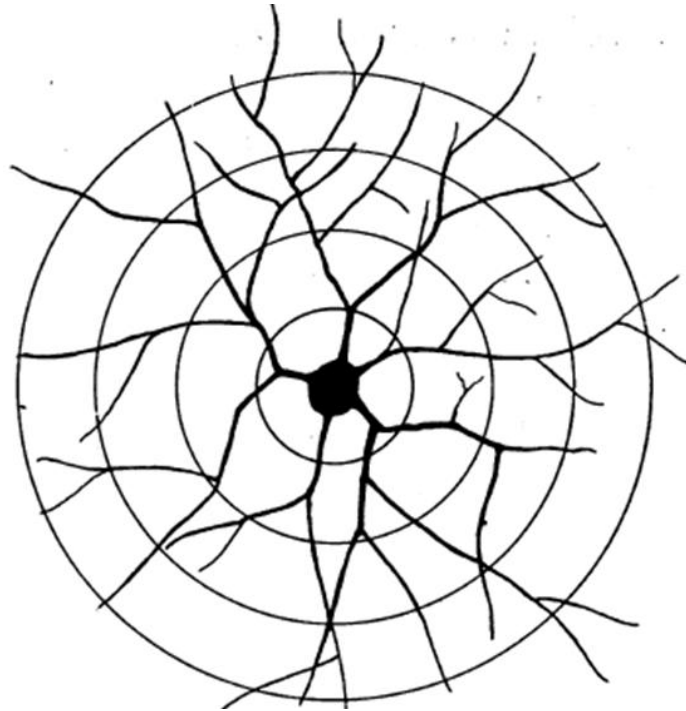


Figure X: *Sholl analysis*

Diagrammatic of a Sholl analysis showing a neuron with concentric circles radiating from the soma superimposed. The number of dendritic intersections is taken from these circles to create a measure of dendritic architecture, the Sholl analysis (Sholl, 1953).

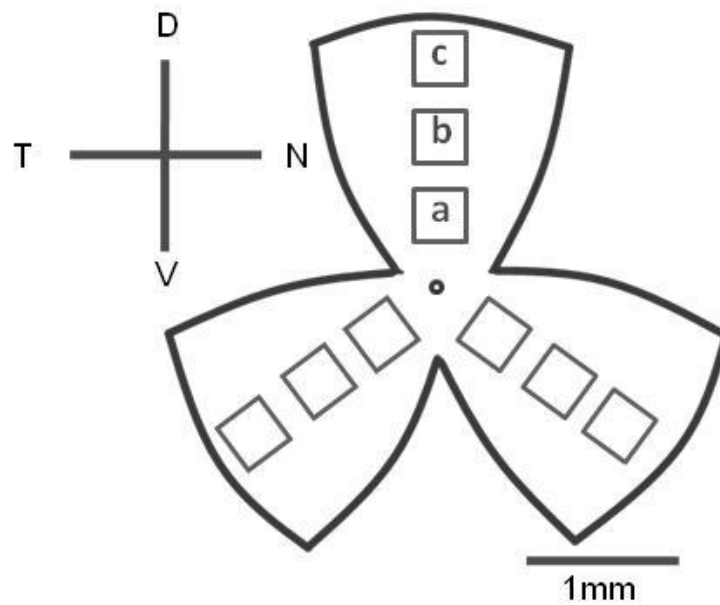


Figure XI: Retinal ganglion cell count locations

Diagrammatic of a flat-mounted retina showing the locations used for retinal ganglion cell and ipRGCs counts.

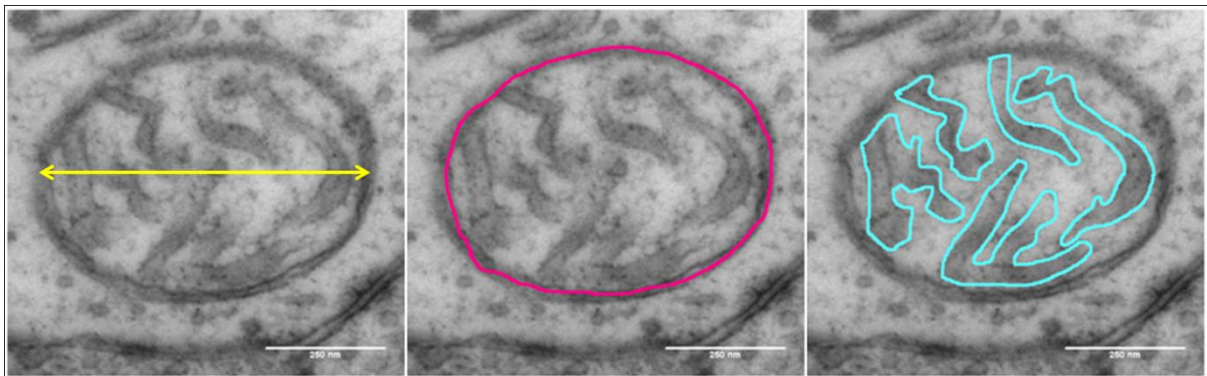


Figure XII: Mitochondria morphometrics

In order to fully analyse mitochondrial morphology 3 major measurements were taken: mitochondrial length (taken as the longest length along the mitochondria, *yellow*), total mitochondrial area (as traced around the mitochondrial outer membrane, *magenta*) and total mitochondrial cristae area (as traced around all individual cristae and summed, *cyan*).

Chapter 3: Aberrant Mitochondrial Morphology in *Opa1*^{+/-} Dendrites

3.1: Introduction

Reduction in *Opa1* protein levels leads to a deficit in mitochondrial fusion and dysfunctional mitochondria have already been shown in other tissues and cell cultures (Li et al., 2004). Therefore the morphology of mitochondria from retinal ganglion cell dendrites in the inner plexiform layer was quantitatively assessed using two methods:

- 1) Electron microscopy to analyse mitochondrial size (length) and matrix to cristae ratio, and;
- 2) Biolistic transfection of plasmid DNA (MitoDsRed: mitochondria) into retinal ganglion cells to allow the specific location of mitochondria in the dendrite to be analysed (*Figure XIII*).

3.2: Mitochondrial Morphology

The retinas of 12 mice (*wt*; $n = 6$, *Opa1*^{+/-}; $n = 6$) aged 12, 14 and 15 months were imaged using electron microscopy to quantitatively assess mitochondrial morphology ($n = 1323$ mitochondria). Mitochondrial average length (AL) was significantly reduced in *Opa1*^{+/-} in all age groups (15 months; AL (nm) \pm SEM; *wt*, 730 ± 20 ; *Opa1*^{+/-}, 602 ± 17 ; $P < 0.0001$), as well as cristae to matrix ratio (C:M) (15 months; C:M (%) \pm SEM; *wt*, 31 ± 1 ; *Opa1*^{+/-}, 15 ± 1 ; $P < 0.0001$). The mitochondrial AL and C:M ratio were similar in sublamina a and sublamina b within age groups. Results show aberrant, fragmented mitochondria compared to *wt* controls.

3.3: Mitochondrial Location and Distribution

ON-centre RGCs of 12 month mice were biolistically labelled with pDsRed2-Mito (MitoDsRed) and pEGFP-N1 (GFP) to label neuronal processes and mitochondria. There was an observed decrease in the dendritic mitochondrial index in *Opa1*^{+/-} mice (*i.e.* less mitochondria per μm of dendrite) (*wt*; 0.775 ± 0.027 , *Opa1*^{+/-}; 0.419 ± 0.016) as well as an increase in mitochondrial number in those dendrites (*i.e.* many small, fragmented mitochondria) (*wt*; 0.113 ± 0.008 , *Opa1*^{+/-}; 0.195 ± 0.007).

3.4: Summary

In summary these data show the importance of mitochondrial fusion as dictated by *Opa1* on the structural integrity of the mitochondrial inner membrane / cristae structure as well as mitochondrial location within the dendrite. It is shown here that retinal ganglion cells in the *Opa1*^{+/-} mouse have aberrant mitochondria with increased levels of mitochondrial fission leading to small mitochondria with abnormal cristae structures. Additionally; in ON-centre retinal ganglion cells there is a shift in the distribution of mitochondria away from the outmost dendrites and towards the cell soma.

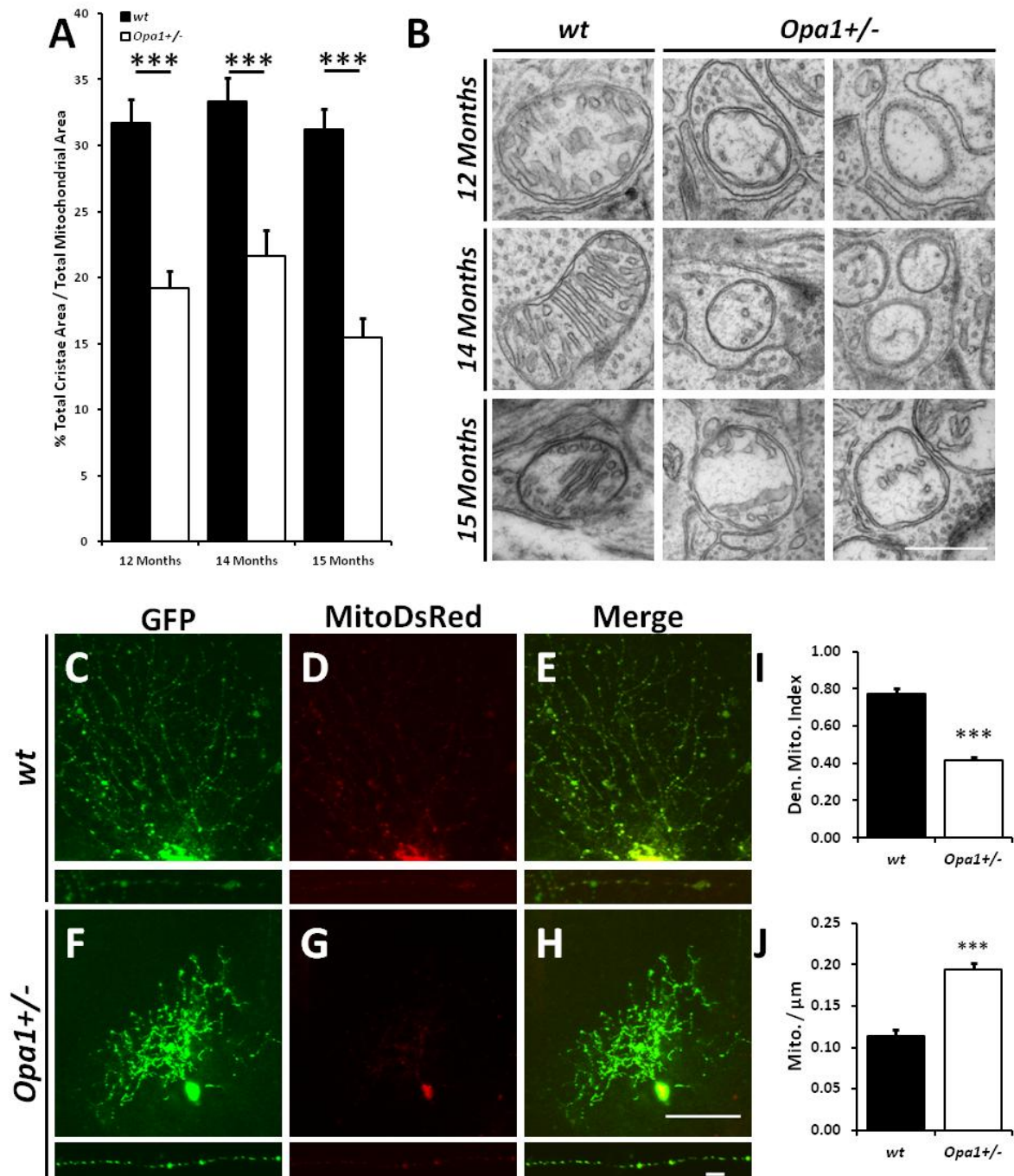


Figure XIII: Aberrant mitochondrial morphology in *Opa1*^{+/-} mice

In order to explore mitochondrial morphology in *wt* and *Opa1*^{+/-} retinal ganglion cell dendrites, mitochondria were imaged using EM or *ex vivo* in retinal whole mounts using Biolistics and their morphometrics (average length, cristae to matrix ratio and mitochondria to dendrite ratio (Den. Mito. Index)) measured using ImageJ.

(A) Total cristae area as a function of mitochondrial area is reduced in *Opa1*^{+/-} mice compared with *wt* controls ($P < 0.0001$). (B) Representative panel of mitochondria from the 3 age groups observed (12, 14, 15 months). (C-E) Samples of biolistically labelled ON-centre RGCs from *wt* (C-E) and *Opa1*^{+/-} mice (F-H). The square panel shows the *en face* view (compressed Z stack- max intensity) the underlying rectangular panels shows a single dendrite typical of the selection used for quantification. Inset plots show the change in mitochondria number (J) (mitochondria / μm dendrite) and a decreased dendritic mitochondrial index (I) (total mitochondrial length / total dendrite length) as a function of genotype.

Scale bar = 500 nm (EM images), 50 μm (C-H; *en face* views panels), 10 μm (C-H; single dendrite views panel). Error bars = standard error of the mean. * = $P < 0.05$, *** = $P < 0.001$ (Mann-Whitney-U).

Chapter 4: Retinal Ganglion Cell Dendropathy in *Opa1*^{+/-} Mice Occurs Without Cell Loss, Is Exacerbated With Age and Localised Exclusively to Sublamina b of the Inner Plexiform Layer

4.1: Introduction

Histological assessments of retinas from patients with dominant optic atrophy show a decrease in the retinal ganglion cell numbers (Kjer et al., 1983) and a thinning of the retinal nerve fibre layer (Milea et al., 2010). Retinal cell populations in *wt* and *Opa1*^{+/-} mice were explored using common nuclear counter stains (Hoechst and To-Pro), γ -synuclein (a retinal ganglion cell specific marker), melanopsin (an intrinsically photosensitive retinal ganglion cell marker (ipRGCs); ipRGCs are γ -synuclein negative) and PKC- α (a rod bipolar cell marker).

Upon inspection of *Opa1*^{+/-} retinas there was no observable deficit in any retinal cell populations, including the retinal ganglion cells, which is a hallmark feature of the human disease. This pointed to retinal ganglion cell dysfunction or atrophy driving visual dysfunction rather than cell loss. To explore this retinal ganglion cells were DiOlistically labelled using carbocyanine dyes which allowed the dendritic trees to be visualised and morphometrically assessed. Changes in retinal ganglion cell dendritic architecture could then be used as a marker of disease. The DiOlistic method was selected to avoid the confounding effects of defective gene expression giving a misleading readout of dendritic structure or the absence of labelled cells through retrograde labelling should there be deficient axonal transport or considerable axonal damage.

4.2: Retinal Cell Populations

Retinal ganglion cell counts were performed on serial 20 μ m thick retinal sections and on whole retinal flat-mounts. For cell counts from retinal flat-mounts counts were taken in a 6 pre-defined areas of retina measuring 300 μ m² (500 μ m from the optic disc; either superior, ventral-nasal or ventral-temporal; or 1000 μ m from the optic disc; either superior, ventral-nasal or ventral-temporal).

Upon examination there was no cell loss across the retina in *Opa1*^{+/-} mice (*Figure XIV*). Changes in retinal ganglion cell dendritic and synaptic architecture and connectivity were explored to elucidate the factors that underlie visual loss in these animals.

The retinal thickness was similar at all ages ($P > 0.05$), and a summary of individual nuclear layer thicknesses is shown in *Table V*. There was no change in nuclear layer thicknesses between *Opa1*^{+/-} and *wt* mice ($P > 0.05$ in all instances).

4.2.1: Retinal Ganglion Cells

Immunohistochemical labelling of γ -synuclein as a retinal ganglion cell specific marker (Surgucheva et al., 2008) indicated preservation of retinal ganglion cell populations ($P > 0.05$) confirming the absence of significant RGC loss in *Opa1*^{+/-} retinas (Davies et al., 2007). To account for ipRGCs flat-mounted retinas were labelled using a melanopsin antibody. ipRGCs populations were unchanged at 24 months (*wt*; 2.15% RGCs = ipRGCs, *Opa1*^{+/-}; 2.21%, $P > 0.05$).

4.2.2: Bipolar Cells

Neuron counts in the inner nuclear layers was based on cell labelling with anti-PKC- α antibodies (rod bipolar cells) There was no change from *wt* bipolar cell count in either the 12 (+3.6%; $P > 0.05$), 14 (-8.3%; $P > 0.05$) or 15 (+2.6%; $P > 0.05$) month age groups, suggesting dysfunction of post- but not pre- synaptic sites.

4.2.3: Photoreceptors

Photoreceptor counts were undertaken using To-Pro-3-Iodide as a nuclear stain in the outer nuclear layer. There was no significant difference in photoreceptor numbers between *wt* and *Opa1*^{+/-} mice (no change; $P > 0.05$).

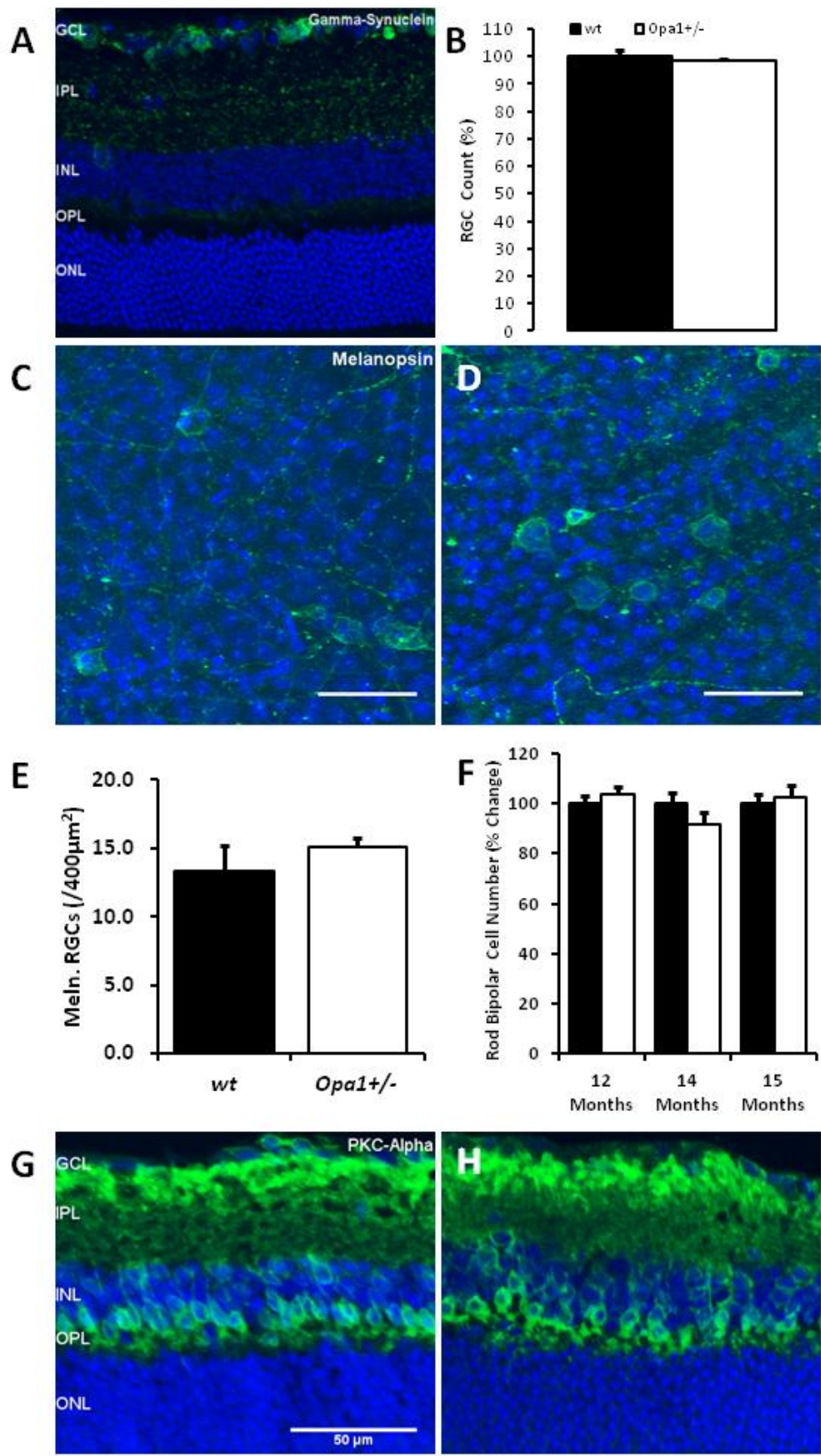


Figure XIV: Retinal cell populations are preserved in *Opa1*^{+/-} mice

Figure XIV: Retinal cell populations are preserved in *Opa1*^{+/-} mice (previous page)

Immunohistochemical labelling against γ -synuclein (green) as a marker of RGCs reveals no loss of RGC populations (B) in the GCL in *Opa1*^{+/-} mice (A) ($P > 0.05$). Additionally, labelling against melanopsin (green) as a marker of ipRGCs on retinal flat mounts (*wt*; (C), *Opa1*^{+/-}; (D)) reveals stable ipRGCs populations (E).

Labelling against PKC-alpha (green) as a marker of bipolar cells reveal no loss of bipolar cell populations (F) and no gross anatomical differences in bipolar cell morphology in *Opa1*^{+/-} mice (H) compare to their *wt* controls (G) ($P > 0.05$). Error bars = standard error of the mean. Scale bars = 50 μ m.

Table IV: Individual nuclear layer thicknesses in *wt* and *Opa1*^{+/-} retina sections

Nuclear layer thickness was calculated from retinal sections of *wt* and *Opa1*^{+/-} mice (*wt*; $n = 12$, *Opa1*^{+/-}; $n = 12$) labelled with To-Pro as a nuclear counter stain. There is no change observed in individual nuclear layer thicknesses between *wt* and *Opa1*^{+/-} mouse retinas in all ages. There is no change in retinal cell populations across the retina (Fig ii).

Key: ONL = outer nuclear layer, INL = inner nuclear layer, GCL = ganglion cell layer, SEM = standard error of the mean, P = Student's t-test P -value.

Layer	Age (months)	<i>wt</i> (μ m \pm SEM)	<i>Opa1</i> ^{+/-} (μ m \pm SEM)	t-test (P)
ONL	12	51.9 \pm 1.6	53.7 \pm 1.9	0.46
INL	12	35.9 \pm 1.8	37.2 \pm 1.9	0.63
GCL	12	9.2 \pm 0.4	10.5 \pm 0.5	0.06
ONL	14	55.7 \pm 1.0	58.6 \pm 1.0	0.21
INL	14	35.9 \pm 1.3	38.1 \pm 1.2	0.21
GCL	14	9.6 \pm 0.3	10.6 \pm 0.4	0.06
ONL	15	52.5 \pm 1.4	51.8 \pm 2.8	0.81
INL	15	28.0 \pm 1.1	31.2 \pm 1.8	0.14
GCL	15	9.8 \pm 0.8	10.1 \pm 0.7	0.74

4.3: Retinal Ganglion Cell Dendropathy

In an absence of cell loss it was hypothesised that low levels of the *Opa1* protein would lead to decreased levels of mitochondrial function. This dysfunction could lead to a low bioavailability of ATP and could lead to retinal ganglion cell atrophy. This atrophy could manifest as dendritic pruning. To explore the possibility of retinal ganglion cell dendritic atrophy flat-mounted adult mice retinas (aged <10 months, 10-15 months or >20 months) were DiOlistically labelled with lipophilic carbocyanine dyes (DiI and DiO) to fully label retinal ganglion cell dendritic processes. Retinal ganglion cells were imaged using an LSM510 confocal microscope and analysed using ImageJ and MATLAB.

In total 145 retinal ganglion cells were identified as ON-centre based on their ramification within the inner plexiform layer and their dendritic field areas, total dendritic lengths and dendritic complexities measured as outlined in Materials and Methods. A panel of ON-centre RGCs across all age groups can be seen in (*Figure XV*). All cells were confirmed to be retinal ganglion cells by the presence of axons running in the retinal nerve fibre layer toward the optic disc.

4.3.1: Dendropathy with Age

These results show a significant decrease in the average total dendritic area of *Opa1*^{+/-} ON-centre retinal ganglion cells in both the 10-15 month group (-24.24%; $C_v=0.68$; $P = 0.054$) (Student's t-test) and the >20 month group (-43.22%; $C_v=0.75$; $P = 0.025$) but not in the <10 month group (-9.24%, $C_v=0.58$, $P = 0.584$).

Similar changes were also seen with measurements of total dendritic length of *Opa1*^{+/-} ON-centre retinal ganglion cells in both the 10-15 month group (-31.66%; $C_v=0.67$; $P = 0.008$) and the >20 month group (-49.55%; $C_v=0.63$; $P = 0.021$) but not the <10 month group (-0.30%; $C_v=0.49$; $P = 0.984$) (Figure XVI). A two-way ANOVA was performed to see if age has an addition affect on dendritic atrophy. For both total dendritic field area and total dendritic length the $F > F_{crit}$ and $P < 0.05$, showing that dendritic atrophy is exacerbated with age.

Dendritic complexities were also analysed using a custom Matlab macro to run a Sholl analysis where dendrites are measured when they intersect graded concentric circles of 10 μ m around the soma (see Gutierrez, 2007). Sholl analyses were run using a ring interval of 10 μ m. Results show a decrease in the dendritic complexities of ON-centre RGCs in both the *Opa1*^{+/-} 10-15 (AUC -21.67%; $P > 0.05$) month group and >20 (AUC -42.12%; $P < 0.05$) month group but not in the <10 month group (AUC -1.29%; $P > 0.05$) (Figure XVII).

To quantify individual dendrite loss across the dendritic field the number of primary, secondary and tertiary dendrites were counted in all retinal ganglion cells. There was a significant decrease in the number of tertiary dendrites in all ages most significant in the >20 month age group ($wt\pm SEM/Opa1^{+/-}\pm SEM$; $16.1\pm 1.9 / 11.3\pm 1.0$) as well as an unchanged dendritic density (>20 month age group; $0.050\pm 0.002 / 0.059\pm 0.008$; $P > 0.05$) signifying a loss of the outer most dendrites in the dendritic field without loss of primary dendrites (Figure XVIII).

4.3.2: Localisation

A further twenty one retinal ganglion cells were identified as OFF-centre based on their ramification within the inner plexiform layer (Xu *et al*, 2007). There was no significant change in the dendritic morphologies of *Opa1*^{+/-} OFF-centre RGCs even in the >20 months group. OFF-centre retinal ganglion cells appear to have an unchanged ($P > 0.05$) dendritic field area and total dendritic length as well as unchanged (AUC; $P > 0.05$) dendritic complexities (Figure XIX, XX).

4.4: Summary

In summary this chapter shows retinal ganglion cell dendritic atrophy which is exacerbated with age and localised to sublamina b of the inner plexiform layer (ON-centre retinal ganglion cells). The dendritic atrophy becomes apparent after 10 months making this finding the earliest observable change in this mouse model. This occurs without retinal ganglion cell loss as made evident by specific labelling using anti- γ -synuclein (specific for retinal ganglion cells) and anti-melanopsin (specific for ipRGCs) and without loss from the retinal ganglion cells input cells, bipolar cells (labelled with anti-PKC- α).

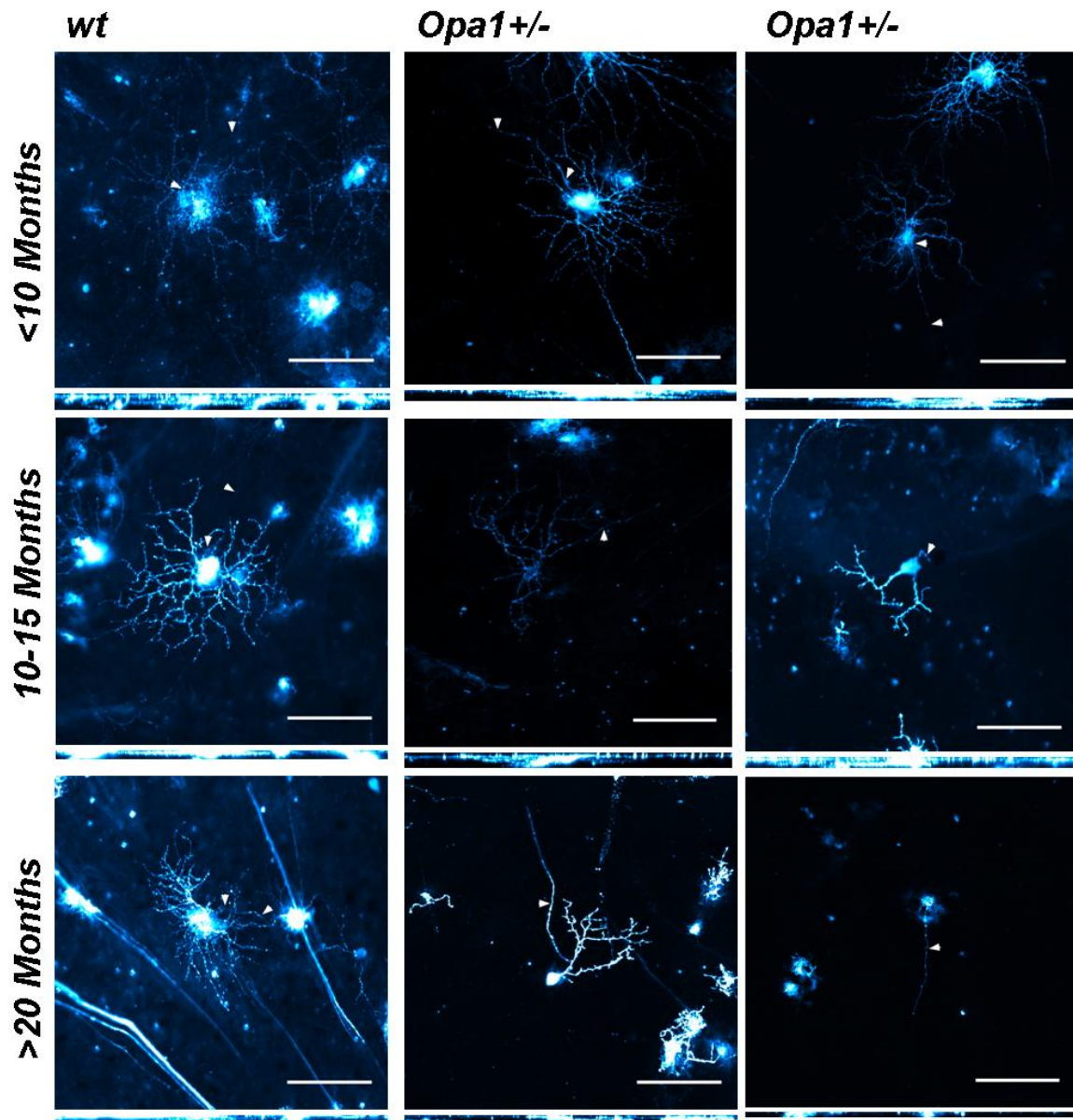


Figure XV: DiOlistically labelled ON-centre retinal ganglion cells

Compressed confocal stacks of DiOlistically labelled wild-type and *Opa1*^{+/-} ON-centre retinal ganglion cells. There is no apparent retinal ganglion cell dendropathy in *Opa1*^{+/-} mice aged <10 months ($n = 4$) compared with their wild-type controls ($n = 4$). There is significant ON-centre retinal ganglion cell dendropathy in both the 10- to 15-month-old *Opa1*^{+/-} mice ($n = 5$) compared with their wild-type controls ($n = 5$) and of the >20-month-old *Opa1*^{+/-} mice ($n = 7$) compared with their wild-type controls ($n = 2$). Bird's-eye views (xy plane) (top) and side-on views (xz plane) (bottom) are shown for cells. Scale bar = 100 μm and is representative of both planes of view; arrow heads = axon.

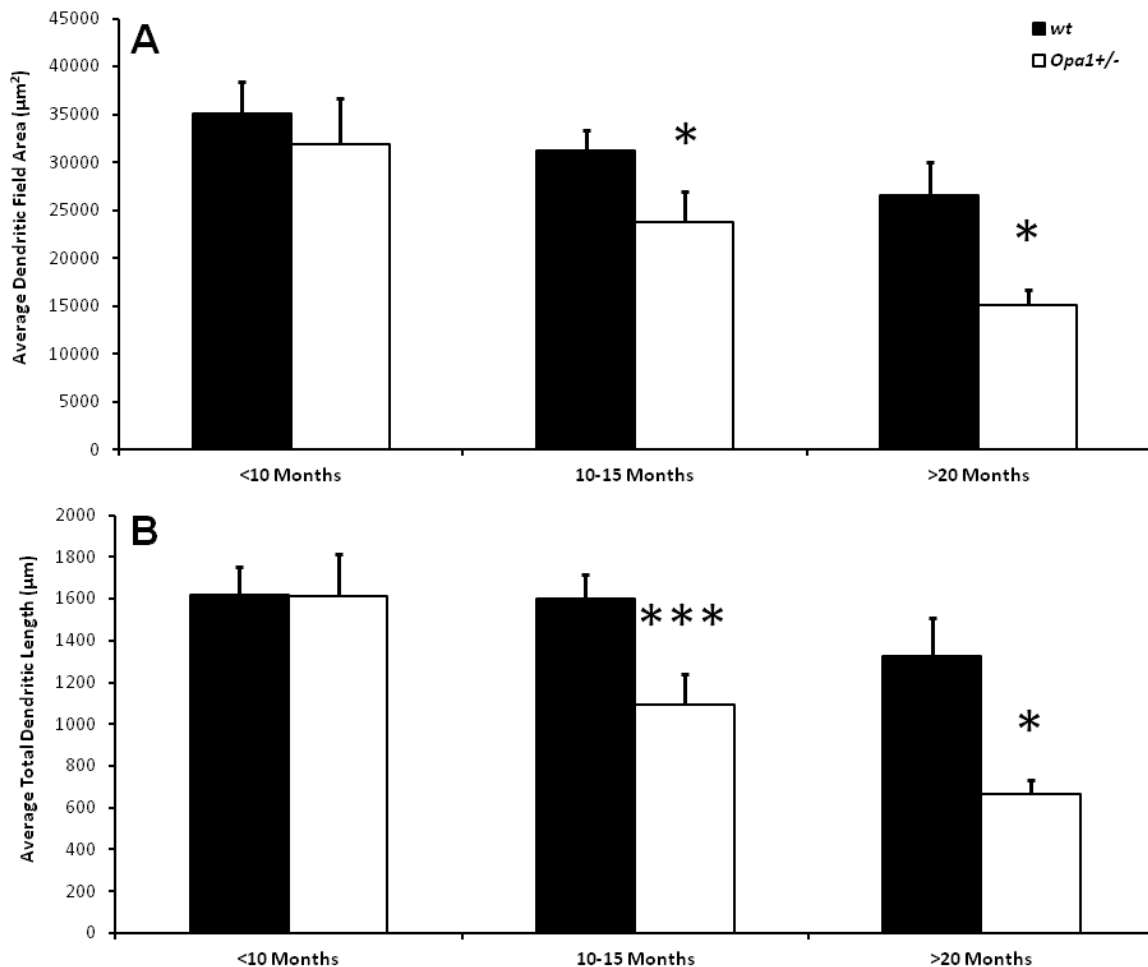


Figure XVI: Dendritic pruning in ON-centre retinal ganglion cells

Opa1 deficiency leads to a reduction in dendritic field area and total dendritic length in on-centre retinal ganglion cells. Average retinal ganglion cell dendritic field area (A) and average total retinal ganglion cell dendritic length (B) in the wild-type and *Opa1*^{+/-} mouse. Results show a significant decrease in both the total dendritic area and average total retinal ganglion cell dendritic length of *Opa1*^{+/-} retinal ganglion cells in both the 10- to 15-month-old group (wild-type $n = 34$, *Opa1*^{+/-} $n = 25$) and the >20-month-old group (wild-type $n = 5$, *Opa1*^{+/-} $n = 44$) but not the <10-month-old group (wild-type $n = 21$, *Opa1*^{+/-} $n = 16$). This decrease is exacerbated in the older (>20-month-old) group. * $P < 0.05$; *** $P < 0.01$; error bars indicate SEM.

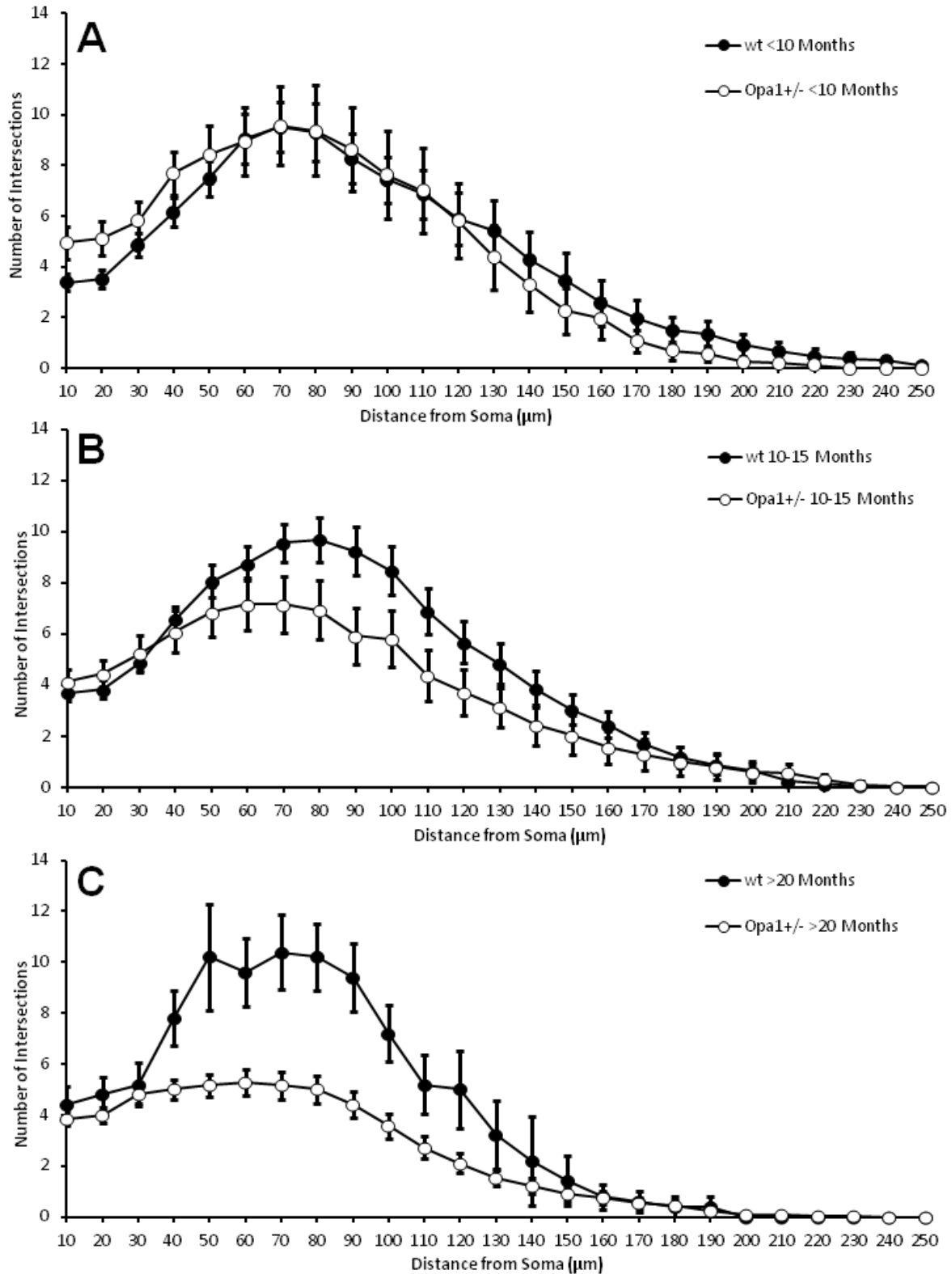


Figure XVII: Sholl analysis of ON-centre retinal ganglion cells

Retinal ganglion cell Sholl analyses of wild type and *Opa1*^{+/-} mice. Results show no difference in dendritic complexity of ON-centre retinal ganglion cells in the <10-month-old

group (A) (wild-type $n = 21$, *Opa1*^{+/-} $n = 16$) (AUC $P = 0.949$) but a clear difference in the 10- to 15-month-old group (B) (wild-type $n = 34$, *Opa1*^{+/-} $n = 25$) (AUC $P = 0.137$) and a significant difference in the >20-month-old group (C) (wild-type $n = 5$, *Opa1*^{+/-} $n = 44$) (AUC $P = 0.047$). Error bars indicate SEM; *wt* =wild-type.

Figure XVIII: Reduction in ON-centre secondary and tertiary dendrites (overleaf)

Opa1 deficiency leads to ON-centre specific dendritic degeneration. Quantification of primary, secondary and tertiary dendrites in these retinal ganglion cells shows a decrease in secondary and tertiary dendrites but not in primary dendrites. * $P < 0.05$.

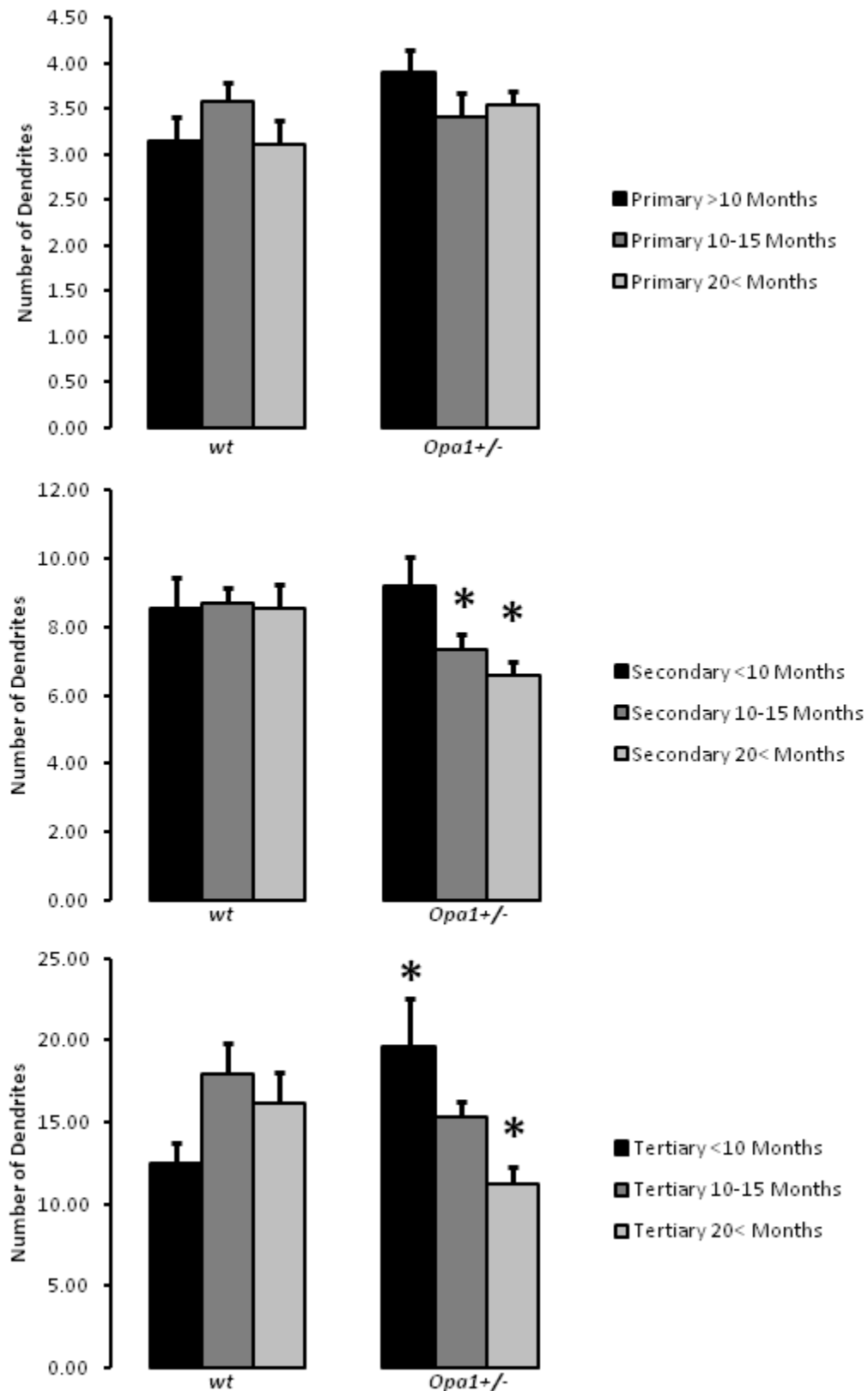


Figure XVIII: Reduction in ON-centre secondary and tertiary dendrites

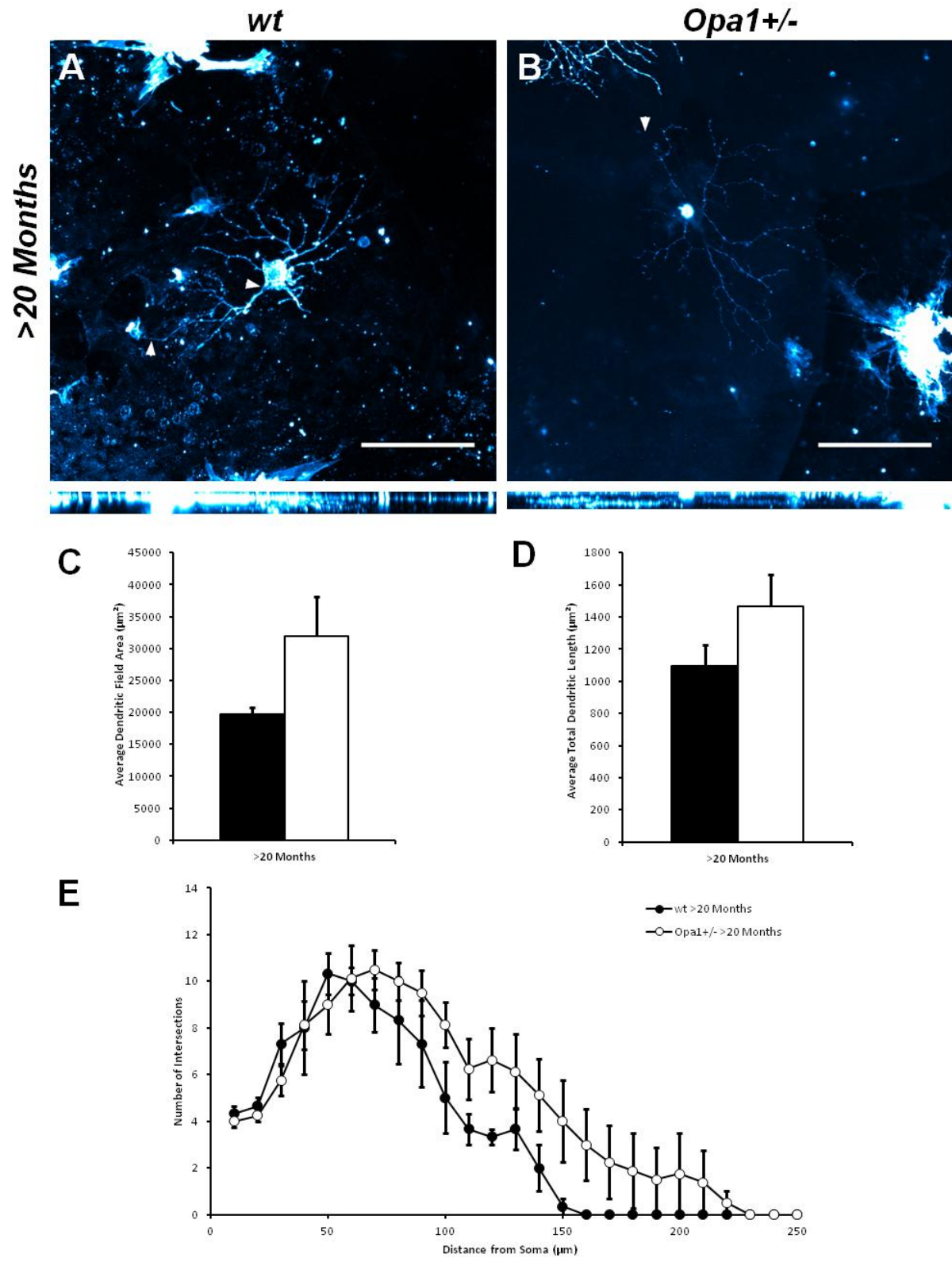


Figure XIX: OFF-centre retinal ganglion cells are unaffected by *Opa1* deficiency

Figure XIX: OFF-centre retinal ganglion cells are unaffected by *Opa1* deficiency (previous page)

Opa1 deficiency has no effect on the dendritic morphology of OFF-centre retinal ganglion cells. Where severe dendritic atrophy is present in the >20-month-old *Opa1*^{+/-} ON-centre retinal ganglion cells, results show no significant change in the dendritic morphologies of *Opa1*^{+/-} OFF-centre retinal ganglion cells ($n = 8$) compared with wild type ($n = 3$). Compressed confocal stacks of DiOlistically labelled wild-type (A) and *Opa1*^{+/-} (B) OFF-centre retinal ganglion cells. Bird's-eye views (xy plane) (top) and side-on views (xz plane) (bottom) are shown for cells. Scale bar = 100 μm and is representative of both planes of view; arrow heads = axon. Average retinal ganglion cell dendritic field area (C) and average total retinal ganglion cell dendritic length (D) in the wild-type and *Opa1*^{+/-} mouse. Results show no significant change between wild-type and *Opa1*^{+/-} mice. $P > 0.05$ for all bars; Student's t-test. (E) Retinal ganglion cell Sholl analyses of wild-type and *Opa1*^{+/-} mice. Although there is a great difference in dendritic complexity of ON-centre retinal ganglion cells in the *Opa1*^{+/-} >20-month-old group, results show no difference in dendritic complexity of OFF-centre retinal ganglion cells in the >20-month-old group. Error bars indicate SEM.

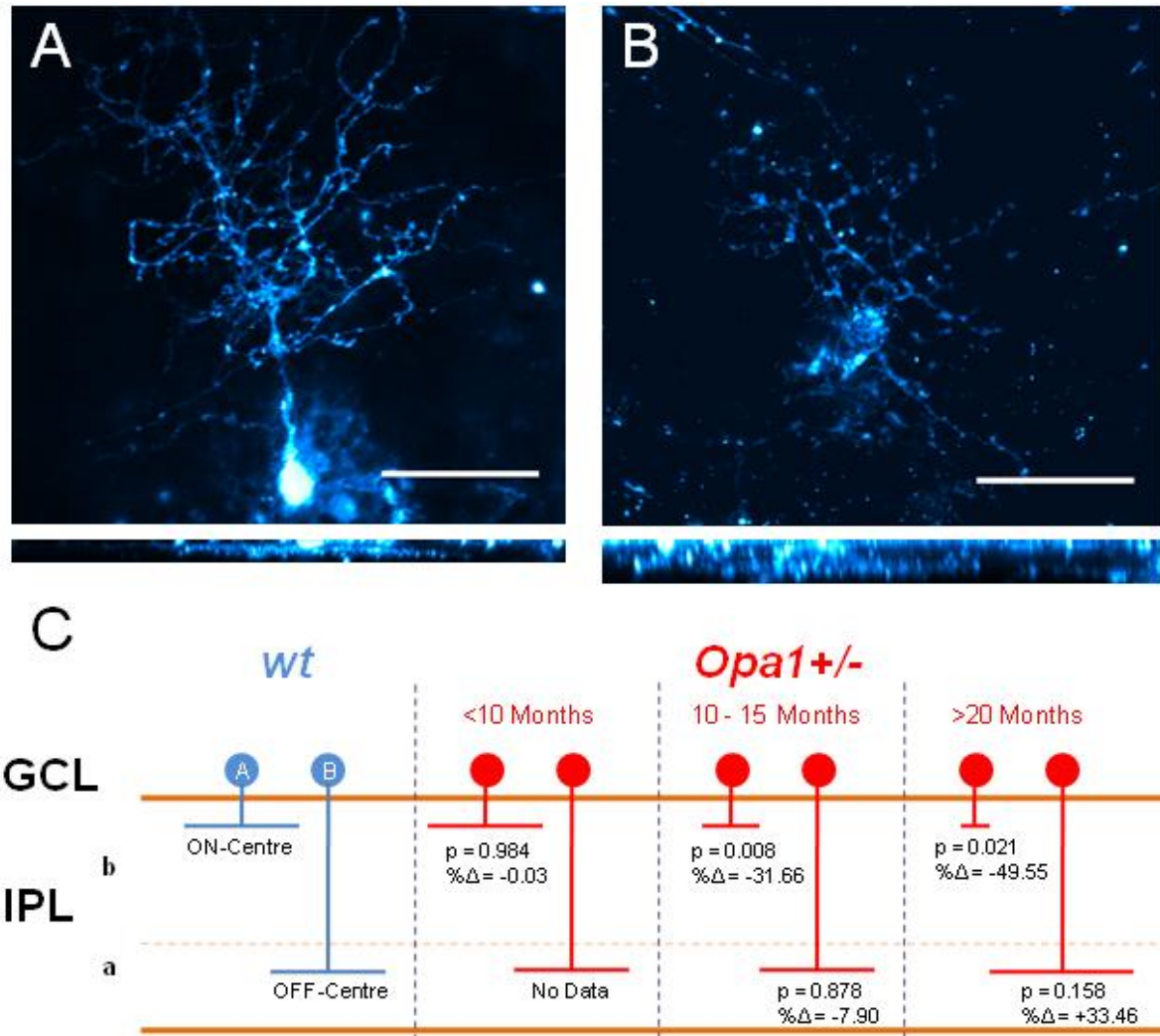


Figure XX: Selective pruning of ON-centre retinal ganglion cells

Opa1 deficiency leads to selective dendritic pruning of ON-centre retinal ganglion cells. Examples of ON- (A) and OFF- (B) centre retinal ganglion cells from an adult (10-month-old) wild-type mouse noting the different levels of dendritic ramification in the inner plexiform layer (Xu et al., 2007) with the dendrites of ON-centre retinal ganglion cells ramifying in sublamina b (close to the level of the cell body) and the dendrites of OFF-centre retinal ganglion cells ramifying in sublamina a (close to the inner nuclear layer). Scale bar = 25 μ m. Total dendritic length is dramatically reduced in the ON-centre retinal ganglion cells of 10- to 15-month-old and >20-month-old mice (C) while remaining statistically unchanged in OFF-centre retinal ganglion cells. *P* = Student's t-test, % Δ = percentage change from wild-type. GCL = ganglion cell layer; IPL = inner plexiform layer.

Chapter 5: *Opa1*^{+/-} Deficiency Leads to the Selective Loss of Glutamatergic Synapses on ON-Centre Retinal Ganglion Cells

5.1: Introduction

Dendritic atrophy was solely localised to sublamina b of the inner plexiform layer *i.e.* it was only observed in ON-centre retinal ganglion cells. To explore this selective neuronal vulnerability sections of the same retinas were labelled with antibodies against mGluR2+3 (the most common glutamate receptor on ON-Centre retinal ganglion cell dendrites) and against GABA A R α S1 (the most common GABA A-ergic receptor on OFF-Centre retinal ganglion cell dendrites), for which the relative luminance of the secondary fluorophores were quantified. In addition, the density of dark, post-synaptic sites specifically on retinal ganglion cell dendrites was quantitatively assessed using electron microscopy.

5.2: Neurotransmitters

mGluR2+3 labelling was reduced at all ages but this was only significant from 14 months (12 month; -5.96%; $P = 0.7535$. 14 month; -22.96%; $P = 0.0347$. 15 month; -23.76%; $P = 0.0113$) consistent with preferential loss of ON-centre retinal ganglion cell dendrites. In contrast, GABA A-ergic relative luminance increased in all age groups (12 month; +21.96%; $P = 0.4350$. 14 month; +37.12%; $P = 0.0457$. 15 month; +58.81%; $P < 0.0001$) (*Figure XXI*). These results are mirrored in the Western blot analysis (*Figure XXV*).

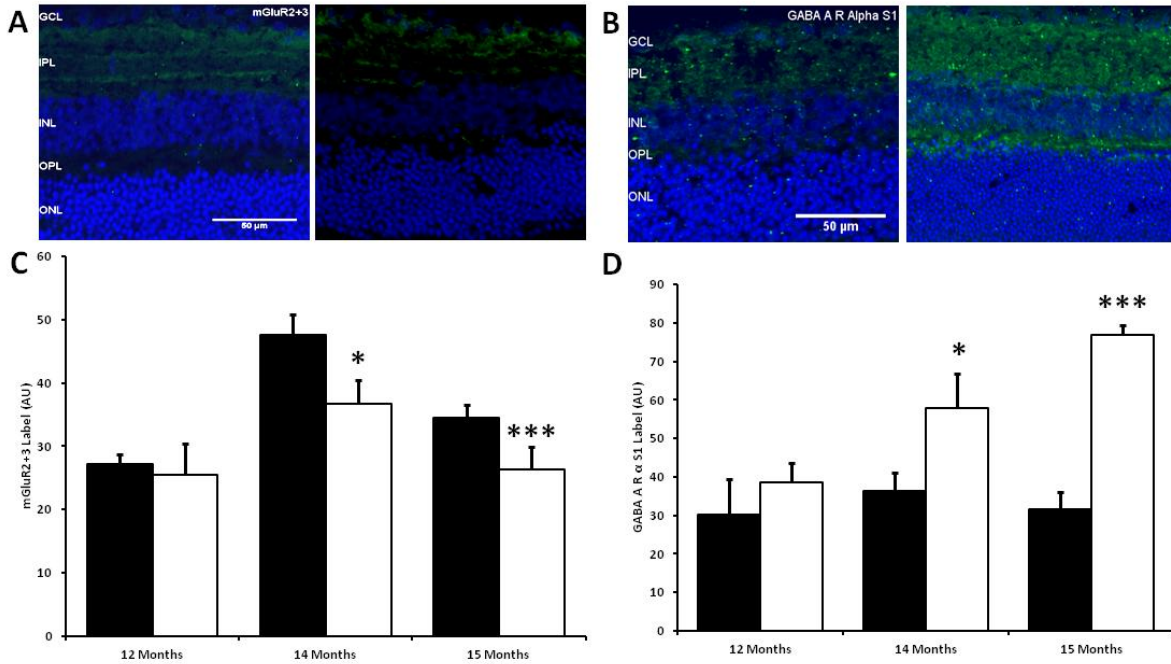


Figure XXI: Glutamatergic synapses are specifically eliminated in *Opa1*^{+/-} mice

Retinal sections were immunohistochemically stained for mGluR2+3 (A, *wt*; left, *Opa1*^{+/-}, right) and GABA A R α S1 (B, *wt*; left, *Opa1*^{+/-}, right). There was a general decrease from 14 months in mGluR2+3 expression in *Opa1*^{+/-} retinas (C) consistent with the changes seen in synaptic density within sublamina b of the inner plexiform layer and ON-centre retinal ganglion cell dendritic degeneration. There was a general increase in GABA A R α S1 expression in all ages which reached significant at 14 months (D).

Key: Error bars = standard error of the mean. * = $P < 0.05$, *** = $P < 0.0001$ (Student's t-test). Black bars = *wt*, white bars = *Opa1*^{+/-}

5.3: Synapses

In order to see whether dendritic pruning is a consequence of a loss of synaptic connectivity 20µm thick sections of fixed retinal tissue were labelled with antibodies against PSD-95 to quantify synaptic integrity within the inner plexiform layer in *Opa1*^{+/-} mice. Secondary fluorophore luminance was reduced in *Opa1*^{+/-} mice at 12 (-21.51%; $P = 0.0626$), 14 (-29.090%; $P = 0.0246$) and 15 (-44.22%; $P = 0.0018$) month age groups. Electron microscopy analysis of post-synaptic sites in *Opa1*^{+/-} and *wt* IPL revealed a steady decrease in post-synaptic density with age and was significant for sublamina b (15 months; %Δ sublamina a, -19.1%, $P > 0.05$; %Δ sublamina b, -33.3%, $P < 0.01$) (*Figure XXII*). These observations were supported by Western blot analysis and qPCR analysis (*Figure XXVI*).

To determine the change at a cellular level in the dendritic distribution of synapses and associated mitochondria, retinal ganglion cells of 12 month mice were biolistically labelled with pE2-Crimson (Crimson) and PSD95:GFP (PSD95) to label neuronal processes and post-synaptic sites. Representative labelled ON-centred retinal ganglion cells are shown in *Figure XXIII*. Quantitative analysis indicates reduced synaptic density along the dendrite. The left shift in the Sholl analysis of post-synaptic sites and mitochondria indicate that a synaptic and mitochondrial deficit towards the most distal portion. The area under the Sholl curve (AUC) showed a 79% ($P < 0.001$) reduction for post-synaptic sites and a 88% reduction ($P < 0.01$) for mitochondria.

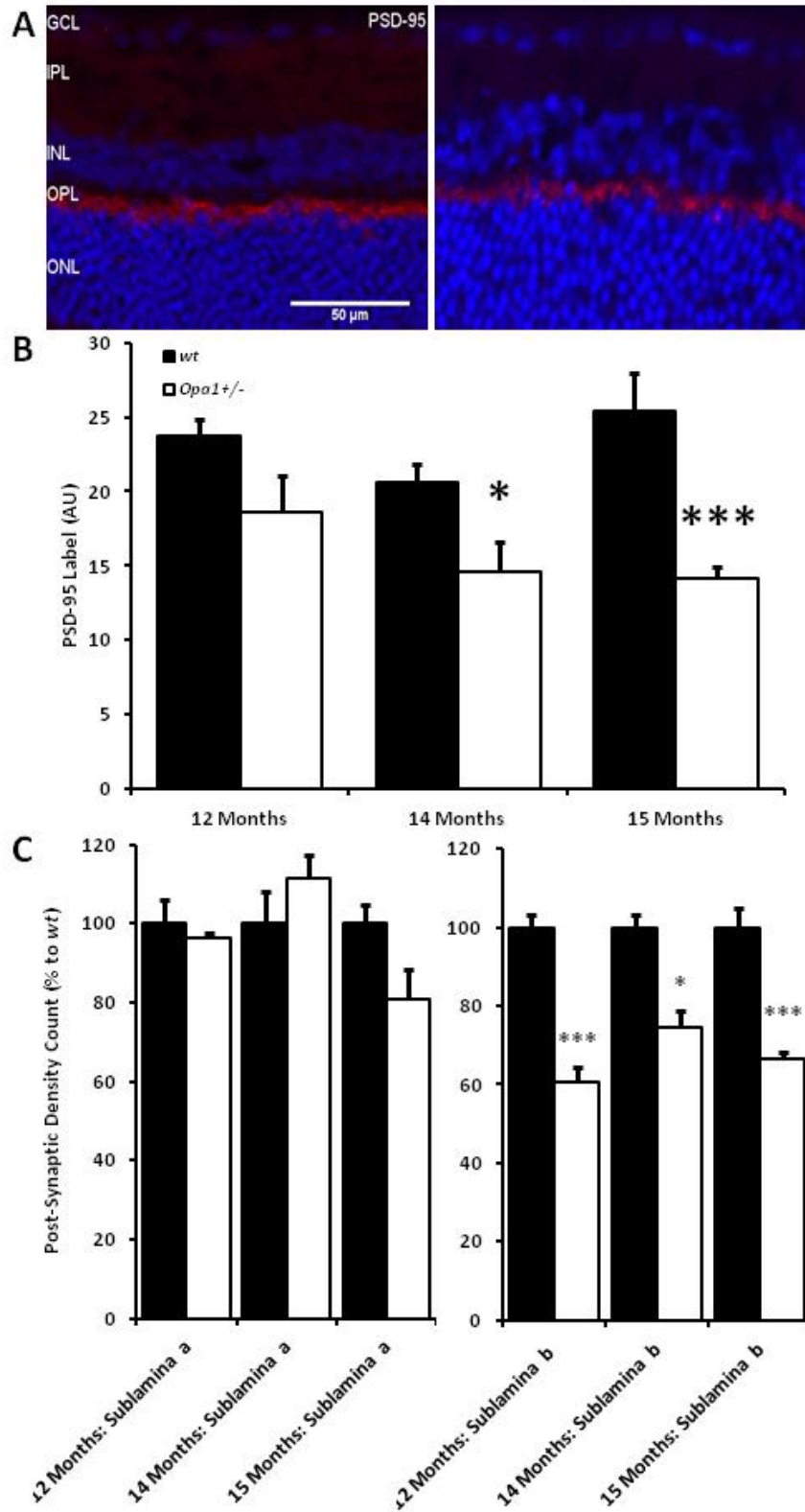


Figure XXII: Reduced retinal connectivity in Opa1^{+/-} mice

Figure XXII: Reduced retinal connectivity in *Opa1*^{+/-} mice (previous page)

To explore synaptic density within the inner plexiform layer retinal sections (A) were labelled with antibodies against PSD-95 and the relative intensity of the secondary fluorophore measured. There was a general decrease in synaptic density within the inner plexiform layer (B) observed in *Opa1*^{+/-} IPL (A, right) over *wt* controls (A, left).

The number of synaptic sites on ON- and OFF- centre retinal ganglion cell dendrites was calculated from EM images from sublamina a (OFF-centre) and sublamina b (ON- centre) of the inner plexiform layer. The reduction in synaptic density is greater in sublamina b and significant by 12 months.

Error bars = standard error of the mean. * = $P < 0.05$, *** = $P < 0.001$ (Student's t-test).

Figure XXIII: Mitochondria and synapses in *Opa1*^{+/-} mice (overleaf)

Representative samples from *wt* (A-C) and *Opa1*^{+/-} (D-F) ON-centre RGCs labelled biolistically with pE2-Crimson (Crimson) and PSD95:GFP (PSD95).

Plots of PSD95 label per unit length of dendrite in *wt* and *Opa1*^{+/-} to show neuronal processes and post-synaptic sites showing a decrease in synaptic density (I). Sholl analyses of post-synaptic sites (G) and mitochondria (H) suggest a synaptic and mitochondrial deficit towards the most distal portion of the dendrite demonstrated by the left-wards shift in the Sholl curve. Percentage comparisons of the area under the curve (AUC) (J) show a 79% reduction in the AUC for post-synaptic sites and an 88% reduction for mitochondria.

Key: black = *wt*, white = *Opa1*^{+/-} in all figures. Error bars = standard error of the mean, scale bars = 50 μ m, ** = $P < 0.01$, *** = $P < 0.001$ (Mann-Whitney-U).

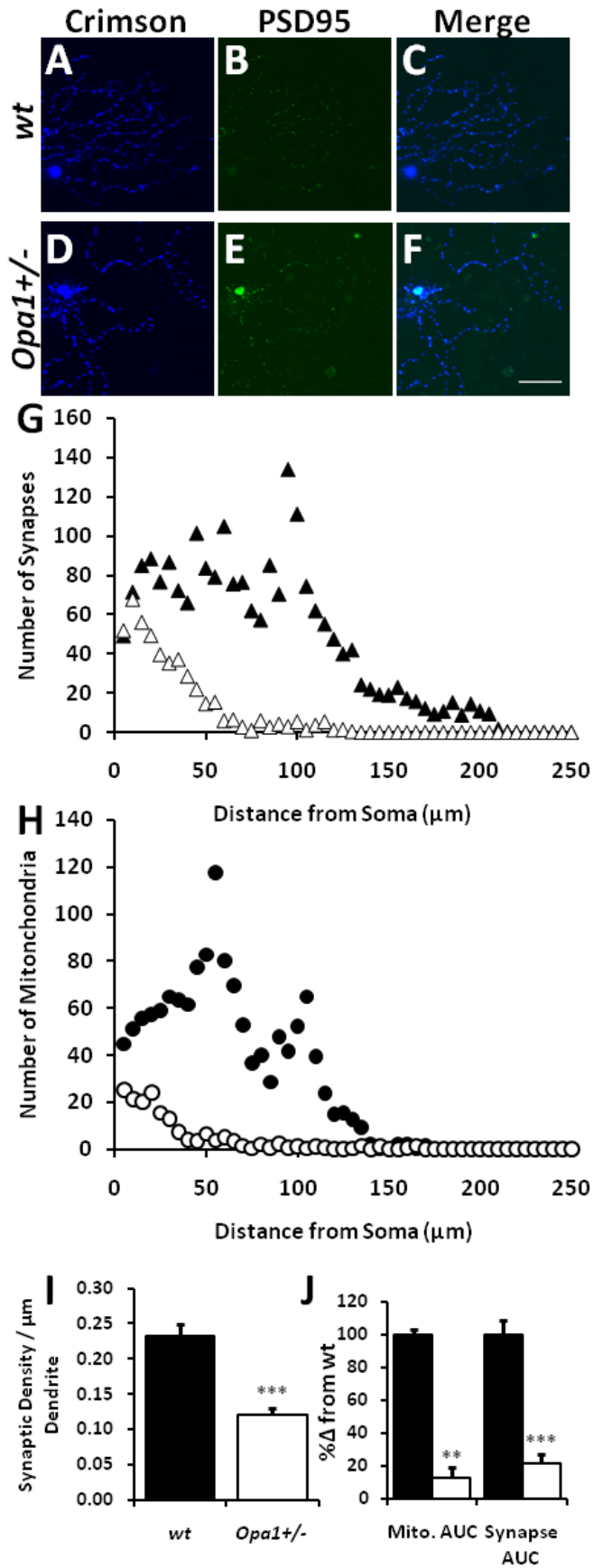


Figure XXIII: Mitochondria and synapses in *Opa1*^{+/-} mice

5.4: Synaptic Vesicles

To determine the subcellular changes underlying the loss of synaptic connectivity we explored synaptic vesicle levels within the synaptic bouton. Retinal sections were labelled with synaptophysin as a marker of synaptic vesicles. An increase in the relative luminance of the secondary fluorophore in the 12 (+122.51%; $P = 0.0026$), 14 (+129.88%; $P = 0.0001$) and 15 (+48.85%; $P = 0.0124$) month age groups.

Electron microscopy analysis of *Opa1*^{+/-} bipolar cell terminals confirmed the increase in the number of synaptic vesicles in aged *Opa1*^{+/-} compared to *wt* (at 15 months (density: synaptic vesicles/ $\mu\text{m}^2 \pm \text{SEM}$); *wt* sublamina a (93.9 \pm 15), b (100.0 \pm 11); *Opa1*^{+/-} sublamina a (194.6 \pm 16.7; $P = 0.0001$), b (240.8 \pm 30.3; $P = 0.0003$) ($P = \text{Mann-Whitney-U}$) (Figure XXIV).

5.5: Summary

This chapter explores the retinal synaptic events happening between 12 and 15 months in the *Opa1*^{+/-}, the time seen to be most vulnerable to the effects of decreased levels of *Opa1* as discussed in the previous chapter. In the 10-15 month age group there was active dendritic degeneration which is accompanied by a decrease in synaptic density and significant changes in both pre- and post- synaptic structure which becomes more prominent with age. In addition there is significant decrease in the levels of mGluR2+3 (the most prominent receptor on ON-centre retinal ganglion cells) which coincides with the dendritic atrophy of ON-centre retinal ganglion cells in this model.

Figure XXIV: Increased synaptic vesicle density in *Opa1*^{+/-} mice (overleaf)

Increased synaptic vesicle count is observed in *Opa1*^{+/-} IPL over *wt* controls as assessed by IHC (A) and EM (F). Representative samples of synapses are shown in B-E (*wt* sublamina a (B); b (C) and *Opa1*^{+/-} sublamina a (D); b (E)). Scale bar = 250nm.

Error bars = standard error of the mean. * = $P < 0.05$, *** = $P < 0.001$ (Mann-Whitney-U).

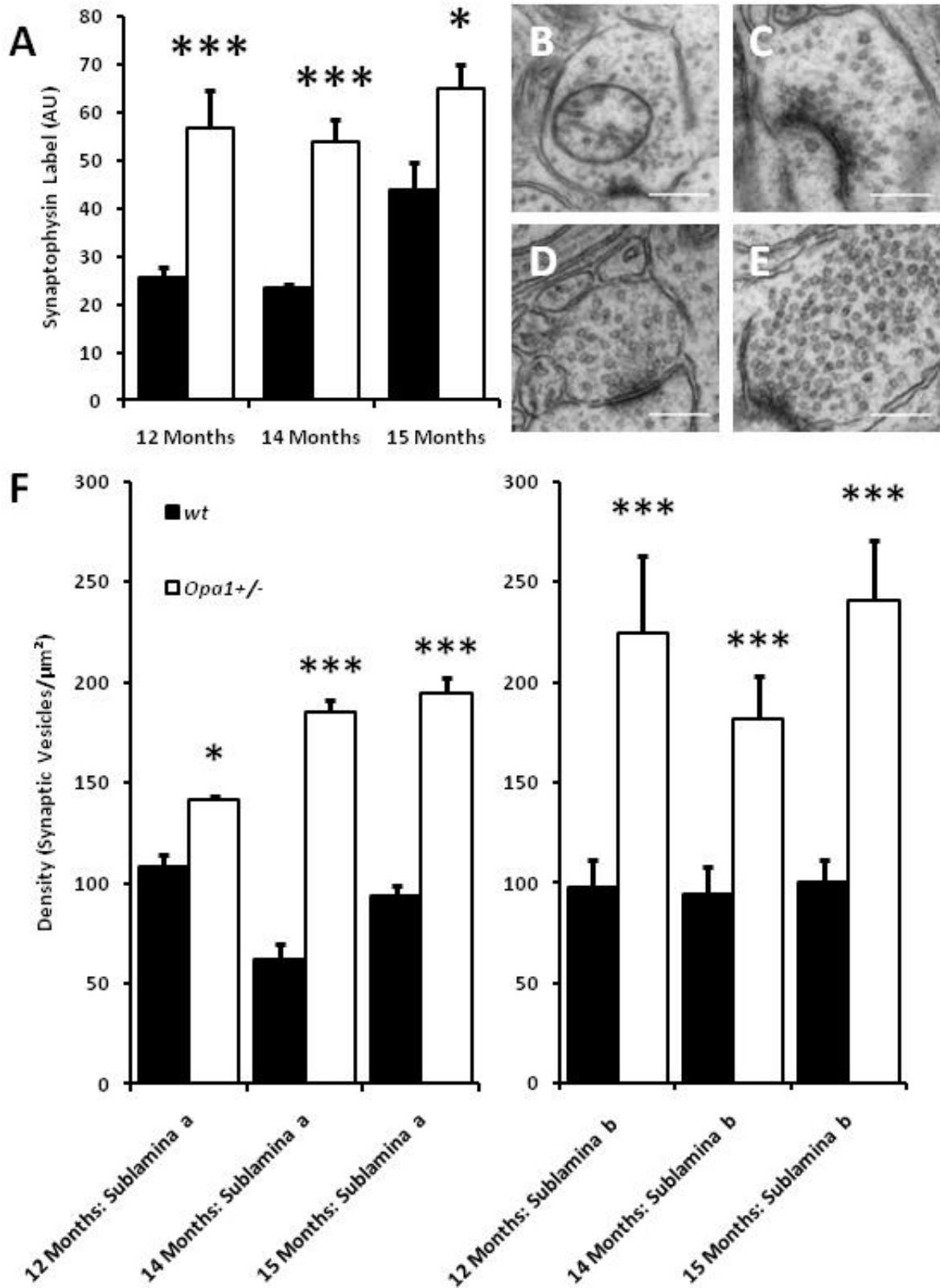


Figure XXIV: Increased synaptic vesicle density in *Opa1*^{+/-} mice

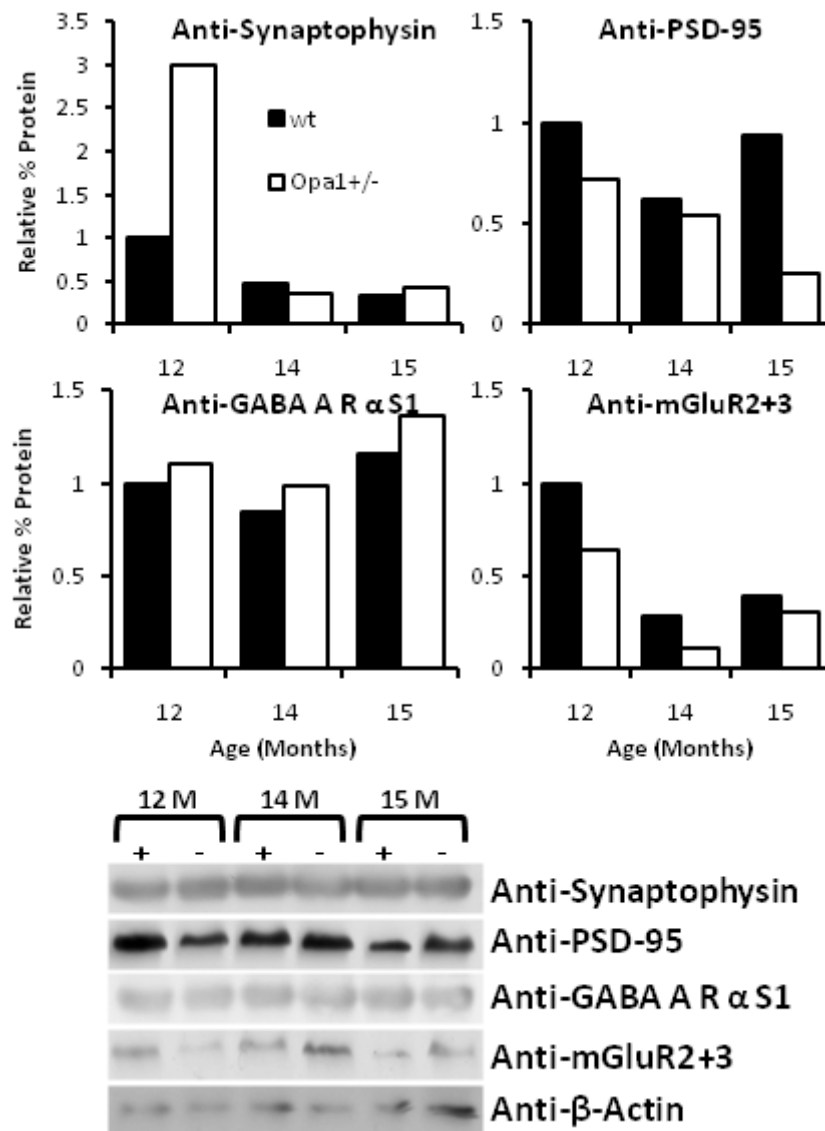


Figure XXV: Western blot densitometry of wt and *Opa1*^{+/-} retinas

Western blot densitometry data from retinas of 12 mice (*wt*; $n = 6$, *Opa1*^{+/-}; $n = 6$) validates findings found by IHC and EM. There is a general decrease in age in PSD-95 (post-synaptic densities) and mGluR2+3 (glutamatergic synapses) which supports previous findings of ON-centre retinal ganglion cell specific degeneration. There is also a general increase in synaptophysin (pre-synaptic vesicles) and GABA A R α S1 (GABA A-ergic synapses). β -actin was used as a loading control. As the data was normalised to a loading control there are no applicable error bars.

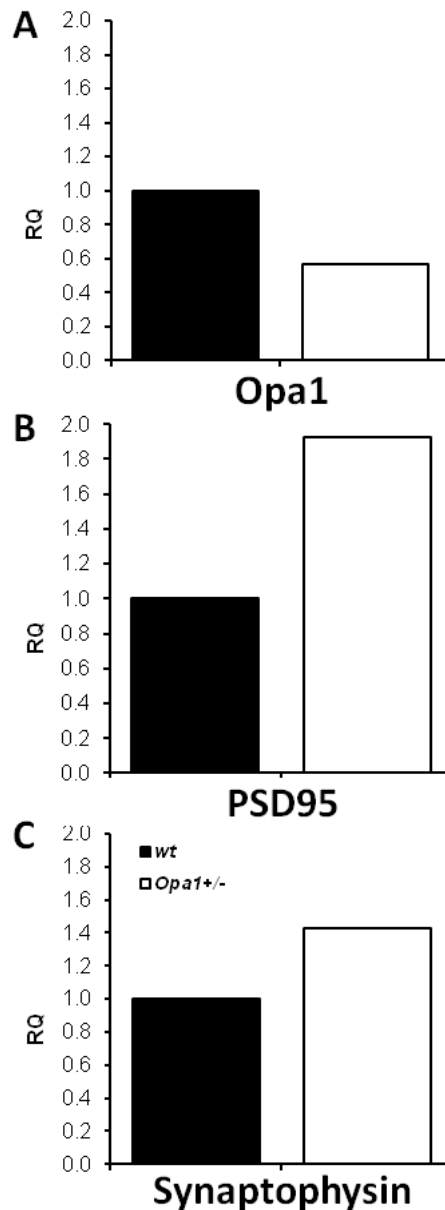


Figure XXVI: qPCR analysis of *wt* and *Opa1*^{+/-} retinas

qPCR analysis of *Opa1* (A), PSD95 (B) and synaptophysin (C) transcripts from 12 month *wt* and *Opa1*^{+/-} retina show an expected decrease in *Opa1* transcript and increase in synaptophysin transcript as mirrored in the data collected from EM, IHC and WB analysis. Interestingly, PSD95 transcription levels are higher in *Opa1*^{+/-} mice suggesting upregulation of PSD95 in response to the destruction of functional synapses on the retinal ganglion cells. The data is presented as ANOVA p-values and therefore there are no applicable error bars.

Chapter 6: Dendritic Spine Atrophy in CA1 Region Pyramidal Neurones

6.1: Introduction

Morphological assessment of the retina of the B6:C3-Opa1^{Q285STOP} mouse has shown that there is a loss of dendrites on ON-centre retinal ganglion cells occurring without soma loss or apoptosis. This work has shown that glutamatergic synapses are particularly affected in Opa1 deficient mice, and therefore such changes may be present in other parts of the central nervous system with a high glutamatergic neuronal population, such as the hippocampus.

Pyramidal neurons of the CA1 region of the hippocampus express Opa1 protein in both their soma and dendrites (Bette et al., 2005). Cognitive deficits have not been documented in patients who carry heterozygous mutations in OPA1 and have clinical signs of ADOA, despite the fact that Opa1 expression is reduced throughout the brain (haploinsufficiency). In the hippocampus approximately 90% of the neuronal cells are glutamatergic and their high energy demand must be met by fully functional mitochondria undergoing the correct ratio of fusion to fission (Vizi and Kiss, 1998; Attwell and Laughlin, 2001). A decrease in spinogenesis in the hippocampus may present as a decrease in hippocampal function *i.e.* memory formation and learning. Using neuronal and synaptic labelling techniques the dendritic architecture and synapse density of *Opa1*^{+/-} CA1 region pyramidal neurones was assessed.

6.2: Changes in Dendritic Spine Density and Morphology

There was a significant decrease in dendritic spine density on both proximal (17% reduction, $P < 0.05$) and distal (15% reduction, $P < 0.05$), basal hippocampal pyramidal dendrites in 15 month old *Opa1*^{+/-} mice compared to *wt* controls. Spine density on the apical proximal dendrites was also significantly decreased (18% reduction, $P < 0.05$) in *Opa1*^{+/-} mice compared to *wt* controls. There was no significant difference in spine density on apical distal dendrites (8% reduction, $P > 0.05$) however they too follow the trend. There was a significant decrease in dendritic spine length on the proximal and distal portions of both apical (proximal; 26% reduction, $P < 0.0001$, distal; 25% reduction, $P < 0.0001$) and basal (proximal; 18% reduction, $P < 0.001$, distal; 15% reduction, $P < 0.0001$) dendrites.

There was a decrease in the number of dendritic spines on the apical dendrites of 23 month old *Opa1*^{+/-} hippocampal pyramidal neurons. This decrease in spine density was significant for both the proximal (28% reduction, $P < 0.01$) and distal (42% reduction, $P < 0.001$) dendrites. There was no significant difference in the spine density on the basal dendrites (proximal; 2% increase, $P > 0.05$, distal; 18% reduction, $P > 0.05$). There was a significant decrease in dendritic spine length on both proximal (26% reduction, $P < 0.0001$) and distal (13% reduction, $P < 0.001$) apical dendrites. There was also a highly significant decrease in spine length on basal proximal dendrites (13% reduction, $P < 0.0001$) but no difference in the spine length on basal distal dendrites (4% reduction, $P > 0.05$).

6.3: Quantification of Post-Synaptic Sites (PSD95) in *Opa1*^{+/-} Mice

Separate brain sections of the same animals were fixed immediately after sectioning and labelled for PSD95 as a marker of post-synaptic sites and the optical density of the secondary fluorophore measured in order to quantify synaptic density in the CA1 region of the hippocampus.

We observed a significant decrease in dendritic complexity in the 23 month *Opa1*^{-/-} mice (optical density \pm SEM; *wt*; 32 \pm 2.9, *Opa1*^{+/-}; 25 \pm 1.8, $P < 0.0001$) but not in the 15 month *Opa1*^{+/-} mice (*wt*; 31 \pm 17.9, *Opa1*^{+/-}; 28 \pm 19.6, $P > 0.05$). This trend suggests a progressive loss of synapses in line with the changes we see at the level of the dendrite.

6.4: Western Blot and qPCR Analysis of Post-Synaptic Sites and Pre-Synaptic Vesicles

Western blot densitometry data from the hippocampus of 12 mice (*wt*; $n = 6$, *Opa1*^{+/-}; $n = 6$) validates findings found by immunohistochemistry in hippocampal tissue. We observed lower levels of the synaptic scaffolding protein PSD95 indicating a loss of post-synaptic sites on hippocampal pyramidal neurons as well as a similar number of pre-synaptic vesicles between *Opa1*^{+/-} and *wt* mice using the vesicle marker synaptophysin indicating that the pre-synaptic sites remain unchanged.

qPCR analysis was performed on dissected mouse hippocampi to detect changes in transcript levels of *Opa1* (expected 50% reduction), PSD95 and synaptophysin. (Similar results to the Western blot densitometry were found in the analysis of the qPCR.) Interestingly, there was an increase in PSD95 transcript suggesting an upregulation of PSD95

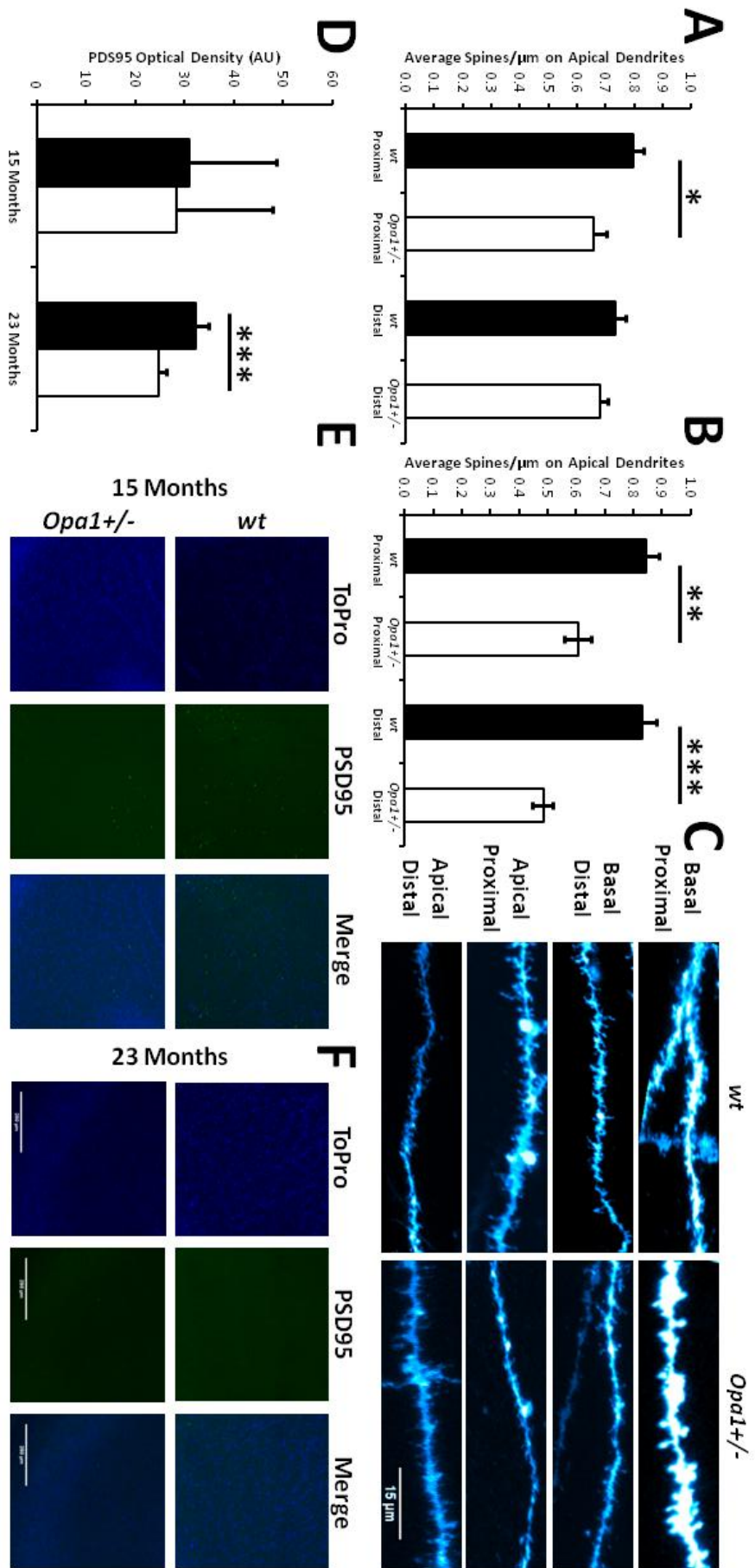
transcript in response to the absence of functional synapses on hippocampal pyramidal neurones. An overview of results is shown in *Figure XXII, XXVIII*.

6.5: Summary

Chapter 4 and 5 of this thesis show a reduction in the dendritic architecture of ON-centre retinal ganglion cells which are primarily glutamatergic. To explore this further the dendritic integrity of another predominantly glutamatergic neuronal population that expresses *Opa1* was analysed, CA1 region pyramidal neurones. This chapter shows a decrease in dendritic spine size and density on CA1 region pyramidal neurones with an associated loss of synaptic sites. Neurological testing performed previously on these mice (see 1.10.3) show a subtle phenotype and it is plausible that there are other *Opa1* related changes happening in other brain regions as well as the hippocampus. This supports the idea of a DOA+ phenotype in this model.

Figure XXVII: Dendritic spine and synapse loss in *Opa1*^{+/-} mice (overleaf)

Hippocampal pyramidal neurons dendrites were quantified in *Opa1*^{+/-} mice to observe whether *Opa1* deficiency has an effect on dendritic spine density or morphology. Using DiOlistic labelling of freshly sectioned hippocampi we observed a significant decrease in spine density on both 15 month (A) and 23 month (B) *Opa1*^{+/-} apical dendritic segments of hippocampal pyramidal neurons (representative samples are shown in C). We also explored synaptic loss in the CA1 region of the hippocampus using antibody labelling against PSD95. We observed no change in 15 month old mice (D, representative samples in E), however there was a significant decrease in synaptic density in 23 month old mice (D, representative samples in F) suggesting a gradual loss of synaptic sites which may manifest into the changes we see at a dendritic level on the *Opa1*^{+/-} pyramidal neurons.



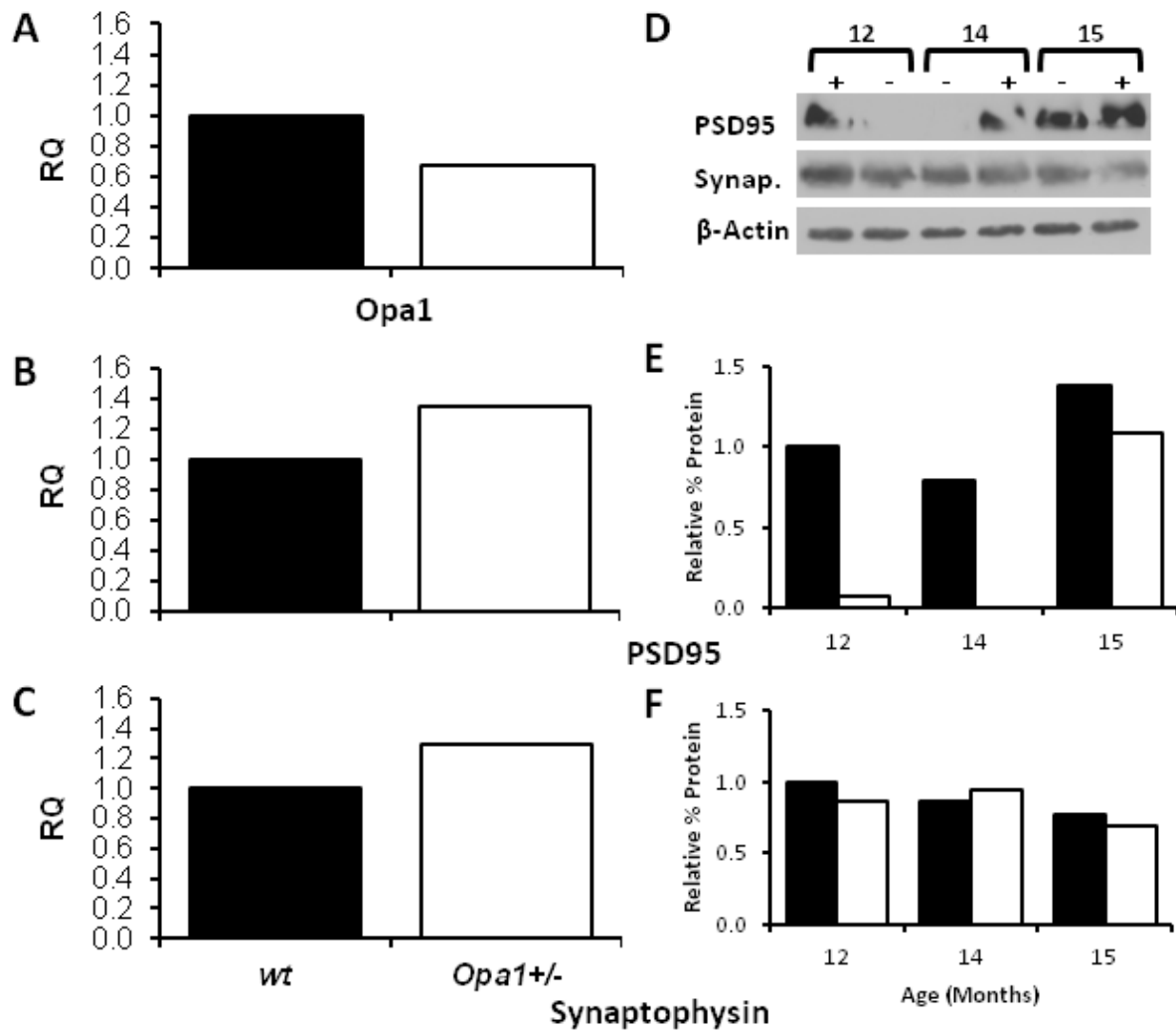


Figure XXVIII: *Opa1*, PSD95 and synaptophysin protein and transcript levels

To validate the findings made by immunohistochemistry, Western blot and qPCR analysis was performed on dissected mouse hippocampi. Western blot densitometry shows the expected changes in PSD95 (D, E) and synaptophysin (D, F) protein levels as observed by immunohistochemistry (β -actin was used as a loading control). Similar results are found in the analysis of the qPCR (A, C). Interestingly there was an increase in PSD95 transcript (B) (although a decrease in protein levels as assessed by Western blot and immunohistochemistry) suggesting an upregulation of PSD95 transcript in response to the elimination of functional synapses / dendritic spines on hippocampal pyramidal neurones. The qPCR data is presented as ANOVA p-values and therefore there are no applicable error bars.

Chapter 7: Method Development of Magnetofections for Neuronal Cell Transfection

7.1: Introduction

The transfection of nucleic acids, especially plasmid DNA and RNAi, into neuronal cells is almost essential for any neurobiologist wanting to investigate the morphology of certain neurons or the role of certain genes or organelles in a subgroup of neurons. The ideal gene transfer method needs to have a high transfection rate / efficiency (or a transfection rate appropriate for use in the study), long expression rates / prolonged expression lasting long enough to see through the experiment and with minimal toxicity. Each one of these factors can be optimised individually but getting all these right for certain applications has proven to be tricky. Neurons especially are hard to deal with being highly sensitive to changes in their environment which included the cells around them.

Magnetofection is the transfection of nucleic acids adhered to cationic magnetic nanoparticles into living cell populations using a magnetic field (a handheld magnet, or a bed of magnets under a culture dish) (McBain et al., 2008; Pankhurst et al., 2009; Yiu et al., 2011). The magnetic nanoparticles are formed from iron oxide and coated with cationic molecules which electrostatically interact with nucleic acids. Using a local magnetic field the magnetic nanoparticles can be concentrated towards the cells / tissue of interest which take up the genetic material by endocytosis. This process can take as little as 10 minutes. Cells and tissue can be kept at their normal culture conditions and within 48 hours the magnetic nanoparticles are localised within the cell cytoplasm or nucleus.

There are several inherent advantages with Magnetofections over traditional transfection techniques (*e.g.* electroporation, lipofection, biolistic transfection) especially when it comes

to neuronal cell lines or neuronal tissue. Primarily; the magnetic nanoparticles are biodegradable and so the issue of toxicity is kept low. Even at very high concentrations the nanoparticles have been shown to be no toxic. The nanoparticles are taken up by the cell, and once degraded, no longer exist in the system and can no longer be effected by extra environmental magnetic fields. The magnetic nanoparticles are relatively cost effective, needing only a small amount for a large application, and there is no need for additional transfection reagents. In addition, there is no need for extra specialised equipment. Magnetofection has been shown to be viable in many cells (and some tissues), with a higher transfection rate, and is simpler and quicker to setup and to run than other transfection techniques (unpublished data, nanoTherics Ltd. UK).

Currently, Magnetofections have been used in a wide range of cell lines and in some tissue explants (unpublished data, nanoTherics Ltd. UK). A key application for Magnetofection therefore must be the delivery of a gene vector or a pharmacological agent to a living system for purposes of gene knockdown in a system (*i.e.* an isolated model of disease), morphological tracking of a cell population (*e.g.* neuronal morphology in a disease state over time) or the addition of a targeted pharmacological agent. The advantage to Magnetofections over traditional transfection techniques is the possibility that a single cell (for example a single retinal ganglion cell) can be imaged in its entirety and that the properties of this cell could be altered limiting the cost for the development of a model. Magnetofections could, potentially allow us to image afferents and dendrites in the same cell. In addition, Magnetofections would also allow larger DNA constructs to be inserted as they get over the cassette limit of AAVs (4.7kb).

Current animal imaging modalities allow scientists to view the retina with a variety of imaging devices allowing single neurons to be imaged in real-time. The series of experiments that follow are designed to see if Magnetofections can be employed to transfect retinal ganglion cells for the purposes of tracking neuronal morphology, mitochondrial distribution and synaptic numbers. The methods and results are detailed below.

7.2: Method Development

7.2.1: *In vitro* retinal labelling using lipophilic dye coated magnetic nanoparticles

Mice were killed by cervical dislocation and the eyes quickly enucleated and placed in chilled (4°C) HBSS (Invitrogen, UK) in 7ml bijoux. The eye was punctured at the limbus and a slit cut in sclera to remove the cornea and sclera anterior to the ora serrata and lens. Vitreous was kept intact. Three cuts were made in the retina using micro-ophthalmic scissors before being flat-mounted ganglion cell layer up on a cell culture insert (Millipore, Billerica, MA) and submerged in custom media. Retinas were incubated at 37°C and 4% CO₂.

For magnetic nanoparticle : lipophilic dye compounds, 80µg of Dil was dissolved in 100µl of methylene chloride at room temperature and 2µl of nTMag100 magnetic nanoparticles (NanoTherics, UK) was added in a fume cupboard, sonicated for 30 minutes and the methylene chloride was left to evaporate. This precipitate was sonicated for 30 minutes; 100µl of PBS was added and sonicated again for 30 minutes.

For *in vitro* retinal labelling using Dil coated magnetic nanoparticles 20-100µl of nanoparticle solution was gently pipetted onto the retina and a handheld rare earth magnet was held underneath the culture for 30 seconds – 2 minutes either stationary or gently moved around. After this time retina cultures were returned to the incubator at 37°C and 4% CO₂ for 35 minutes to allow diffusion of dye through neuronal processes. Retinas were then fixed in 4% PFA, mounted in ProLong Gold AntiFade Reagent, coverslipped and sealed with nail polish. Retinas were imaged within 24 hours.

7.2.2: *In vivo* retinal labelling using lipophilic dye coated magnetic nanoparticles

For *in vivo* retinal labelling, male, brown Norwegian rats were anaesthetised using iso-fluorane and pupils dilated using tripicamide. Dil coated magnetic nanoparticles were prepared as above and 5µl of solution was injected intravitreally. Following this a handheld rare earth magnet was held close to the eye at four different quadrants (nasal, temporal, inferior, superior) to the eye for 30 seconds (2 minutes in total) to allow dispersal of the solution across the retina. Rats were allowed to recover and were sacrificed 72 hours later. Retinas were prepared as above and imaged within 24 hours.

7.2.3: *In vitro* retinal and neuronal labelling using plasmid coated magnetic nanoparticles

For magnetic nanoparticle : plasmid DNA compounds 200ng of plasmid DNA (either GFP, YFP or DsRed2-mito (Clontech)) was added to 10µl of serum free media and 0.2µl of nTMag100 magnetic nanoparticles and incubated at room temperature for 20 minutes after which 100µl of custom media was added and the solution was kept at 37°C.

For *in vitro* retinal labelling adult mouse retinas were dissected as previously described and kept at 37°C and 4% CO₂ in custom media. 20-100µl of magnetic nanoparticle : plasmid DNA solution was gently pipetted onto the retina and a handheld magnet was held underneath the culture for 30 seconds – 2 minutes either stationary or gently moved around. Retinas were returned to the incubator at 37°C and 4% CO₂ for 48-72 hours and then processed as above.

For *in vitro* labelling of cells cell cultures of RGC5 (retinal cell line) cells were kept in compliment media at 37°C and 4% CO₂, magnetic nanoparticle : plasmid DNA solution was

prepared as above and the ratios of components changed over various experiments (see results). The solution was applied over cells in culture and a handheld magnet was held underneath the culture for 30 seconds – 2 minutes either stationary or gently moved around or stationary for 24 hours. Retinas were returned to the incubator at 37°C and 4% CO₂ for 48-72 hours and then processed as above.

7.2.4: *In vivo* retinal labelling using plasmid coated magnetic nanoparticles

For *in vivo* retinal labelling, male, brown Norwegian rats were anaesthetised using isoflurane and pupils dilated using tripicamide. Plasmid DNA coated magnetic nanoparticles were prepared as above and 5µl of solution was injected intravitreally. Following this a handheld rare earth magnet was held close to the eye at four different quadrants (nasal, temporal, inferior, superior) to the eye for 30 seconds (2 minutes in total) to allow dispersal of the solution across the retina. Rats were allowed to recover and were sacrificed 72 hours later. Retinas were prepared as above and imaged within 24 hours.

7.2.5: Plasmid validation

For plasmid validation cell cultures of SH-SY5Y (human neuroblastoma cell line) cell lines were kept in complete media at 37°C and 4% CO₂. The magnetic nanoparticle : plasmid DNA solution was prepared as above. The solution was applied over cells in culture and 24-well plates were placed on a magnetofect-nano cell transfection device (NanoTherics) at 3Hz for 1 hour at 37°C. Cell lines were kept for 48 hours, fixed in 4% PFA, mounted, coverslipped and imaged within 24 hours.

7.3: Results

7.3.1: *In vitro* labelling of retinal ganglion cells using lipophilic dyes

Whole adult mouse retinas in culture were labelled using lipophilic dye (DiI) coated magnetic nanoparticles and subjected to a small local magnetic field (from a rare earth magnet) for 10 seconds to 2 minutes. Times greater than 45 seconds lead to the retinas being overly labelled (*i.e.* many dendrites and cells labelled so that individual morphologies of cells was unclear, similar to that of 'over shooting' using a DiOlistic method). Retinas were sufficiently labelled after just 30 seconds compared with control retinas (*i.e.* retinas treated with just the magnet and no magnetic beads, or retinas treated with the dye : magnetic nanoparticle solution but no magnet) allowing morphologies of individual retinal ganglion cells to be shown (*Figure XXIX*). This was sufficient data to move onto the next stage of experimentation: *in vivo* labelling of retinal cells.

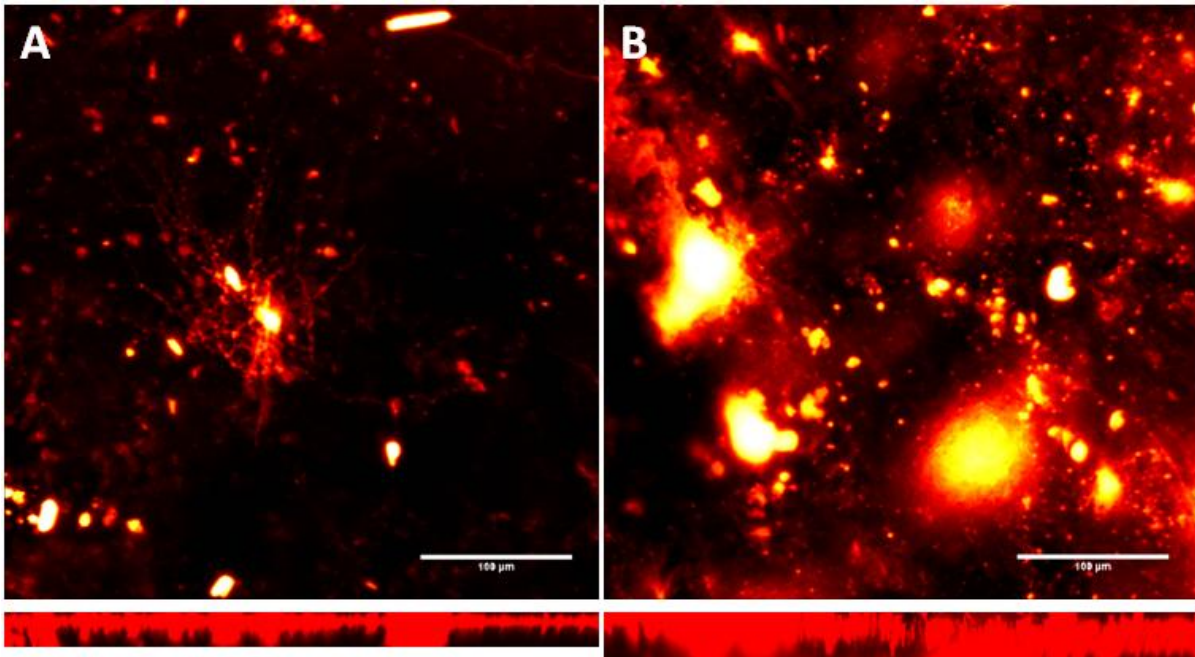


Figure XXIX: Magnetolistically labelled retinal ganglion cells

Magnetic nanoparticles in PBS were coated in a DiI solution, pipetted onto mouse retina in culture and subjected to a local magnetic field from a hand-held rare-earth magnet. (A) shows two retinal ganglion cells that have had the dye 'pulled' into them by the magnet. No labelling was present on control retinas with no magnet field (B).

7.3.2: *In vivo* labelling of retinal ganglion cells using lipophilic dyes

Adult brown Norwegian rats were intravitreally injected with the Dil coated nanoparticles previously described and a small local magnetic field was applied to the nasal, temporal, superior and inferior quadrants of the eye for 30 seconds per quadrant. The rat was left to recover and sacrificed 72 hours later. Although there was no staining of retinal ganglion cells there was labelling of axonal processes throughout the eye (*Figure XXX*).

Figure XXX: Magnetolistically labelled retinal ganglion cell axons *in vivo* (overleaf)

Magnetic nanoparticles coated in a Dil solution were intravitreally injected into the eyes of adult brown Norwegian rats and a local magnetic field was created at the nasal, temporal, superior and inferior quadrants of the eye. Although there was no labelling of retinal ganglion cell dendritic processes there was substantial labelling of retinal ganglion cell bodies (A) and axons (B-F).

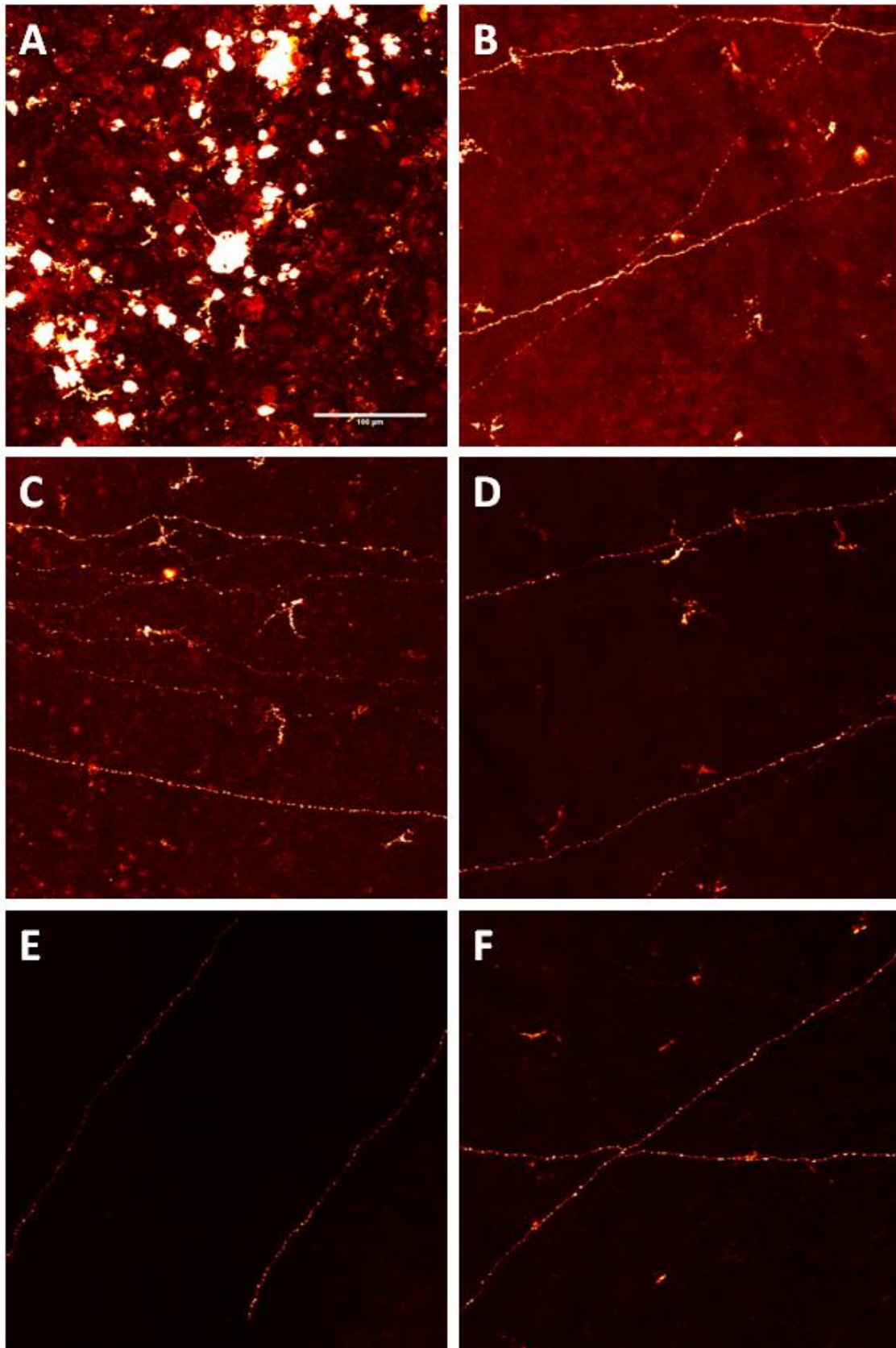


Figure XXX: Magnetotistically labelled retinal ganglion cell axons in vivo

7.3.3: *In vitro* labelling of cell cultures using plasmid DNA

RGC5 cells were kept in culture and treated with plasmid DNA adhered to magnetic nanoparticles in complete media. The cell cultures were subjected to a light magnetic field using the same magnet (mentioned above) for 30, 60, 90, 120 or 210 seconds or 24 hours. Cells were sufficiently labelled compared to control counterparts with YFP and DsRed2-Mito with just seconds of applied magnet time. Additional magnet time (*i.e.* the 24 hour scenario) made no noticeable difference (*Figure XXXI*).

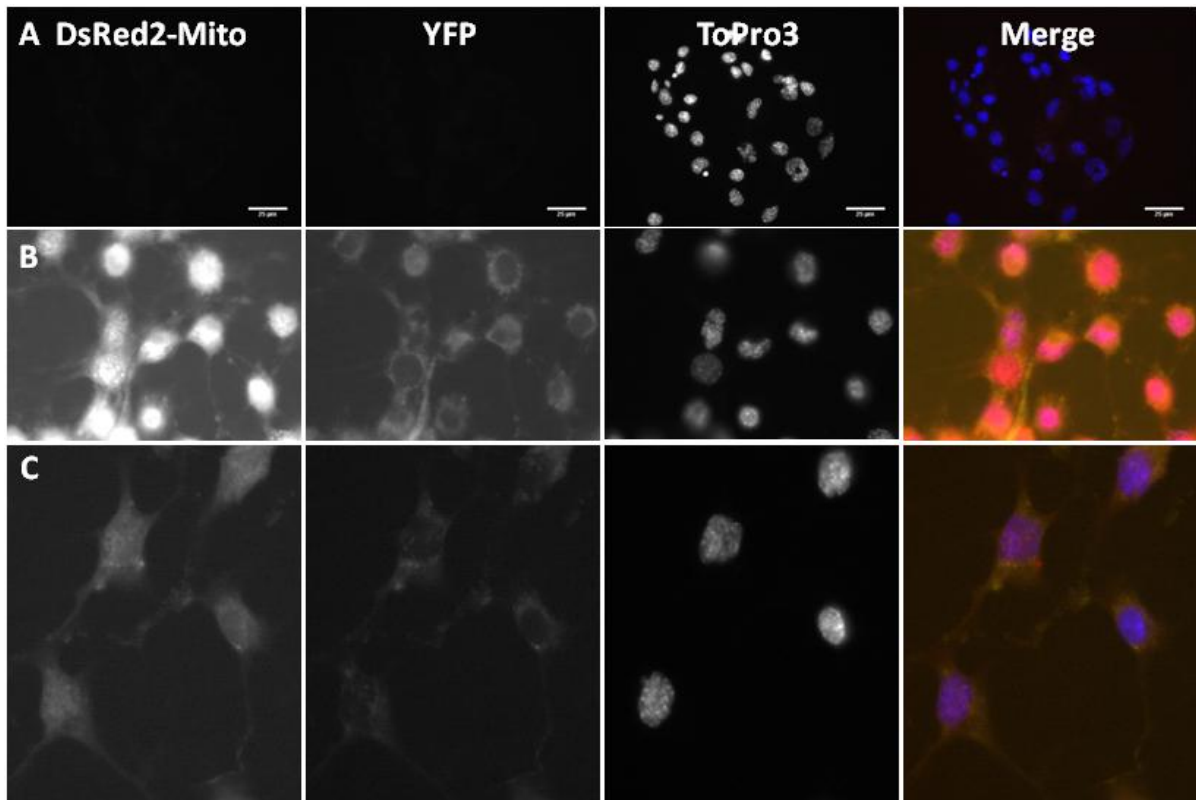


Figure XXXI: Magnetofections: RGC-5 culture

RGC-5 cultures was successfully labelled using magnetic transfection of plasmid DNA (DsRed2-mito; mitochondria, YFP; cell labelling, ToPro3, nuclear counter stain). Labelling was efficient with just 90 seconds exposure to a local magnetic field (B) compared with non-magnetic field control (A). There was no increase in labelling efficiency when the magnetic field exposure time was increased up to 24 hours (C).

7.3.4: *In vivo* labelling of retinal cells using plasmid DNA

Intact adult mouse retinas were kept in culture conditions (as previously described) and treated with plasmid DNA adhered to magnetic nanoparticles in complete media. Retinas were subjected to a light magnetic field using the same magnet (mentioned above) for 30, 60 or 90 seconds or 24 hours. Retinas were processed and imaged but there was no labelling compared with control retinas (*Figure XXXII*).

In addition, retinas were placed in 6-well culture plates and subjected to a light magnetic field for 30-60 minutes using a magnefect-nano cell transfection device with the same plasmid DNA : magnetic nanoparticle solution. There was no labelling compared with control retinas.

The plasmid DNA : magnetic nanoparticle : media ratio was changed throughout these two experiments. A detailed table of ratios attempted are seen in *Table IV*.

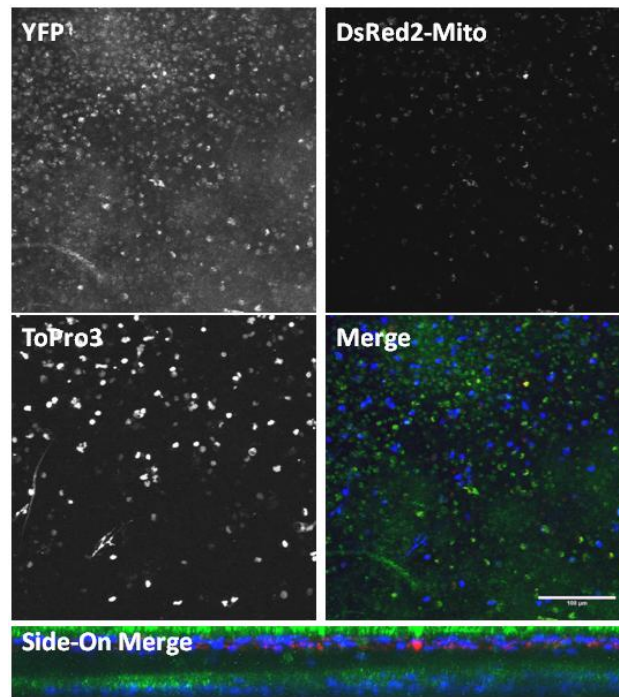


Figure XXXII: Magnetofection: Intraocular injections

The eyes of brown Norwegian rats were intravitreally injected with plasmid coated magnetic nanoparticles. There was moderate labelling of cell bodies in the photoreceptive cell layer with YFP and in the processes of a few cells with DsRed2-Mito.

7.3.5: Plasmid validation

For plasmid validation cell cultures of SH-SY5Y cell lines were kept in compliment media and the same magnetic nanoparticle : plasmid DNA solution was prepared as above. The solution was applied over cells in culture and 24-well plates were placed on a magnefect-nano cell transfection device 1 hour at 37°C. Cell cultures were processed and imaged. Biolistic transfection of retinal ganglions (mentioned above) added an additional plasmid validation trail.

Table V: Magnetofection trails

Tables detailing the Magnetofection trails performed on health retinal flat-mounts in culture including the combinations of reagents (*upper table*), combinations of plasmids (*middle table*) and combinations of settings on the nanoTherics 'magnetfect nano II' (*lower table*).

Trials	Plasmid DNA	nTMag Beads	Serum Free Media	Complete Media
1	1	1	1	1000
2	1	1	1	2000
3	2	2	1	1000
4	2	2	2	1000
5	1	5	20	500
6	1	5	50	500
7	10	1	1000	1000

Combination	GFP	YFP	E2-Crimson	DsRed2-Mito	PSD-95GFP
1	x				
2		x			
3			x		
4			x	x	
5	x			x	
6			x		x
7		x	x		x

Setting	Time	Hz
1	30	3
2	30	4
3	45	3
4	45	4
5	60	3
6	60	4

7.5: Magnetofections Discussion

Although the ultimate goal of the experiment, to label retinal cells using plasmid DNA adherant to magnetic nanoparticles *in vivo*, was not achieved, the labelling of axonal processes *in vivo* using lipophilic dyes and the labelling of cell cultures with plasmid DNA without using proprietary equipment is promising. The best setting for plasmid DNA delivery by Magnetofection was using YFP and DsRed2-mito plasmids with an applied magnet time of 60 seconds on RGC5 cultures. This gave a high yield of clearly labelled cells with complete mitochondrial labelling and labelling of cell processes. The simplicity of the experiment, coupled its low cost, short preparation time and its reproducibility means that this is an experimental paradigm that could easily be used in a laboratory setting. In addition there was no obvious toxicity in either the cell or retina cultures.

There are several possible explanations as to why *in vivo* Magnetofections did not work. Originally it was suggested that the vitreous on the retina provided a barrier stopping the magnetic particles from moving. This posed two problems. Firstly; this would mean that Magnetofection could not be used in an *in vivo* setting as the vitreous could not be removed, and secondly, on *in vitro* retinal cultures with the vitreous removed Magnetofection of retinal cells was unobtainable. The magnet strength was then optimised. Changing the parameters using a range of various rare earth magnets and magnetic plates provided by NanoTherics the experiments were repeated but Magnetofection was still unachievable. There was no change when changing the parameters of the plasmid DNA : magnetic nanoparticles : media ratio. It is plausible that the varicosity of the retina, as well as, magnet strength, field size and the cell's own intrinsic ability to endocytose the bead construct all have a role to play in as to why *in vivo* Magnetofections didn't work.

Theoretically, *in vivo* magnetofection is attainable; however the magnetic and bead parameters have to be optimised even further. Future research should focus on specialised magnetic field generators (*e.g.* can fit closer to the eye), working out the exact varicosity of the retina and how this will affect bead : plasmid DNA constructs and the need for any additional transfection reagents or bead coatings.

Chapter 8: Discussion

8.1: Retinal Ganglion Cell Dendropathy in a Mouse Model of Dominant Optic Atrophy

Evidence of dendritic pruning in a mouse model of *Opa1* dominant optic atrophy is shown here for the first time. The effects of the *Opa1*^{Q285STOP} (exon 8) mutation in this mouse model appear to be more subtle than those seen in some patients with ADOA allowing the mechanism of disease to be elucidated leading to the development of potential therapeutics rather than attempting to solve irreversible neuronal loss without a tangible marker of disease state.

The *Opa1*^{+/-} mouse phenotype becomes *clinically* apparent only after ca. 12 months and is slowly progressive with age. Visual deficits manifest as a reduction in visual acuity (measured by optokinetic drum (Davies et al., 2007)), a reduction in the photopic negative response (light adapted ERG) thought to represent retinal ganglion cell function and reduction in the P2 positive deflection (light adapted visual evoked potential) at 11-13 months (Barnard et al., 2011). An accompanying reduction in muscle power is apparent on rotarod testing (unpublished data) as well as wider neurological defects. Previous examination of the optic nerve in the *Opa1*^{+/-} mouse by electron microscopy reveals a loss of fibre bundle myelination as well as disrupted mitochondrial morphology which is accompanied by increased autophagy in retinal ganglion cells from 12 to 24 months of age (White et al., 2009). The retinal ganglion cell dendropathy shown here precedes clinical visual loss and occurs without retinal ganglion cell loss as confirmed by nuclear staining, γ -synuclein staining and labelling of ipRGCs using melanopsin.

But why do retinal ganglion cells show a specific vulnerability to mitochondrial dysfunction? The retinal ganglion cell population is unique in the challenges it faces in the central nervous system. Retinal ganglion cell axons are only myelinated when they exit the eye and enter the optic nerve. This places a high metabolic demand on the retinal ganglion cell as saltatory conduction of action potentials can only occur after exiting the eye (which can be as much as 2000µm for cells in the periphery of the retina). These requirements manifest as the presence of a large number of mitochondria within axon hillock, at the nodes of Ranvier and within dendritic processes. If mitochondrial motility ceases or the throughput of energy from functional mitochondria decreases this could have dire repercussions on the retinal ganglion cell. Whilst this theory is convincing it may nevertheless not be the case. The evidence put forward in this thesis points towards the specific elimination of glutamatergic synapses and in order to explore this further pilot studies were performed on another highly glutamatergic region of the central nervous system, the CA1 region of the hippocampus. Using a DiOlistic method our group explored the dendritic integrity of CA1 region pyramidal neurons in adult (15 month) and aged (23 month) *Opa1*^{+/-} mice. We observed a decrease in dendritic spine density on the apical proximal sections (closer than 100µm to the cell soma) of *Opa1*^{+/-} pyramidal neuron dendrites in both ages. Repeated trials showed the same findings. We observed lower levels of the synaptic scaffolding protein PSD95 as observed by immunohistochemistry indicating a loss of post-synaptic sites on hippocampal pyramidal neurons as well as a similar number of pre-synaptic vesicles between *Opa1*^{+/-} and *wt* mice using the vesicle marker synaptophysin indicating that the pre-synaptic sites remain unchanged. This was validated in our Western blots. We also observed a high proportion of short spines in the *Opa1*^{+/-} mice, which may be due to a decrease in synaptic activity and a

reduction in PSD95. Interestingly this degeneration occurs without apparent deficits in learning and memory tasks.

A high proportion of short spines in the *Opa1*^{+/-} mice was observed, which may be due to a decrease in synaptic activity and a reduction in the synaptic scaffolding protein PSD95. Dominant optic atrophy would not be unique in this; a reduction in spine size is observed in various neurological disorders including schizophrenia and Down's syndrome.

In wildtype mice an increase in synaptic activity or induction of LTP causes an increase in spine growth which is not seen in the *Opa1*^{+/-} mice. *In vivo* imaging studies on dendritic spines have shown that they may be highly motile. Their shape and length may change rapidly, with some smaller spines retracting and disappearing completely. However in aged animals this motility decreases and spines become more stable (Stuart et al., 1999).

Li et al. (2004) found that an overexpression of *OPA1*, leading to increased mitochondrial fusion, reduced the number of dendritic mitochondria and led to a decrease in spine and synapse number. In this model a ca. 50% decrease in *Opa1* expression leads to a decreased spine density and a decrease in synaptic density. This suggests that the fine balance of mitochondrial fusion and fission is essential in maintaining dendritic spine and synapse density in health and disease.

These data highlight the role that *Opa1* has to play on other neurones in the central nervous system and in the body as a whole. This is seen clinically in patients with ADOA+ phenotype symptoms which include heart defects and sensorineural deafness. It would be interesting to examine, post-mortem, the hippocampus of ADOA patients as well as their ability to

perform memory tasks to see whether the observations found in the mouse model translate to the human population.

8.2: Mechanism of Disease

Mitochondria are dynamic, morphologically diverse organelles and the classic text book image of a perfectly oval, bean shaped mitochondria floating in a cytoplasmic soup could not be further from the truth. Mitochondria continuously fuse, divide and move throughout the cell to sites of requirement, for example the synapse. Functional mitochondria are actively recruited to the synapse whereas dysfunctional mitochondria are actively transported to the soma and undergo mitophagy. Once at the synapse mitochondrial movement is inhibited in properly functioning neurones (*i.e.* synaptically active) by a morphological change from elongated to a rounder morphology (Greenwood and Connolly, 2007). Mitochondrial morphology is therefore crucial so that mitochondria travel in the right direction along the dendrite. This is probably an integral component of the *Opa1*^{+/-} disease model where mitochondrial dynamics are shifted towards fission leaving small, fragmented mitochondria at synaptic sites which are then actively returned to the soma and undergo mitophagy thereby reducing the number of mitochondria at an already compromised synaptic site. Studies show there are less mitochondria generally in dendrites than there are in axonal segments and that the mitochondria in dendrites are more metabolically active as well as being less motile (Overly, Rieff and Hollenbeck, 1996; Cheng et al., 2010). This can only act to increase the cellular stress imposed on synaptic sites within the retinal ganglion cell. This may also help explain why there is relatively little axonal loss in the optic nerve and considerable dendritic degeneration in this model.

The process connecting changes in mitochondrial fusion with reduced visual function has been elusive (Yu-Wai-Man, Griffiths and Chinnery, 2011). Whilst loss of retinal ganglion cells by apoptosis has been proposed as the mechanism (Heiduschka et al., 2010), the *Opa1*^{+/-}

mice do not show statistically significant age-dependent loss of retinal ganglion cells on retinal sections and whole mounts and TUNEL staining has not indicated an increase in apoptosis (unpublished data), which is consistent with this observation. In contrast, these data indicate a marked change in retinal ganglion cell connectivity as the origin of the development of visual defects.

Studies in human OPA1 ADOA patients have been limited by the paucity of pathological material. Retinal ganglion cell numbers from patients with ADOA are lacking and broad conclusions are based on the study of two elderly ADOA patients with severe and advanced end-stage disease, in whom no retinal ganglion cell counts were undertaken only measures of thickness and arbitrary measures of 'degeneration' (Kjer et al., 1983). However, electrophysiological studies in patients are consistent with both the loss of retinal ganglion cells as evidenced by changes in the PERG P50:N95 ratio, as well as retinal ganglion cell dysfunction resulting in delayed visually evoked potential responses (Berninger, Jaeger and Krastel, 1991; Holder et al., 1998; Holder, 2004).

In the *Opa1*^{+/-} mouse dendritic atrophy appears to be most active around 10-15 months of age with some retinal ganglion cells appearing relatively healthy (non-significant levels of degeneration observed) with others having severely compromised dendritic architectures. To investigate the time-course and mechanism of dendritic atrophy the 10-15 month age group was subcategorised into 12, 14 and 15 month cohorts. Elucidation of the mechanism of disease was sought by proposing the following questions using a range of methodologies including electron microscopy, immunohistochemistry, Biologics, Western blot analysis and quantitative RT-PCR:

- i) Is dendritic atrophy driven post-synaptically at a synaptic level;
- ii) Is dendritic atrophy driven pre-synaptically by loss of input from bipolar cells;
- iii) Do *Opa1*^{+/-} retinal ganglion cells maintain a normal distribution of mitochondria and synapses?

The density and localisation of post-synaptic sites were explored using various experimental modalities. A reduction in the synaptic scaffolding protein, PSD95, analysed using immunohistochemistry was found in all age cohorts which was exacerbated with age. This was mirrored in the Western blot analysis. As with retinal ganglion cell dendritic atrophy analysis of dark post-synaptic densities by electron microscopy revealed synaptic loss was restricted to sublamina b of the inner plexiform layer *i.e.*, ON-centre retinal ganglion cells. These data are indicative of synaptic atrophy and suggests synaptic atrophy that coincides or precedes dendritic pruning.

Further data confirm the hypothesis that visual dysfunction is driven from the retinal ganglion cell rather than earlier in the visual pathway. Counts of photoreceptive cells and bipolar cells using nuclear stains and PKC- α (a marker of rod bipolar cells) show that cell populations are maintained across all age groups compared with *wt* controls. Published visual electrophysiology data on *Opa1*^{+/-} mice at 11-13 months of age show deficits at the level of the retinal ganglion cell without deficits to cells in the outer retina, again supporting retinal ganglion cell dysfunction over retinal ganglion cell loss or loss of input from other parts of the visual pathway (Barnard et al. 2011).

Synaptic vesicle density in the terminal arbors of bipolar cells in whole retinal sections were examined by electron microscopy and immunohistochemistry labelling for the synaptic vesicle protein synaptophysin. There was an increased luminance of the secondary

fluorophore in immunohistochemically labelled retinas for synaptophysin in all ages indicating an increase in synaptic vesicle number which was mirrored by the Western blot analysis and increased synaptophysin transcript levels as assessed by qPCR. Electron microscopy analysis of bipolar cell terminal arbors as well shows an increase in synaptic vesicle density in all ages analysed. This again suggests that bipolar cells undergo normal inputs and function (*i.e.* producing vesicle bodies) but the increased synaptic vesicle density may be due to low levels of recycling at the post-synaptic site or the bipolar cell itself not having enough available energy to undergo proper or efficient synaptic vesicle transfer leading to a build up of vesicles. Within the synaptic bouton mitochondria are essential for cycling of the reserve pool synaptic vesicles as well as being essential for the general organisation of the synaptic bouton therefore it is unsurprising that Opa1 deficiency manifests as a build up of synaptic vesicles possibly representing decreased levels of vesicle recycling (Chan, 2006a).

The retinal ganglion cell soma and dendrite is unique in the central nervous system in that it is frequently exposed to high levels of light. This has led to theories (Wataha et al., 2004; Osborne et al., 2006) that ambient light may exacerbate mitochondrial dysfunction by mechanisms including higher generated levels of reactive oxygen species from mitochondrial photosensitisers and suppressed levels of oxidative phosphorylation. Light exposure studies on rat retinal cultures show enhanced levels of apoptosis (increased number of TUNEL positive cells) caused by cleavage of caspase-3 by light into the caspase-3 active form (Lascaratos et al., 2007).

8.3: The Pharmacological Properties of Retina Ganglion Cells Determines Their Fate

ON and OFF pathways in the mammalian retina are partially separated in the visual pathways at the thalamic and cortical levels, with different stimulus and neurotransmitter requirements (Pourcho, 1996; Xu and Tian, 2007; Marc, 2008). The differential effects of the mutation on dendritic morphology in the ON and OFF pathways are of interest since it may shed light on the mechanisms of dendrite change in *Opa1*^{+/-} mice.

The neuropharmacology of the retinal ganglion cell has a strong influence on neuronal viability in the *Opa1*^{+/-} mouse. A selective loss of glutamatergic but not GABAergic synaptic sites with age in *Opa1*^{+/-} mice as indicated by changes on immunohistochemistry and western-blot analysis was observed. One explanation for this is that these GABAergic synapses on OFF-centre retinal ganglion cells have a lower energy demand as they operate near the $\Delta E_{q_{\text{chl}}}$ and the polarized changes are small. The observed selective neuronal vulnerability may therefore reflect the higher energy demands of ON-centre retinal ganglion cells (Mattson and Magnus, 2006). This higher energy requirement may be the cells' downfall as the *OPA1* deficient mitochondria may not be able to support the cells' metabolic needs. The retinal ganglion cell may go through a phase of low bioavailability of ATP leading to a lower rate of synaptic firing. This leads to a period of low activity whereby synaptic sites are depleted, synaptic connections fail and the dendrites atrophy, leading to the loss of visual function we see in this mouse phenotype. It has been previously shown that the maintenance of retinal ganglion cell dendritic architecture depends on glutamatergic signalling in both the mature and immature retina, supporting our findings that an absence

of glutamatergic synapses leads to dendritic degeneration (Bodnarenko et al., 1995; Wong et al., 2000; Sernagor, Eglén and Wong, 2001).

A further suggestion to the mechanism of the specific dendritic degeneration in ON- centre retinal ganglion cells is that the retinal ganglion cells go through the starting sequence of excitotoxicity leading up to dendrite loss. Under the conditions of low energy availability caused by dysfunctional mitochondria and continued stimulation at glutamatergic synapses there is a higher influx of Ca^{2+} into the postsynaptic membrane which can trigger apoptosis (although this is not seen in this model) and higher levels of reactive oxygen species produced. High concentrations of reactive oxygen species can induce lipid peroxidation leading to the dysfunction of ATPases which further decreases the bioavailability of ATP, the dysregulation of ions (*e.g.* Ca^{2+}) and lead to excitotoxicity. Loss of synaptic sites has shown to be a cellular defence against excitotoxicity (Ikegaya et al., 2001; Mizielinska et al., 2009). This is a pathway that is commonly shared in other neurodegenerative disorders which is exacerbated by certain proteins that sensitise neurones to excitotoxic damage; for example amyloid β in Alzheimer's disease, dopamine in Parkinson's disease and huntingtin in Huntington's disease. Additionally, glutamate, rather than GABA is essential for retinal ganglion cell stratification during and post- development (Bodnarenko et al., 1995).

The dendropathy shown in ON-centre retinal ganglion cells increases with age and this may be due to the increased reactive oxygen species production in these cells as mentioned above. Evidence for this comes from studies in the rat cerebral cortex where older rats have increased reactive oxygen species levels and enhanced mitochondrial swelling in response to higher Ca^{2+} loads. This may be a contributing factor to dendritic loss in this model.

The functional difference between the ON- and OFF- centre pathways may hold a clue as to the specific degeneration of ON-centre retinal ganglion cells. It has been shown in humans (Komban, Alonso and Zaidi, 2011) that the OFF- centre pathway is processed at a higher rate than the ON-, light sensitive pathway, and that the OFF- pathway is better represented in the visual cortex, perhaps promoting OFF- pathway survival. If these findings hold true in mice then the faster processing of the OFF- pathway could promote synaptic exchange quicker and strengthen synapses on OFF-centre retinal ganglion cells thus increasing mitochondrial recruitment to the synapse and effectively saving the OFF- centre retinal ganglion cells from degeneration.

Although not observed in this mouse model, the glutamatergic synapses on retinal ganglion cell dendrites may already be destined to their fate. The selective blocking of glutamatergic receptors (either/both AMPA or NMDA receptors) in isolated retina leads to a decrease in dendritic growth, leading to a decrease in overall dendritic complexity. AMPA receptor trafficking in the synapses stabilises dendritic branches and, in addition, also escorts other proteins to the synapse. A problem with AMPA trafficking (perhaps caused by low energy bioavailability or dysfunctional mitochondria for example) therefore can have dire consequences downstream. Proteins are not recruited efficiently to the synapse leading to poor assembly of the post-synaptic density which, in turn, can lead to the synaptic failure of glutamatergic synapses, leading to defects in retinal ganglion cell dendritic architecture (Xia, Nawy and Carroll, 2007).

Downstream problems associated with altering AMPA receptor trafficking may also shed light onto why the bipolar cell terminal arbours were becoming highly densely populated with pre-synaptic vesicles. By interfering with AMPA receptor trafficking, one group

(Ruthazer and Aizenman, 2010) showed that the post-synaptic sites take longer to mature (*i.e.*, less instances of mature sites) and that pre-synaptic sites become clustered with vesicles over the course of hours. This effect was more prominent in the brains of older animals.

8.4: The Importance of Mitochondria in Neuronal Health, Survival and Plasticity

The role of mitochondria in synaptic plasticity has mostly been studied in glutamatergic neurons where they are essential members of the synaptic transmission process as they are the major contributors to the neurons' energy demands. This energy is required for the influx and release of calcium ions as well as maintaining various ion gradients. Mitochondria, therefore, are found in areas of high energy demand; around the nucleus and in the dendritic shafts of the neuron with their movement and distribution coordinated by the balance of mitochondria fusion and fission as dictated by Drp1 and OPA1.

The role of *OPA1* and disrupted mitochondrial fusion in the pathophysiology of ADOA is not an unique association; mitochondrial dysfunction is increasingly recognised as a key contributor to neuronal dysfunction and loss in classic neurodegenerative diseases such as Alzheimer's (Wang et al., 2008), Huntington's (Kieper et al., 2010) and Parkinson's disease (Abou-Sleiman et al., 2006; Otera and Mihara, 2011). In Alzheimer's disease models (Wang et al., 2008) a decrease in synaptic and mitochondrial density in the periphery of the cell has been shown in addition to a general redistribution of mitochondria towards the soma, similar to the findings shown in the *Opa1*^{+/-} mouse. In these neurodegenerative disease states the rate of neuronal loss is slow and accompanied by prolonged periods of neural dysfunction in the absence of demonstrable neuronal loss and atrophy and changes in mitochondrial dynamics may be a common final pathway that leads to neuronal dysfunction (Cho et al., 2010). The high dependence of neurons on mitochondria leaves them highly susceptible to any changes in energy stasis (Mattson and Magnus, 2006). Mitochondrial structure, number and their distribution within the axon, dendrite and synapse are thus

integral to neuronal physiological function and health (Selkoe, 2002; Mattson et al., 2008; Cheng et al., 2010; Cho et al., 2010).

The role of Opa1 itself is of consequence in another optic neuropathy, glaucoma (Ju et al., 2008; Ju et al., 2009a; Ju et al., 2009b; Ju et al., 2010). Recent studies show that transfection of pre-glaucomatous DBA/2J eyes (a mouse model of heredity glaucoma) with mOpa1 using AAV2 lead to increased retinal ganglion cell survival at 2 months of age suggesting a role for Opa1 in glaucoma. These results however are not conclusive; DBA/2J mice have a variable phenotype including the levels of retinal ganglion cell death observed and these mice were examined at 2 months of age were widespread retinal ganglion cell loss is not observed until 9 months of age. A repeat of this study on mice of this age would yield interesting results. In addition, in retinal ganglion cell cultures (RGC-5) subjected to a high hydrostatic pressure an upregulation of Opa1 is seen within 2 days of the initial hypertensive shock. Interestingly Opa1 was downregulated after 3 days of pressure treatment suggesting that Opa1 is initially upregulated in response to mitochondrial stress and that after 3 days the mitochondria are actively damaged by the high hydrostatic pressure. Opa1 may have protective effects on neurones lowering apoptotic stress by limited cytochrome c release. It would be interesting to induce high intraocular pressure in the *Opa1*^{+/-} mouse to evaluate comparative levels of retinal ganglion cell damage.

8.5: Implications for Therapeutics Interventions

These findings reveal a potentially useful window of opportunity for the exploration of therapeutic intervention in the mouse model of ADOA starting at a point in the disease pathway before significant visual and retinal ganglion cell loss.

In the *Opa1*^{+/-} mouse, dysfunctional mitochondria in retinal ganglion cells could lead to damage by increased reactive oxygen species, lipid peroxidation leading to energy depletion (through ATPase dysfunction), slower vesicle recycling leading to synaptic, and consequently dendritic, atrophy as well as lower rates of Ca²⁺ sequestering (shown to cause neuritic degeneration). Preferential loss of ON-centre retinal ganglion cells has a number of implications including the disruption of a light-sensitive pathway (though a survival of a dark-sensitive pathway) leading to visual dysfunction and ultimately loss of vision. Analysis of mutations in OPA1 ADOA patients suggests two principle mechanisms by which OPA1 mutation affects mitochondrial function: haploinsufficiency (nonsense mutations) and a potential dominant negative effect (missense mutations). Data from patient fibroblasts (Arnoult et al., 2005; Olichow et al., 2007; Amati-Bonneau et al., 2009) suggest a number of cellular effects such as mtDNA deletions, fusion defects, reduced ATP synthesis, increase in susceptibility to apoptosis or vulnerable to oxidative stress.

Damage and cell death of retinal ganglion cells may be induced by high levels of reactive oxygen species / oxidative stress. Mitochondria are significant generators of reactive oxygen species and this makes modulation of mitochondrial function an ideal target for therapeutic intervention. Evidence from the *Drosophila* mutant (Yarosh, Monserrate and Tong, 2008), dOpa1, show an increase in reactive oxygen production due to mutations in *Opa1* and that

antioxidants such as Vitamin E are able to reverse the disease phenotype. Since mitochondria are significant generators of reactive oxygen they are particularly vulnerable to oxidative stress. Mitochondrial function may be modulated in a number of ways, including agents that may increase ATP production (idebenone (Chinnery and Turnbull, 2001; Kerr, 2010; Klopstock et al., 2011)), agents which can reduce reactive oxygen production; co-enzyme Q₁₀ (Nakajima et al., 2008), antioxidants; vitamin E (Khanna et al., 2006) and Brazilian green propolis (Inokuchi et al., 2006), as well as minocycline (Shimazawa et al., 2005), superoxide dismutase 1 (SOD1) (Yarosh et al., 2008) and resveratrol (Kaeberlein, 2010) and those agents which may modulate the mitochondrial permeability transition pore and inhibit loss of mitochondrial membrane potential (cyclosporine (Cook et al., 2009)).

The selective loss of glutamatergic retinal ganglion cells provides a useful insight into the selective vulnerability of neurons in mitochondrial disease associated with chronic neurodegeneration, and may help elucidate similar mechanisms of neurodegeneration in other diseases where mitochondrial dynamics have shown to be altered (Wang et al., 2008; Cho et al., 2010).

References

Abou-Sleiman P M, Muqit M M K, and Wood N W (2006) Expanding insights of mitochondrial dysfunction in Parkinson's disease. *Nature Reviews Neuroscience* 7: 207-219.

Aijaz S, Erskine L, Jeffery G, Bhattacharya S S, and Votruba M (2004) Developmental expression profile of the optic atrophy gene product: OPA1 is not localized exclusively in the mammalian retinal ganglion cell layer, Invest. *Ophthalmol. Visual Sci.* 45: 1667-1673.

Akaishi Y, Uchiyama H, Ito H, and Shimizu Y (1995) A morphological-study of the retinal ganglion-cells of the afghan pika (*ochotona-rufescens*). *Neuroscience Research* 22: 1-12.

Alavi M V, Bette S, Schimpf S, Schuettauf F, Schraermeyer U, Wehrl H F, Ruttiger L et al. (2007) A splice site mutation in the murine Opa1 gene features pathology of autosomal dominant optic atrophy. *Brain : a journal of neurology* 130: 1029-1042.

Alavi M V, Fuhrmann N, Nguyen H P, Yu-Wai-Man P, Heiduschka P, Chinnery P F, and Wissinger B (2009) Subtle neurological and metabolic abnormalities in an Opa1 mouse model of autosomal dominant optic atrophy. *Experimental neurology* 220: 404-409.

Alexander C, Votruba M, Pesch U E, Thiselton D L, Mayer S, Moore a, Rodriguez M et al. (2000) OPA1, encoding a dynamin-related GTPase, is mutated in autosomal dominant optic atrophy linked to chromosome 3q28. *Nature genetics* 26: 211-215.

Amati-Bonneau P, Milea D, Bonneau D, Chevrollier A, Ferré M, Guillet V, Gueguen N et al. (2009) OPA1-associated disorders: phenotypes and pathophysiology. *The international journal of biochemistry & cell biology* 41: 1855-1865.

Arnoult D, Grodet A, Lee Y J, Estaquier J, and Blackstone C (2005) Release of OPA1 during apoptosis participates in the rapid and complete release of cytochrome c and subsequent mitochondrial fragmentation. *Journal of Biological Chemistry* 280: 35742-35750.

Attwell D, and Laughlin S B (2001) An energy budget for signaling in the grey matter of the brain. *Journal of Cerebral Blood Flow and Metabolism* 21: 1133-1145.

Barboni P, Carbonelli M, Savini G, Foscarini B, Parisi V, Valentino M L, Carta A et al. (2010) OPA1 Mutations Associated with Dominant Optic Atrophy Influence Optic Nerve Head Size. *Ophthalmology* 117: 1547-1553.

Barnard A R, Charbel Issa P, Perganta G, Williams P A, Davies V J, Sekaran S, Votruba M et al. (2011) Specific deficits in visual electrophysiology in a mouse model of dominant optic atrophy. *Experimental eye research* 93: 771-777.

Barnard A R, Issa P C, Perganta G, Williams P A, Davies V J, Sekaran S, Votruba M et al. Specific deficits in visual electrophysiology in a mouse model of dominant optic atrophy. *Experimental Eye Research*.

Beal M F (2001) Experimental models of Parkinson's disease. *Nature Reviews Neuroscience* 2: 325-332.

Bear MF (1995) Mechanism for a sliding synaptic modification threshold. *Neuron* 15: 1-4.

Berninger T A, Jaeger W, and Krastel H (1991) Electrophysiology and color perimetry in dominant infantile optic atrophy. *British Journal of Ophthalmology* 75: 49-52.

Berson D M (2003) Strange vision: ganglion cells as circadian photoreceptors. *Trends in Neurosciences* 26: 314-320.

Bette S, Schlaszus H, Wissinger B, Meyermann R, and Mittelbronn M (2005) OPA1, associated with autosomal dominant optic atrophy, is widely expressed in the human brain. *Acta Neuropathologica* 109: 393-399.

Bodnarenko S R, Jeyarasasingam G, and Chalupa L M (1995) Development and regulation of dendritic stratification in retinal ganglion-cells by glutamate-mediated afferent activity. *Journal of Neuroscience* 15: 7037-7045.

Boycott B B, Dowling J E, and Kolb H (1969) Organization of primate retina - light microscopy - a second type of midget bipolar cell in primate retina. *Philosophical Transactions of the Royal Society of London Series B-Biological Sciences* 255: 109-&.

Carelli V, Chiara, Valentino M L, Barboni P, Ross-Cisneros F N, and Sadun A a (2009) Retinal ganglion cell neurodegeneration in mitochondrial inherited disorders. *Biochimica et biophysica acta* 1787: 518-528.

Carelli V, Ross-Cisneros F N, and Sadun A a (2002) Optic nerve degeneration and mitochondrial dysfunction: genetic and acquired optic neuropathies. *Neurochemistry international* 40: 573-584.

Cervený K L, Tamura Y, Zhang Z, Jensen R E, and Sesaki H (2007) Regulation of mitochondrial fusion and division. *Trends in Cell Biology* 17: 563-569.

Chalupa L, and Werner J (2004) *The Visual Neurosciences*. 1st ed. The MIT Press.

- Chan D C (2006a) Mitochondria: Dynamic organelles in disease, aging, and development. *Cell* 125: 1241-1252.
- Chan D C (2006b) Mitochondrial fusion and fission in mammals. *Annual Review of Cell and Developmental Biology* 22: 79-99.
- Chen H, and Chan D C (2005) Emerging functions of mammalian mitochondrial fusion and fission, Hum. *Mol. Genet.* 14.
- Chen H, and Chan D C (2006) Critical dependence of neurons on mitochondrial dynamics. *Current Opinion in Cell Biology* 18: 453-459.
- Chen H C, Detmer S A, Ewald A J, Griffin E E, Fraser S E, and Chan D C (2003) Mitofusins Mfn1 and Mfn2 coordinately regulate mitochondrial fusion and are essential for embryonic development. *Journal of Cell Biology* 160: 189-200.
- Cheng A W, Hou Y, and Mattson M P (2010) Mitochondria and neuroplasticity. *Asn Neuro* 2: 243-256.
- Chetkovich D M, Bunn R C, Kuo S-H, Kawasaki Y, Kohwi M, and Brecht D S (2002) Postsynaptic Targeting of Alternative Postsynaptic Density-95 Isoforms by Distinct Mechanisms. *J. Neurosci.* 22: 6415-6425.
- Chinnery P F, and Turnbull D M (2001) Epidemiology and treatment of mitochondrial disorders. *American Journal of Medical Genetics* 106: 94-101.
- Cho D-H, Nakamura T, and Lipton S A (2010) Mitochondrial dynamics in cell death and neurodegeneration. *Cellular and Molecular Life Sciences* 67: 3435-3447.
- Cook A M, Whitlow J, Hatton J, and Young B (2009) Cyclosporine A for neuroprotection: establishing dosing guidelines for safe and effective use. *Expert Opinion on Drug Safety* 8: 411-419.
- Coombs J, van der List D, Wang G Y, and Chalupa L M (2006) Morphological properties of mouse retinal ganglion cells. *Neuroscience* 140: 123-136.
- Crooks J, and Kolb H (1992) Localization of gaba, glycine, glutamate and tyrosine-hydroxylase in the human retina. *Journal of Comparative Neurology* 315: 287-302.
- Dacey D M, and Petersen M R (1992) Dendritic field size and morphology of midget and parasol ganglion cells of the human retina. *Proceedings of the National Academy of Sciences of the United States of America* 89: 9666-9670.

Davanger S, Ottersen O P, and Stormmathisen J (1991) Glutamate, gaba, and glycine in the human retina - an immunocytochemical investigation. *Journal of Comparative Neurology* 311: 483-494.

Davies V J, Hollins A J, Piechota M J, Yip W, Davies J R, White K E, Nicols P P et al. (2007) Opa1 deficiency in a mouse model of autosomal dominant optic atrophy impairs mitochondrial morphology, optic nerve structure and visual function. *Hum. Mol. Genet.* 16: 1307-1318.

de Brito O M, and Scorrano L (2009) Mitofusin-2 regulates mitochondrial and endoplasmic reticulum morphology and tethering: The role of Ras. *Mitochondrion* 9: 222-226.

Delettre C, Lenaers G, Griffoin J M, Gigarel N, Lorenzo C, Belenguer P, Pelloquin L et al. (2000) Nuclear gene OPA1, encoding a mitochondrial dynamin-related protein, is mutated in dominant optic atrophy. *Nature Genetics* 26: 207-210.

Delettre C, Lenaers G, Pelloquin L, Belenguer P, and Hamel C P (2002) OPA1 (Kjer type) dominant optic atrophy: a novel mitochondrial disease. *Molecular genetics and metabolism* 75: 97-107.

Delivani P, and Martin S J (2006) Mitochondrial membrane remodeling in apoptosis: an inside story. *Cell Death and Differentiation* 13: 2007-2010.

Dhruv N T, Tailby C, Sokol S H, Majaj N J, and Lennie P (2009) Nonlinear Signal Summation in Magnocellular Neurons of the Macaque Lateral Geniculate Nucleus. *J Neurophysiol* 102: 1921-1929.

Diller L, Packer O S, Verweij J, McMahon M J, Williams D R, and Dacey D M (2004) L and M cone contributions to the midget and parasol ganglion cell receptive fields of macaque monkey retina. *Journal of Neuroscience* 24: 1079-1088.

Dohm J A, Lee S J, Hardwick J M, Hill R B, and Gittis A G (2004) Cytosolic domain of the human mitochondrial fission protein Fis1 adopts a TPR fold. *Proteins-Structure Function and Genetics* 54: 153-156.

Doi M, Uji Y, and Yamamura H (1995) Morphological classification of retinal ganglion-cells in mice. *Journal of Comparative Neurology* 356: 368-386.

Dong W, Sun W, Zhang Y, Chen X, and He S (2004) Dendritic relationship between starburst amacrine cells and direction-selective ganglion cells in the rabbit retina. *The Journal of physiology* 556: 11-17.

Dowling J E (1987) *The Retina: An Approachable Part of the Brain*. 1st ed. The Belknap Press of Harvard University Press.

Dowling J E, and Werblin F S (1969) Organization of retina of mudpuppy neoturus maculosus .i. synaptic structure. *Journal of Neurophysiology* 32: 315-&.

Ferré M, Amati-Bonneau P, Tourmen Y, Malthiery Y, and Reynier P (2005) *eOPA1*: An online database for *OPA1* mutations. *Human Mutation* 25: 423-428.

Fournier A V, Damji K F, Epstein D L, and Pollock S C (2001) Disc excavation in dominant optic atrophy. *Ophthalmology* 108: 1595-1602.

Frank S, Gaume B, Bergmann-Leitner E S, Leitner W W, Robert E G, Catez F, Smith C L et al. (2001) The role of dynamin-related protein 1, a mediator of mitochondrial fission, in apoptosis. *Developmental Cell* 1: 515-525.

Frezza C, Cipolat S, Brito M D, O M, M B, G.v, Rudka T et al. (2006) *OPA1* controls apoptotic cristae remodeling independently from mitochondrial fusion. *Cell* 126: 177-189.

Gan W B, Grutzendler J, Wong W T, Wong R O, and Lichtman J W (2000) Multicolor "DiOlistic" labeling of the nervous system using lipophilic dye combinations. *Neuron* 27: 219-225.

Ghosh K K, Goodchild A K, Sefton A E, and Martin P R (1996) Morphology of retinal ganglion cells in a New World monkey, the marmoset *Callithrix jacchus*. *Journal of Comparative Neurology* 366: 76-92.

Ghosh K K, Goodchild A N N K, Sefton A N N E, and Martin P R (2006) Morphology of Retinal Ganglion Cells in a New World Monkey, the Marmoset. *Journal of Comparative Neurology* 92: 76-92.

Greenwood S M, and Connolly C N (2007) Dendritic and mitochondrial changes during glutamate excitotoxicity. *Neuropharmacology* 53: 891-898.

Grutzendler J, Helmin K, Tsai J, and Gan W B (2007) Various dendritic abnormalities are associated with fibrillar amyloid deposits in Alzheimer's disease. *Imaging and the Aging Brain* 1097: 30-39.

Gutierrez H, and Davies A M (2007) A fast and accurate procedure for deriving the Sholl profile in quantitative studies of neuronal morphology. *Journal of Neuroscience Methods* 163: 24-30.

Hausser M, Spruston N, and Stuart G J (2000) Diversity and dynamics of dendritic signaling. *Science* 290: 739-744.

Heiduschka P, Schnichels S, Fuhrmann N, Hofmeister S, Schraermeyer U, Wissinger B, and Alavi M V (2010) Electrophysiological and Histologic Assessment of Retinal Ganglion Cell Fate in a Mouse Model for *OPA1*-Associated Autosomal Dominant Optic Atrophy. *Investigative Ophthalmology & Visual Science* 51: 1424-1431.

Higley MJ, Sabatini BL (2008) Calcium signaling in dendrites and spines: practical and functional considerations. *Neuron* 59: 902-913.

Hinshaw J E, and Schmid S L (1995) Dynamin self-assembles into rings suggesting a mechanism for coated vesicle budding. *Nature* 374: 190-192.

Holder G E (2004) Electrophysiological assessment of optic nerve disease. *Eye (London, England)* 18: 1133-1143.

Holder G E, Votruba M, Carter A C, Bhattacharya S S, Fitzke F W, and Moore A T (1998) Electrophysiological findings in dominant optic atrophy (DOA) linking to the OPA1 locus on chromosome 3q 28-qter. *Documenta Ophthalmologica* 95: 217-228.

Huang T, Santarelli R, and Starr A (2009) Mutation of OPA1 gene causes deafness by affecting function of auditory nerve terminals. *Brain research* 1300: 97-104.

Ikegaya Y, Kim J A, Baba M, Iwatsubo T, Nishiyama N, and Matsuki N (2001) Rapid and reversible changes in dendrite morphology and synaptic efficacy following NMDA receptor activation: implication for a cellular defense against excitotoxicity. *Journal of Cell Science* 114: 4083-4093.

Inokuchi Y, Shimazawa M, Nakajima Y, Suemori S, Mishima S, and Hara H (2006) Brazilian green propolis protects against retinal damage in vitro and in vivo. *Evidence-based complementary and alternative medicine : eCAM* 3: 71-77.

Jan Y N, and Jan L Y (2001) Dendrites. *Genes & Development* 15: 2627-2641.

Jeon C J, Strettoi E, and Masland R H (1998) The major cell populations of the mouse retina. *Journal of Neuroscience* 18: 8936-8946.

Johnston D, and Narayanan R (2008) Active dendrites: colorful wings of the mysterious butterflies. *Trends in Neurosciences* 31: 309-316.

Johnston P B, Gaster R N, Smith V C, and Tripathi R C (1979) Clinicopathologic study of autosomal dominant optic atrophy. *American Journal of Ophthalmology* 88: 868-875.

Ju W-K, Kim K-Y, Angert M, Duong-Polk K X, Lindsey J D, Ellisman M H, and Weinreb R N (2009a) Memantine blocks mitochondrial OPA1 and cytochrome c release and subsequent apoptotic cell death in glaucomatous retina. *Investigative ophthalmology & visual science* 50: 707-716.

Ju W-K, Kim K-Y, Duong-Polk K X, Lindsey J D, Ellisman M H, and Weinreb R N (2010) Increased optic atrophy type 1 expression protects retinal ganglion cells in a mouse model of glaucoma. *Molecular Vision* 16: 1331-1342.

Ju W-K, Kim K-Y, Lindsey J D, Angert M, Duong-Polk K X, Scott R T, Kim J J et al. (2008) Intraocular pressure elevation induces mitochondrial fission and triggers OPA1 release in glaucomatous optic nerve. *Investigative ophthalmology & visual science* 49: 4903-4911.

Ju W-K, Kim K-Y, Lindsey J D, Angert M, Patel A, Scott R T, Liu Q et al. (2009b) Elevated hydrostatic pressure triggers release of OPA1 and cytochrome C, and induces apoptotic cell death in differentiated RGC-5 cells. *Molecular vision* 15: 120-134.

Ju W K, Misaka T, Kushnareva Y, Nakagomi S, Agarwal N, Kubo Y, Lipton S A et al. (2005) expression in the normal rat retina and optic nerve, *J. Comp. Neurol.* 488: 1-10.

Kaeberlein M (2010) Resveratrol and rapamycin: are they anti-aging drugs? *Bioessays* 32: 96-99.

Kerr D S (2010) Treatment of mitochondrial electron transport chain disorders: A review of clinical trials over the past decade. *Molecular Genetics and Metabolism* 99: 246-255.

Khanna S, Roy S, Parinandi N L, Maurer M, and Sen C K (2006) Characterization of the potent neuroprotective properties of the natural vitamin E alpha-tocotrienol. *Journal of Neurochemistry* 98: 1474-1486.

Kieper N, Holmstroem K M, Ciceri D, Fiesel F C, Wolburg H, Ziviani E, Whitworth A J et al. (2010) Modulation of mitochondrial function and morphology by interaction of Omi/HtrA2 with the mitochondrial fusion factor OPA1. *Experimental Cell Research* 316: 1213-1224.

Kjer B, Eiberg H, Kjer P, and Rosenberg T (1996) Dominant optic atrophy mapped to chromosome 3q region .2. Clinical and epidemiological aspects. *Acta Ophthalmologica Scandinavica* 74: 3-7.

Kjer P, Jensen O A, and Klinken L (1983) Histopathology of eye, optic-nerve and brain in a case of dominant optic atrophy. *Acta Ophthalmologica* 61: 300-312.

Klopstock T, Yu-Wai-Man P, Dimitriadis K, Rouleau J, Heck S, Bailie M, Atawan A et al. (2011) A randomized placebo-controlled trial of idebenone in Leber's hereditary optic neuropathy. *Brain* 134: 2677-2686.

Knott A B, and Bossy-Wetzel E (2008) Impairing the Mitochondrial Fission and Fusion Balance: A New Mechanism of Neurodegeneration. In: Gibson G E, Ratan R R, and Beal M F [eds.] *Mitochondria and Oxidative Stress in Neurodegenerative Disorders*. Vol. 1147. pp. 283-292.

Komban S J, Alonso J-M, and Zaidi Q (2011) Darks Are Processed Faster Than Lights. *Journal of Neuroscience* 31: 8654-8658.

Kong J-H, Fish D R, Rockhill R L, and Masland R H (2005) Diversity of ganglion cells in the mouse retina: unsupervised morphological classification and its limits. *The Journal of comparative neurology* 489: 293-310.

- Lackner L L, and Nunnari J M (2009) The molecular mechanism and cellular functions of mitochondrial division. *Biochimica et Biophysica Acta (BBA) - Molecular Basis of Disease* 1792: 1138-1144.
- Lascaratos G, Ji D, Wood J P M, and Osborne N N (2007) Visible light affects mitochondrial function and induces neuronal death in retinal cell cultures. *Vision Research* 47: 1191-1201.
- Lawrence E (2005) *Henderson's Dictionary of Biology*. 13th ed. Pearson.
- Laycock R, Crewther S G, and Crewther D P (2007) A role for the 'magnocellular advantage' in visual impairments in neuro developmental and psychiatric disorders. *Neuroscience and Biobehavioral Reviews* 31: 363-376.
- Lee S, Jeong S-Y, Lim W-C, Kim S, Park Y-Y, Sun X, Youle R J et al. (2007) Mitochondrial fission and fusion mediators, hFis1 and OPA1, modulate cellular senescence. *The Journal of biological chemistry* 282: 22977-22983.
- Lenaers G, Reynier P, Elachouri G, Soukkaieh C, Olichon A, Belenguer P, Baricault L et al. (2009) OPA1 functions in mitochondria and dysfunctions in optic nerve. *The international journal of biochemistry & cell biology* 41: 1866-1874.
- Li Z, Okamoto K, Hayashi Y, and Sheng M (2004) The importance of dendritic mitochondria in the morphogenesis and plasticity of spines and synapses. *Cell* 119: 873-887.
- Liesa M, Palacin M, and Zorzano A (2009) Mitochondrial Dynamics in Mammalian Health and Disease. *Physiological Reviews* 89: 799-845.
- Malenka R C (1995) LTP and LTD: Dynamic and Interactive Processes of Synaptic Plasticity. *The Neuroscientist* 1: 35-42.
- Marc R (2008) Functional anatomy of the neural retina. In: Albert D, Miller J, and Azar D [eds.] *Albert & Jakobiec's principles and practice of ophthalmology*. Vol. 2. Saunders/Elsevier, pp. 1-28.
- Marc R E, Jones B W, Watt C B, and Strettoi E (2003) Neural remodeling in retinal degeneration. *Progress in Retinal and Eye Research* 22: 607-655.
- Matthews G (2005) Making the retina approachable. *Journal of Neurophysiology* 93: 3034-3035.
- Mattson M P, Gleichmann M, and Cheng A (2008) Mitochondria in Neuroplasticity and Neurological Disorders. *Neuron* 60: 748-766.

- Mattson M P, and Magnus T (2006) Ageing and neuronal vulnerability. *Nature Reviews Neuroscience* 7: 278-294.
- McBain S C, Griesenbach U, Xenariou S, Keramane A, Batich C D, Alton E W F W, and Dobson J (2008) Magnetic nanoparticles as gene delivery agents: enhanced transfection in the presence of oscillating magnet arrays. *Nanotechnology* 19.
- Merkwirth C, and Langer T (2008) Mitofusin 2 Builds a Bridge between ER and Mitochondria. *Cell* 135: 1165-1167.
- Milea D, Sander B, Wegener M, Jensen H, Kjer B, Jorgensen T M, Lund-Andersen H et al. (2010) Axonal loss occurs early in dominant optic atrophy. *Acta Ophthalmologica* 88: 342-346.
- Milone M, Younge B R, Wang J, Zhang S, and Wong L-J (2009) Mitochondrial disorder with OPA1 mutation lacking optic atrophy. *Mitochondrion* 9: 279-281.
- Misaka T, Miyashita T, and Kubo Y (2002) Primary structure of a dynamin-related mouse mitochondrial GTPase and its distribution in brain, subcellular localization, and effect on mitochondrial morphology. *J. Biol. Chem.* 277: 15834-15842.
- Miyata K, Nakamura M, Kondo M, Lin J, Ueno S, Miyake Y, and Terasaki H (2007) Reduction of oscillatory potentials and photopic negative response in patients with autosomal dominant optic atrophy with OPA1 mutations. *Investigative Ophthalmology & Visual Science* 48: 820-824.
- Mizielinska S M, Greenwood S M, Tummala H, and Connolly C N (2009) Rapid dendritic and axonal responses to neuronal insults. *Biochemical Society Transactions* 37: 1389-1393.
- Morgan J, and Wong R O (2007) Development of cell types and synaptic connections in the retina. In: Kolb H, Fernandez E, and Nelson R [eds.] *Webvision: The organization of the retina and visual system*. [Internet].
- Mozdy A D, McCaffery J M, and Shaw J M (2000) Dnm1p GTPase-mediated mitochondrial fission is a multi-step process requiring the novel integral membrane component Fis1p. *Journal of Cell Biology* 151: 367-379.
- Nakajima Y, Inokuchi Y, Nishi M, Shimazawa M, Otsubo K, and Hara H (2008) Coenzyme Q(10) protects retinal cells against oxidative stress in vitro and in vivo. *Brain Research* 1226: 226-233.
- Nelson R, Famiglietti E V, and Kolb H (1978) Intracellular staining reveals different levels of stratification for on- and off-center ganglion cells in cat retina. *Journal of neurophysiology* 41: 472-483.

O'Brien J A, and Lummis S C R (2006) Biolistic transfection of neuronal cultures using a hand-held gene gun. *Nature Protocols* 1: 977-981.

Oesch N, Euler T, and Taylor W R (2005) Direction-selective dendritic action potentials in rabbit retina. *Neuron* 47: 739-750.

Olichon A, Emorine L J, Descoins E, Pelloquin L, Brichese L, Gas N, Guillou E et al. (2002) The human dynamin-related protein OPA1 is anchored to the mitochondrial inner membrane facing the inter-membrane space. *FEBS Lett.* 523: 171-176.

Olichon A, Guillou E, Delettre C, Landes T, Arnaune-Pelloquin L, Emorine L J, Mils V et al. (2006) Mitochondrial dynamics and disease, OPA1. *Biochimica Et Biophysica Acta-Molecular Cell Research* 1763: 500-509.

Olichow A, Landes T, Arnaune-Pelloquin L, Emorine L J, Mils V, Guichev A, Delettre C et al. (2007) Effects of OPA1 mutations mitochondrial morphology and apoptosis: Relevance to ADOA pathogenesis. *Journal of Cellular Physiology* 211: 423-430.

Osborne N N, Lascaratos G, Bron a J, Chidlow G, and Wood J P M (2006) A hypothesis to suggest that light is a risk factor in glaucoma and the mitochondrial optic neuropathies. *The British journal of ophthalmology* 90: 237-241.

Otera H, and Mihara K (2011) Molecular mechanisms and physiologic functions of mitochondrial dynamics. *Journal of Biochemistry* 149: 241-251.

Overly C C, Rieff H I, and Hollenbeck P J (1996) Organelle motility and metabolism in axons vs dendrites of cultured hippocampal neurons. *Journal of Cell Science* 109: 971-980.

Pankhurst Q A, Thanh N K T, Jones S K, and Dobson J (2009) Progress in applications of magnetic nanoparticles in biomedicine. *Journal of Physics D-Applied Physics* 42.

Perez-Cruz C, Nolte M W, van Gaalen M M, Rustay N R, Termont A, Tanghe A, Kirchhoff F et al. (2011) Reduced Spine Density in Specific Regions of CA1 Pyramidal Neurons in Two Transgenic Mouse Models of Alzheimer's Disease. *Journal of Neuroscience* 31: 3926-3934.

Pesch U E A, Leo-Kottler B, Mayor S, Jurklies B, Kellner U, Apfelstedt-Sylla E, Zrenner E et al. (2001) OPA1 mutations in patients with autosomal dominant optic atrophy and evidence for semi-dominant inheritance. *Human Molecular Genetics* 10: 1359-1368.

Pignatelli V, and Strettoi E (2004) Bipolar cells of the mouse retina: a gene gun, morphological study. *The Journal of comparative neurology* 476: 254-266.

Pinto L H, Invergo B, Shimomura K, Takahashi J S, and Troy J B (2007) Interpretation of the mouse electroretinogram. *Documenta Ophthalmologica* 115: 127-136.

Poderoso C, Converso D P, Maloberti P, Duarte A, Neuman I, Galli S, Maciel F C et al. (2008) A Mitochondrial Kinase Complex Is Essential to Mediate an ERK1/2-Dependent Phosphorylation of a Key Regulatory Protein in Steroid Biosynthesis. *Plos One* 3: 11.

Pourcho R G (1982) Dopaminergic amacrine cells in the cat retina. *Brain Research* 252: 101-109.

Pourcho R G (1996) Neurotransmitters in the retina. *Current Eye Research* 15: 797-803.

Puomila A, Huoponen K, Mantyjarvi M, Hamalainen P, Paananen R, Sankila E M, Savontaus M L et al. (2005) Dominant optic atrophy: correlation between clinical and molecular genetic studies. *Acta Ophthalmologica Scandinavica* 83: 337-346.

Ramon y Cajal S (1889a) Nota preventiva sobre la estructura de la médula embrionaria *Gaceta Medica Catalana* 12: 132-174.

Ramon y Cajal S (1889b) Nuevas aplicaciones del método de coloración de Golgi *Gaceta Medica Catalana* 12: 1-8.

Reynolds E S (1963) Use of lead citrate at high pH as an electron-opaque stain in electron microscopy. *Journal of Cell Biology* 17: 208-&.

Rizzuto R, Marchi S, Bonora M, Aguiari P, Bononi A, De Stefani D, Giorgi C et al. (2009) Ca²⁺ transfer from the ER to mitochondria: When, how and why. *Biochimica Et Biophysica Acta-Bioenergetics* 1787: 1342-1351.

Rizzuto R, Pinton P, Carrington W, Fay F S, Fogarty K E, Lifshitz L M, Tuft R A et al. (1998) Close contacts with the endoplasmic reticulum as determinants of mitochondrial Ca²⁺ responses. *Science* 280: 1763-1766.

Rossier M F (2006) T channels and steroid biosynthesis: in search of a link with mitochondria. *Cell Calcium* 40: 155-164.

Ruggiero L, Allen C N, Brown R L, and Robinson D W (2009) The development of melanopsin-containing retinal ganglion cells in mice with early retinal degeneration. *European Journal of Neuroscience* 29: 359-367.

Ruthazer E S, and Aizenman C D (2010) Learning to see: patterned visual activity and the development of visual function. *Trends in Neurosciences* 33: 183-192.

Sanes J R, and Zipursky S L (2010) Design Principles of Insect and Vertebrate Visual Systems. *Neuron* 66: 15-36.

Santel A, Frank S, Gaume B, Herrier M, Youle R J, and Fuller M T (2003) Mitofusin-1 protein is a generally expressed mediator of mitochondrial fusion in mammalian cells. *Journal of Cell Science* 116: 2763-2774.

Sawamiphak S, Ritter M, and Acker-Palmer A (2010) Preparation of retinal explant cultures to study ex vivo tip endothelial cell responses. *Nature Protocols* 5: 1659-1665.

Saxena S, and Caroni P (2011) Selective Neuronal Vulnerability in Neurodegenerative Diseases: from Stressor Thresholds to Degeneration. *Neuron* 71: 35-48.

Schmitz S K, Hjorth J J J, Joemai R M S, Wijntjes R, Eijgenraam S, de Bruijn P, Georgiou C et al. (2011) Automated analysis of neuronal morphology, synapse number and synaptic recruitment. *Journal of Neuroscience Methods* 195: 185-193.

Selkoe D J (2002) Alzheimer's disease is a synaptic failure. *Science* 298: 789-791.

Sernagor E, Eglén S J, and Wong R O L (2001) Development of retinal ganglion cell structure and function. *Progress in Retinal and Eye Research* 20: 139-174.

Shah M, Hammond R, and Hoffman D (2010) Dendritic ion channel trafficking and plasticity. *Trends in Neurosciences* 33: 307-316.

Shimazawa M, Yamashima T, Agarwal N, and Hara H (2005) Neuroprotective effects of minocycline against in vitro and in vivo retinal ganglion cell damage. *Brain Research* 1053: 185-194.

Sholl D A (1953) Dendritic organization in the neurons of the visual and motor cortices of the cat. *Journal of Anatomy* 87: 387-&.

Silver R A (2010) Neuronal arithmetic. *Nature Reviews Neuroscience* 11: 474-489.

Smith R S, John S W M, Nishina P M, and Sundberg J P (2002) *Systemic evaluation of the mouse eye; anatomy, pathology, and biometrics*. Boca Raton, Florida: CRC Press.

Stevens C F (1998) Neuronal diversity: Too many cell types for comfort? *Current Biology* 8: R708-R710.

Stojanovski D, Koutsopoulos O S, Okamoto K, and Ryan M T (2004) Levels of human Fis1 at the mitochondrial outer membrane regulate mitochondrial morphology. *J Cell Sci* 117: 1201-1210.

Stuart G, Spruston N, and Hausser M (1999) *Dendrites*. 1st ed. Oxford.

Sun W, Deng Q, Levick W R, and He S (2006) ON direction-selective ganglion cells in the mouse retina. *Journal of Physiology-London* 576: 197-202.

Sun W, Li N, and He S (2002a) Large-scale morphological survey of rat retinal ganglion cells. *Visual neuroscience* 19: 483-493.

Sun W Z, Li N, and He S G (2002b) Large-scale morphological survey of mouse retinal ganglion cells. *Journal of Comparative Neurology* 451: 115-126.

Surgucheva I, Weisman A D, Goldberg J L, Shnyra A, and Surguchov A (2008) gamma-Synuclein as a marker of retinal ganglion cells. *Molecular Vision* 14: 1540-1548.

Tang S, Le P K, Tse S, Wallace D C, and Huang T (2009) Heterozygous Mutation of Opa1 in Drosophila Shortens Lifespan Mediated through Increased Reactive Oxygen Species Production. *Plos One* 4.

Taylor E, Davies J, Powell K, Davies V, and Votruba M (2010) Heterozygous B6;C3-*Opa1*^{Q285stop} Mouse Model of Dominant Optic Atrophy Displays Subtle Neuromuscular Features With Age but No Increase in Severity on a B6;C3-*Opa3*^{L122p} Background. *Investigative Ophthalmology and Visual Science* 51: E-Abstract 1451.

Ulfhake B, and Kellerth J O (1981) A quantitative light microscopic study of the dendrites of cat spinal alpha-motoneurons after intracellular staining with horseradish-peroxidase. *Journal of Comparative Neurology* 202: 571-583.

Van Bergen N J, Crowston J G, Kearns L S, Staffieri S E, Hewitt A W, Cohn A C, Mackey D A et al. (2011) Mitochondrial Oxidative Phosphorylation Compensation May Preserve Vision in Patients with OPA1-Linked Autosomal Dominant Optic Atrophy. *Plos One* 6.

Vizi E S, and Kiss J P (1998) Neurochemistry and pharmacology of the major hippocampal transmitter systems: Synaptic and nonsynaptic interactions. *Hippocampus* 8: 566-607.

Votruba M (2004) Molecular genetic basis of primary inherited optic neuropathies. *Eye (London, England)* 18: 1126-1132.

Votruba M, Moore a T, and Bhattacharya S S (1997) Genetic refinement of dominant optic atrophy (OPA1) locus to within a 2 cM interval of chromosome 3q. *Journal of Medical Genetics* 34: 117-121.

Votruba M, Moore A T, and Bhattacharya S S (1998) Clinical features, molecular genetics, and pathophysiology of dominant optic atrophy. *J. Med. Genet.* 35: 793-800.

Votruba M, Thiselton D, and Bhattacharya S S (2003) Optic disc morphology of patients with OPA1 autosomal dominant optic atrophy. *British Journal of Ophthalmology* 87: 48-53.

Wang X L, Su B, Siedlak S L, Moreira P I, Fujioka H, Wang Y, Casadesus G et al. (2008) Amyloid-beta overproduction causes abnormal mitochondrial dynamics via differential modulation of mitochondrial fission/fusion proteins. *Proceedings of the National Academy of Sciences of the United States of America* 105: 19318-19323.

Wataha J C, Lewis J B, Lockwood P E, Hsu S, Messer R L, Rueggeberg F A, and Bouillaguet S (2004) Blue light differentially modulates cell survival and growth. *Journal of Dental Research* 83: 104-108.

Watanabe M, and Rodieck R W (1989) Parasol and midget ganglion cells of the primate retina. *J. Comp. Neurol* 289: 434-454.

Waterham H R, Koster J, van Roermund C W T, Mooyer P A W, Wanders R J A, and Leonard J V (2007) A lethal defect of mitochondrial and peroxisomal fission. *New England Journal of Medicine* 356: 1736-1741.

Werblin F S (1972) Lateral interactions at inner plexiform layer of vertebrate retina - antagonistic responses to change. *Science* 175: 1008-&.

Werblin F S, and Dowling J E (1969) Organization of retina of mudpuppy necturus maculosus .2. intracellular recording. *Journal of Neurophysiology* 32: 339-&.

White K E, Davies V J, Hogan V E, Piechota M J, Nichols P P, Turnbull D M, and Votruba M (2009) OPA1 Deficiency Associated with Increased Autophagy in Retinal Ganglion Cells in a Murine Model of Dominant Optic Atrophy. *Investigative Ophthalmology & Visual Science* 50: 2567-2571.

Williams P A, Morgan J E, and Votruba M (2010) Opa1 deficiency in a mouse model of dominant optic atrophy leads to retinal ganglion cell dendropathy. *Brain* 133: 2942-2951.

Williams P A, Morgan J E, and Votruba M (2011) Mouse models of dominant optic atrophy: What do they tell us about the pathophysiology of visual loss? *Vision Research* 51: 229-234.

Wong W T, Faulkner-Jones B E, Sanes J R, and Wong R O L (2000) Rapid dendritic remodeling in the developing retina: Dependence on neurotransmission and reciprocal regulation by Rac and Rho. *Journal of Neuroscience* 20: 5024-5036.

Xia Y, Nawy S, and Carroll R C (2007) Activity-dependent synaptic plasticity in retinal ganglion cells. *Journal of Neuroscience* 27: 12221-12229.

Xu H P, and Tian N (2007) Retinal ganglion cell dendrites undergo a visual activity-dependent redistribution after eye opening. *Journal of Comparative Neurology* 503: 244-259.

Yamada E S, Silveira L C L, Perry V H, and Franco E C S (2001) M and P retinal ganglion cells of the owl monkey: morphology, size and photoreceptor convergence. *Vision Research* 41: 119-131.

Yarosh W, Monserrate J, and Tong J J (2008) The molecular mechanisms of OPA1-mediated optic atrophy in *Drosophila* model and prospects for antioxidant treatment. *PLoS Genet.* 4, e6.

Yiu H H P, McBain S C, Lethbridge Z A D, Lees M R, Palona I, Olariu C I, and Dobson J (2011) Novel Magnetite-Silica Nanocomposite (Fe₃O₄-SBA-15) Particles for DNA Binding and Gene Delivery Aided by a Magnet Array. *Journal of Nanoscience and Nanotechnology* 11: 3586-3591.

Yoon Y, Krueger E W, Oswald B J, and McNiven M A (2003) The mitochondrial protein hFis1 regulates mitochondrial fission in mammalian cells through an interaction with the dynamin-like protein DLP1. *Molecular and Cellular Biology* 23: 5409-5420.

Yu T, Fox R J, Burwell L S, and Yoon Y (2005) Regulation of mitochondrial fission and apoptosis by the mitochondrial outer membrane protein hFis1. *J Cell Sci* 118: 4141-4151.

Yu-Wai-Man P, Davies V J, Piechota M J, Cree L M, Votruba M, and Chinnery P F (2009) Secondary mtDNA Defects Do Not Cause Optic Nerve Dysfunction in a Mouse Model of Dominant Optic Atrophy. *Investigative Ophthalmology & Visual Science* 50: 4561-4566.

Yu-Wai-Man P, Griffiths P G, and Chinnery P F (2011) Mitochondrial optic neuropathies - Disease mechanisms and therapeutic strategies. *Progress in Retinal and Eye Research* 30: 81-114.

Yu-Wai-Man P, Griffiths P G, Gorman G S, Lourenco C M, Wright A F, Auer-Grumbach M, Toscano A et al. (2010) Multi-system neurological disease is common in patients with OPA1 mutations. *Brain* 133: 771-786.

Zhang Y, and Chan D C (2007) New insights into mitochondrial fusion. *Febs Letters* 581: 2168-2173.

Appendix: DiOlistic Method Development

In general reagents and antibodies worked out of the box following the established product literature, however in order to effectively label retinal ganglion cells using DiOlistics significant method development was required.

For DiOlistic method development the methods found in the literature were initially followed (Sun et al., 2002b) but gave sub-optimum results with retinal ganglion cells being poorly labelled and with a low yield (2-3 cells per retina). To increase the quality of the labelling of retinal ganglion cells the Dil / DiO concentration was increased by a factor of 2, 3, 5 and 10 from those found in the literature (ratio of 3:100, Dil : methylene chloride) with the most optimum results being a ratio of 1:10 (Dil : methylene chloride)(~3.3 fold increase). In addition, changes were made to the ballistic pressure of the gene gun. Test retinas from C57/B6 mice were shot once or twice with differing pressures between 80 and 200psi. To avoid 'overshooting' (excessive labelling rendering the cell unsuitable for analysis) the optimum pressure (allowing clear, distinct cells) was found to be 100psi. Retinas were only required to be shot once for optimum labelling at this pressure. These changes allowed a lower gain and smaller aperture on the confocal microscope and this, in turn, allowed for clearer and higher quality images to be generated. Adjusting the pressure of the gene gun also generated a greater yield of cells per retina. Figure XXXIII demonstrates the effects of varying pressures and dye concentrations on retinal ganglion cells labelling and image quality.

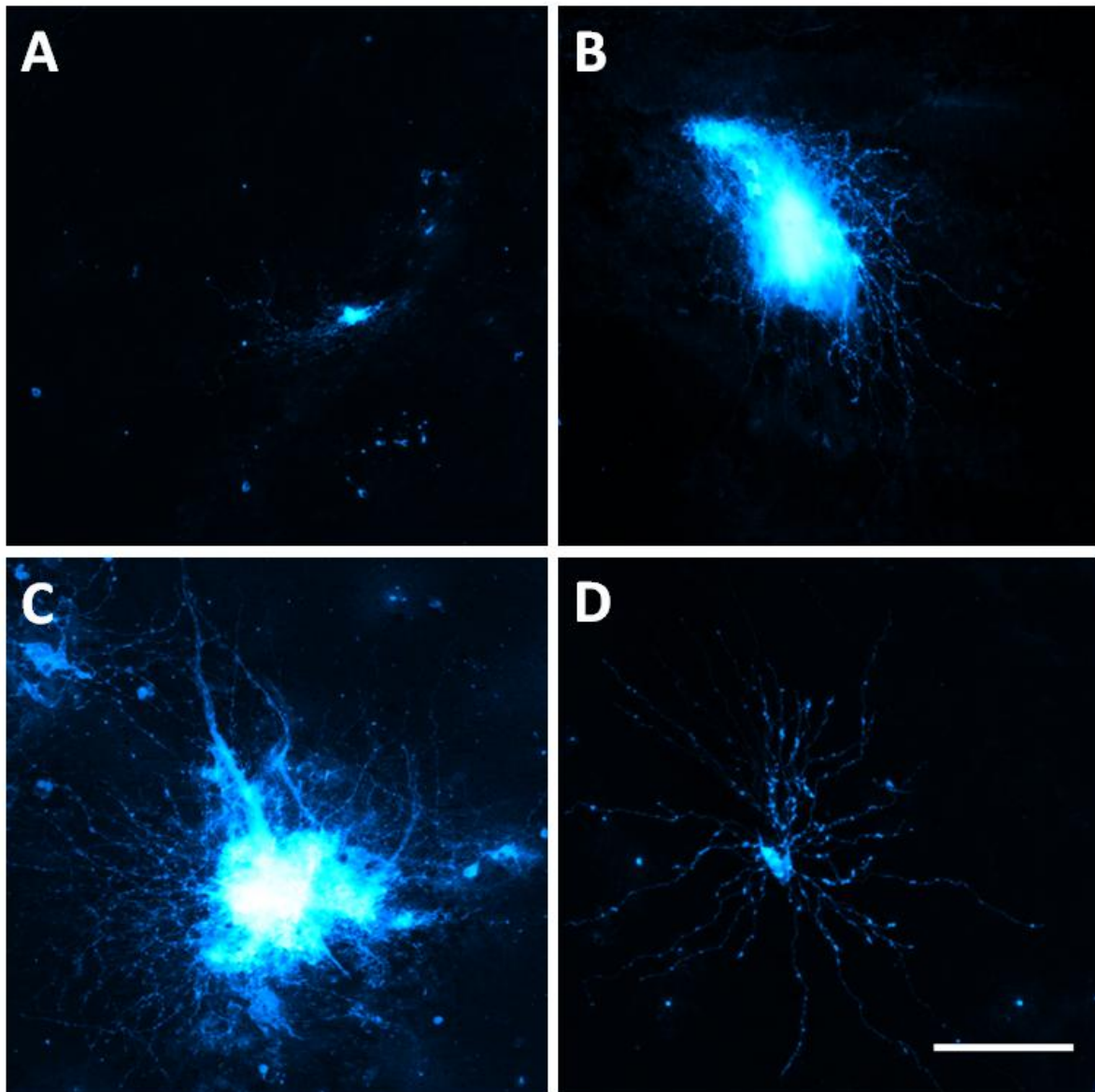


Figure XXXIII: *DiOlistic method development*

There is a delicate balance between the dye concentration and the shooting pressure of the gene gun that determines the quality and yield of viable retinal ganglion cells. Labelled cells need to have clear somas and distinct dendritic trees for quantitative analysis. If the dye concentration or shooting pressure is too low (A; low pressure [80psi]) or too high (B; high pressure [120psi]) it results in a too bright or too dull image that cannot be corrected through editing the microscope settings or through image processing. Likewise, shooting twice at a low pressure (C; shot twice [80psi]) does not correct this. Retinas shot once at 100psi gave the best quality and yield of retinal ganglion cells (D). Error bar = 100 μ m.

Papers Arising From This Thesis

Williams PA, Morgan JE, Votruba M (2010). Opa1 deficiency in a mouse model of dominant optic atrophy leads to retinal ganglion cell dendropathy. *Brain* 133(10): 2942-2951

Williams PA, Morgan JE, Votruba M (2011). Mouse models of dominant optic atrophy: What do they tell us about the pathophysiology of visual loss? *Vision Research* 51(2): 229-234

Williams PA, Piechota G, von Ruhland C, Taylor E, Morgan JE, Votruba M (2011). Opa1 is essential for retinal ganglion cell synaptic architecture and connectivity. *Brain* 135(2): 493-505